Title
Conservation and Divergence of Genetic Interactions and Functions Regulating Cilia and Embryogenesis

Author
Yee, Laura

Publication Date
2015

Peer reviewed|Thesis/dissertation

Conservation and Divergence of Genetic Interactions and Functions Regulating Cilia and Embryogenesis

by

Laura Yee

DISSERTATION

Submitted in partial satisfaction of the requirements for the degree of

DOCTOR OF PHILOSOPHY

in

Developmental Biology

in the

GRADUATE DIVISION

of the

UNIVERSITY OF CALIFORNIA, SAN FRANCISCO

Dedication and Acknowledgements

This PhD has been a team effort. I could not have made it to the finish line without the support of my labmates, family, and friends.

The work in Chapter 2 was done in collaboration with Francesc Garcia-Gonzalo, Rachel Bowie, Chunmei Li, Julie Kennedy, Oliver Blacque, and Michel R. Leroux, and will be submitted as a manuscript shortly. Thank you for all your hard work.

I would like to thank the members of the Ashrafi lab for adopting me into their lab to work on the worm part of the project. I'd especially like to thank Brian Lee and Jason Liu for teaching me all about worms.

I am most grateful to all the members of the Reiter lab who have been there with me day by day. A big thank you goes to Bill Dowdle for teaching me all things mouse, Colin Dinsmore for scientific advice, Nicole Santos for moral support, and Saori Haigo for keeping me on track. I would like to thank Francesc Garcia-Gonzalo in particular for collaborating with me on the genetic interactions project. It has a great experience working with you.

To my classmates Hayley, Theresa, Vanessa, and Anna, it has been a fun, tough journey together. We've made it!

My thesis committee members, Kaveh Ashrafi, Pat O'Farrell and David Agard have provided thoughtful suggestions for my projects. Thank you for your feedback and advice.

Finally, I am most indebted to my advisor, Jeremy Reiter. Thank you for your sincere enthusiasm for science, for challenging me, and for your guidance.

This is dedicated to SBL, RKY, and CBS.

Conservation and Divergence of Genetic Interactions and Functions Regulating Cilia and Embryogenesis

Laura Yee

Abstract

Ciliopathies, diseases that arise from defective ciliary function, afflict many tissues to various degrees. However the genetic basis underlying the range of phenotypes is unclear. Two protein complexes at the ciliary transition zone are linked to the ciliopathies Meckel syndrome (MKS) and nephronophthisis (NPHP); the BBSome is a third complex linked to Bardet-Biedl syndrome. To model the complex inheritance of ciliopathies, we made double mutants between MKS, NPHP, and BBS genes, focusing on *tctn-1*, the *C. elegans* ortholog of the Tectonic family of ciliopathy genes. Loss of TCTN-1 or TCTN-1 and an MKS complex component does not disrupt ciliary structure. In contrast, loss of TCTN-1 and an NPHP complex component disrupts ciliary structure, as does loss of an NPHP and a BBS complex component. Thus, the MKS, NPHP and BBS complexes have overlapping ciliogenic functions in *C. elegans*. Similar genetic interactions that modify ciliopathy phenotypes are conserved in mammals, as mice mutant for both an MKS family gene and an NPHP family gene display exacerbated phenotypes compared to single mutants. *Tctn1* and *Bbs1* also show a synthetic genetic interaction in mammals. Together, our data support the hypothesis that multiple mutations within an individual organism may explain the expressivity observed in ciliopathy patients.

In addition, we investigated the role of *Odr4* in mammals, a gene that is required for the localization of GPCRs to cilia in *C. elegans.* Preliminary studies demonstrate that *Odr4* is required for embryonic development and binds to the Ufm1-specific protease, UfSP2.

Table of Contents

List of Tables

List of Figures

Chapter 1: Introduction

Primary cilia serve as the cell's antenna, projecting from surface of most cells and sensing both intercellular and environmental cues. These cellular antennas are composed of a precise set of proteins that enable them to carry out specialized functions, including regulating embryonic development, kidney function, vision, and olfaction (1, 2). As such, human disorders caused by ciliary dysfunction can affect several different tissues to varying degrees, and are collectively known as ciliopathies.

Ciliopathies, including Meckel syndrome (MKS), nephronophthisis (NPHP), and Bardet-Biedl syndrome (BBSome) represent an array of diseases that range from mild to severe. Clinical manifestations of ciliopathies such as retinal degeneration, kidney disease, neural tube malformations, and obesity are often overlapping, and even mutations in the same gene can result in multiple phenotypes (3, 4). Thus the genetic basis behind ciliopathies is poorly understood.

C. elegans has been an invaluable model in which to study cilia and ciliopathy genes. The *C. elegans* genome contains orthologs for genes associated with MKS and NPHP, and orthologs for nearly all the BBSome genes. Unlike in mammals, cilia are present only at the tip of sensory neuron dendrites, and thus are restricted to sensory roles in *C. elegans*. Twelve bilateral sets of amhpid neurons in the head and two sets of phasmid neurons in the tail are primarily responsible chemosensation. Each class of amphid neurons expresses a specific set of GPCR receptors and thus is responsible for sensing a corresponding set of odorants (5, 6). In particular, the receptor ODR-10 localizes to the cilia of AWA neurons, and binds the odorant diacetyl (7).

Although the *C. elegans* system provides genetic and molecular means to study ciliary defects, nematodes do not recapitulate the phenotypes observed in human ciliopathy patients. Thus mouse models of ciliary dysfunction have been instrumental in furthering the understanding of ciliopathies. Mutations in genes that completely ablate cilia have revealed that cilia are required for embryonic development: cilia play an essential role in transducing the Shh signaling pathway during neural tube development and patterning of the limb bud (1, 8). As genes mutated in ciliopathies have been identified, mice strains baring these mutations have emerged as disease models. Conversely, gene mutations originating in mice that affect cilia have subsequently been identified in human ciliopathy patients (9-11).

Using the power of *C. elegans* genetic combined with the phenotypic relevance of mice to human disease, we have studied gene combinations affecting cilia and embryogenesis. We have attempted to dissect the basis of phenotypic variation seen in human ciliopathy patients by creating double mutants of ciliopathy genes in *C. elegans* and mice. Additionally, we tested whether the gene require for ODR-10 localization to cilia in *C. elegans* performed a similar function in mammals.

Chapter 2: Conserved genetic interactions between MKS, NPHP, and BBS ciliopathy complexes cooperatively support ciliogenesis

Abstract

Mutations in genes encoding cilia proteins cause human ciliopathies, diverse disorders affecting many tissues. Individual genes can be linked to ciliopathies with dramatically different phenotypes, suggesting that genetic modifiers may participate in their pathogenesis. The ciliary transition zone contains two protein complexes affected in the ciliopathies Meckel syndrome (MKS) and nephronophthisis (NPHP). The BBSome is a third protein complex, affected in the ciliopathy Bardet-Biedl syndrome (BBS). We tested whether mutations in MKS, NPHP and BBS complex genes modify the phenotypic consequences of one another in both *C. elegans* and mice. We identified TCTN-1, the *C. elegans* ortholog of vertebrate MKS complex components called Tectonics, as a transition zone protein. Neither disruption of TCTN-1 alone or together with MKS complex components abrogated ciliary structure in *C. elegans*. In contrast, disruption of TCTN-1 together with either of two NPHP complex components, NPHP-1 or NPHP-4, compromised ciliary structure. Similarly, disruption of an NPHP complex component and the BBS complex component BBS-5 individually did not compromise ciliary structure, but together did. As in nematodes, disrupting two components of the mouse MKS complex did not cause additive phenotypes compared to single mutants. However, disrupting both Tctn1 and either Nphp1 or Nphp4 exacerbated defects in ciliogenesis and cilia-associated developmental events, as did disrupting both Tctn1 and the BBSome component Bbs1. This study demonstrates that ciliary complexes act in parallel to support ciliary function, suggesting that different human ciliopathy phenotypes could arise from genetic interactions between distinct biochemical complexes.

Introduction

Despite accelerating success in identifying genetic variations, the relationship between genotype and phenotype in humans often remains obscure. Even for many Mendelian diseases, the expressivity of disease alleles is not always predictable, indicating that additional genetic and epigenetic influences modify the disease-causing mutations. The genetic influences could include many common genetic variants with small effects, rare variants with large effects, and allele-specific gene-gene interactions. In turn, the phenotypic outcome of these genetic interactions can be affected by synergistic changes in gene expression, protein interactions, or compromise of overlapping functions (12-15).

Ciliopathies, which arise from disrupted ciliary function, are prominent examples of disorders with complex inheritance. The clinical manifestations of ciliopathies are often variable and overlapping. For example, Meckel syndrome (MKS) is characterized by cystic kidney dysplasia, polydactyly, and occipital meningoencephalocoele. Nephronophthisis (NPHP), the most common genetic cause of renal failure in children, is characterized by cystic kidney dysplasia without limb or brain malformations. Bardet-Biedl syndrome **(**BBS), a disorder associated with at least nineteen loci, is characterized by cystic kidney dysplasia, polydactyly, retinal degeneration, obesity, and learning difficulties. Although BBS has been traditionally considered an autosomal recessive disorder affecting a single locus, in some instances three mutations in two loci are required to cause disease (16-20). Thus, mutations in two loci can be required for a ciliopathy to be penetrant.

As reflected by the broad spectrum of ciliopathy-associated phenotypes, primary cilia play numerous, often tissue-specific, roles in mammals. For example, cilia sense odorants and light, control growth in the kidney, and transduce the Hedgehog (Hh) signaling pathway, thereby

playing integral functions in embryonic development and adult tissue homeostasis (1). To transduce signals, cilia maintain compositions distinct from those of other cellular compartments. How cilia exclude some proteins while allowing others access remains a fundamental question (21). Previous work has suggested that the transition zone, a region at the base of the cilium between the basal body and the axoneme proper, may be involved in this process (22, 23). The transition zone is defined ultrastructurally by the presence of Y-links that connect the microtubule core to the ciliary membrane (24, 25). In mice, the proteins Tctn1, Tctn2, Tmem231, Tmem67, Mks1, B9d1, B9d2, Cep290 and Cc2d2a co-localize to the transition zone and form a large biochemical complex, the MKS complex (26-28). A biochemically distinct complex that includes Nphp1 and Nphp4, termed the NPHP complex, also localizes to the transition zone (29).

Mammals possess cilia on many cell types, whereas *C. elegans* cilia are confined to the dendritic tips of 60 select sensory neurons in hermaphrodites. As in mammals, the *C. elegans* orthologs of the MKS complex genes, *tmem-231, mks-1*, *mksr-1* (the ortholog of *B9d1*), *mksr-2* (the ortholog of *B9d2*), *mks-3* (the ortholog of *Tmem67*), and *mks-6* (the ortholog of *Cc2d2a*), as well as the orthologs of the NPHP complex genes *nphp-1* and *nphp-4,* encode transition zone proteins (23, 30-35). Individual loss of function of these genes does not dramatically compromise *C. elegans* ciliary structure (33). However, loss of function of one of several MKS complex genes when combined with loss of function of either *nphp-1* or *nphp-4* synergistically compromises ciliary structure in *C. elegans* (31-33).

Like MKS and NPHP complex proteins, many proteins associated with BBS form a large complex, the BBSome (36). The BBSome functions as a vesicular coat that transports select GPCRs to the cilium through an association with intraflagellar transport (IFT) machinery (37, 38). In contrast to MKS or NPHP components, abrogating the function of individual BBS components

in *C. elegans* disrupts ciliary structure (39). Whether the BBSome works together with the transition zone is unknown. However, mutation in *MKS1* can cause BBS, and mutation in *BBS4* can modify the ciliopathy phenotypes of *Cep290*, suggesting that the BBSome and transition zone may share some functions (40, 41).

We hypothesized that genetic interactions between MKS, NPHP, and BBS complex genes could contribute to the wide phenotypic spectrum observed in human ciliopathies. To test this hypothesis, we generated animals with intra- and inter-complex double mutations, with an emphasis on the ciliopathy gene *Tectonic1* (*Tctn1*). We previously found that Tctn1 is an essential component of the transition zone required for cilium-dependent Hh signaling in mice (26, 42). Here, we identify the *C. elegans* ortholog of *Tctn1*, *tctn-1*, and find that it also encodes a transition zone protein. Loss of TCTN-1 does not disrupt *C. elegans* ciliary structure, similar to other transition zone genes. *tctn-1* genetically interacts with *nphp-4* and *nphp-1*, but not with the MKS complex genes *mks-1*, *mksr-1*, *mksr-2* and *mks-3*, thereby genetically placing *tctn-1* within the MKS module. These genetic interactions in nematodes predicted mammalian genetic interactions, as combining mouse *Tctn1* and *Nphp4* mutations also resulted in synthetic ciliary phenotypes. Additional double mutations between one gene of the MKS complex and one gene of the NPHP complex yielded similar synthetic effects, suggesting that the genetic interactions between MKS and NPHP complex components may pertain to many members. In contrast, double mouse mutations between genes within the same family did not show such an interaction, consistent with findings in *C. elegans*. Furthermore, both *C. elegans* and mammals exhibited a genetic synergy between mutations affecting the transition zone and the BBSome, indicating that the MKS, NPHP, and BBS complexes share overlapping functions in ciliogenesis. Hence, mutations affecting distinct ciliopathy protein complexes synthetically interact to modify ciliary phenotypes.

Results

C.elegans Tectonic is a transition zone component

By sequence homology, we identified a single *C. elegans* ortholog of the three vertebrate *Tectonic* genes, *E04A4.6,* which we refer to as *tctn-1*. Mammalian Tectonics possess a signal peptide and a domain of unknown function (DUF1619) characteristic of the family. *C. elegans tctn-1* also possesses a signal peptide and is most homologous to other Tectonics in the C-terminal region (Supplementary Fig. 1). In nematodes, ciliary genes often contain a conserved X-box sequence that acts as a binding site for the ciliogenic RFX transcription factor, DAF-19 (43, 44). Consistent with a ciliary function, *tctn-1* has a predicted X-box sequence (Fig. 1A), is strongly downregulated in *daf-19* mutants, and is preferentially expressed in ciliated sensory neurons (45-47). For these reasons, we surmised that *tctn-1* was likely to have a ciliary function in *C. elegans*.

To investigate whether nematode TCTN-1 localizes to cilia, we generated a strain that expresses a carboxy-terminal GFP-tagged version of TCTN-1 under a *bbs-8* promoter active in ciliated cells (48). To visualize cilia, we marked basal bodies and axonemes with a tdTomato-tagged ciliary dynein light intermediate chain, XBX-1. TCTN-1-GFP was enriched specifically at the transition zone of cilia, immediately distal to the basal body and proximal to the axoneme (Fig. 1B).

tctn-1 genetically interacts with NPHP complex genes, but not MKS complex genes

To investigate the function of TCTN-1, we obtained the *E04A4.6*(*ok3021*) mutant from the *C. elegans* Gene Knockout Consortium. The *ok3021* allele contains a 515 base pair deletion spanning exons three and four of *tctn-1*, and generates a premature stop codon (Fig. 1A),

resulting in a truncated protein predicted to consist of the first 194 amino acid residues, as compared to wild type which is predicted to consist of 466 residues. Thus, the *ok3021* allele is likely to disrupt the function of *tctn-1*.

Homozygous *tctn-1* mutants exhibited no alteration of growth, size, egg laying, brood size, or cilium-associated sensory behaviors (osmotic avoidance or chemotaxis to diacetyl or butanone) (Supplementary Fig. 2). Additionally, the sensory neurons of *tctn-1* mutants were indistinguishable from those of the wild type N2 reference strain in their ability to take up the hydrophobic dye, DiI. This dye filling assay is a simple method of testing the structural integrity of cilia on six head (amphid) neurons and two tail (phasmid) neurons (49), and suggests that ciliary structure is not grossly compromised in the absence of TCTN-1 (Fig. 2A-C). Other *C. elegans* transition zone mutants such as *nphp-1*, *nphp-4*, *mks-1*, *mksr-1*, *mksr-2*, and *mks-3* mutants, similarly possess largely normal ciliary structure (Fig. 2A-C) (31, 32, 34).

Previous studies have found that a mutation in either of the *C. elegans* homologs of the NPHP complex components *nphp-1* or *nphp-4,* combined with a mutation in an MKS complex gene, synergistically disrupts ciliary structure and consequently causes defects in dye filling of ciliated neurons (31-33). To test whether *tctn-1* functions as an MKS complex or NPHP complex gene, we generated double mutants between *tctn-1* and MKS complex genes or NPHP complex genes. Double mutations affecting *tctn-1* and any of four MKS complex genes (*tctn-1; mks-1, tctn-1; mksr-1, tctn-1; mksr-2, and tctn-1; mks-3*) did not alter dye filling, similar to *tctn-1* single mutants (Fig. 2A, B).

In contrast, dye filling in *tctn-1; nphp-4* double mutant sensory neurons was dramatically disrupted compared to *tctn-1* or *nphp-4* single mutants (Fig. 2A, C). In *tctn-1; nphp-4* double mutants only a few or no amphid neurons were able to dye fill, resulting in decreased fluorescence relative to either single mutant (Fig. 2A, C). Therefore, *tctn-1* synergistically disrupts ciliary structure when combined with NPHP but not MKS complex mutations, genetically placing *tctn-1* within the MKS complex.

TCTN-1 and NPHP-4 have overlapping function in supporting ciliary structure

The inability of the sensory neurons of *tctn-1; nphp-4* mutants to dye fill suggested that their ciliary structure or morphology was defective. *tctn-1; nphp-4* phasmid cilia, visualized by expressing the fluorescently tagged ciliary protein XBX-1::tdTomato, were shorter than cilia of wild type or either single mutant (Supplementary Fig. 3A, B). Additionally, many *tctn-1; nphp-4* cilia were mispositioned; for example, they were frequently abnormally close to the cell body at the ends of short dendrites, or not projecting posteriorly (Supplementary Fig. 3C, D)**.** These perturbations in ciliary position are similar to those caused by concurrent loss of NPHP-4 and other MKS complex components (31, 33).

To gain further insight into how TCTN-1 and NPHP-4 cooperatively support ciliogenesis, we examined the amphid channel cilia of *tctn-1* and *nphp-4* single mutants, and *tctn-1; nphp-4* double mutants using transmission electron microscopy. In *tctn-1* single mutants, the ten cilia of both amphid channel pores were indistinguishable from wild type. Notably, the ciliary transition zones of *tctn-1* mutants contained intact Y-links and exhibited no overt abnormalities, suggesting that TCTN-1 is not an essential structural component of the transition zone (Fig. 2D). In contrast, *nphp-4* single mutants displayed cilia with moderate ultrastructural defects. In addition to the modest shortening of 1-3 axonemes in one amphid pore (the other pore is normal) and the increased occurrence of open B-tubules in the middle segment previously

described (23, 30-35), some *nphp-4* mutants exhibited a small accumulation of vesicles in the periciliary membrane compartment (PCMC) (Fig. 2D). We also detected defects in the transition zone of *nphp-4* mutants (Lambacher *et al.*, manuscript in revision). Y-links, the structural hallmark of the transition zone, were frequently reduced in number and appeared less electron dense in *nphp-4* mutants. Despite the reduction in Y-links, the ciliary membrane remained closely opposed to the axoneme in most *nphp-4* transition zones. The only exceptions were the transition zones of the biciliated ADF and ADL neurons; in *nphp-4* mutants, these transition zones were frequently fully disconnected from the ciliary membrane and positioned ectopically in the distal dendrite region (Fig. 2D).

The ciliary structure of *tctn-1; nphp-4* double mutants was more severely disrupted than that of *nphp-4* single mutants. In *tctn-1; nphp-4* mutants, at least 3-4 axonemes were missing in the middle and distal regions of both amphid pores, and remaining axonemes frequently possessed fewer microtubule doublets (Fig. 2D). Additionally, *tctn-1; nphp-4* mutant cilia displayed defects in Y-links at the transition zone similar to *nphp-4* mutants: Y-links were either thinner than wild type or missing, and in some cases, transition zone microtubules were completely disconnected from the ciliary membrane (Fig. 2D). An accumulation of membranes and vesicles was also observed in the PCMC of *tctn-1; nphp-4* mutants. In contrast, *tctn-1; mks-3* double mutants displayed no abnormalities in ciliary ultrastructure (Supplementary Fig. 3E), consistent with the lack of genetic interaction between *tctn-1* and other MKS complex components. Taken together, we conclude that ciliary structure is dependent on the overlapping functions of TCTN-1 and NPHP-4.

TCTN-1 contributes to ciliary gate function, but not to transition zone protein composition

We hypothesized that disruption of Y-links in *nphp-4* single mutants and *tctn-1; nphp-4* double mutants could reflect an abnormal composition of the transition zone. Using established

markers of the ciliary base and axoneme, we assessed the localization of several fluorescently tagged transition zone proteins. MKSR-1, MKS-5, MKS-6 and NPHP-4 all localized to the transition zone of *tctn-1* mutants in a manner indistinguishable from wild type (Fig. 3A-D). Similarly, despite the reduction in Y-links identified in *nphp-4* and *tctn-1; nphp-4* mutants, MKSR-1, MKS-6 and NPHP-4 localized to the transition zone of these mutants equivalently to wild type (Fig. 3A, C, D). MKS-5 also localized to the transition zone of *nphp-4* and *tctn-1; nphp-4* mutants, although it partially mislocalized distally along the ciliary axoneme (Fig. 3B).

The transition zone is proposed to function as a ciliary gate, controlling which proteins enter the cilium and which proteins are excluded (33, 50). The small GTPase, ARL-13 and its ortholog Arl13b localize to cilia in *C. elegans* and vertebrates, respectively (51, 52). To test if *C. elegans* TCTN-1 regulates the localization of ARL-13, we examined a fusion of ARL-13 and GFP. As in wild type animals, in *tctn-1* single and *tctn-1; nphp-4* double mutants, ARL-13::GFP localized along the length of the axoneme, indicating that TCTN-1 is not required for ARL-13::GFP to enter, or to be retained within the cilium (Fig. 3E).

We tested whether TCTN-1 participated in the complementary function of the ciliary gate, excluding non-ciliary proteins from the cilium, by examining the localization of a fluorescently tagged protein, TRAM-1a::tdTomato, which is normally excluded from the cilium (33). In wild type animals, TRAM-1a::tdTomato was confined to a ring of periciliary membrane at the distal end of the dendrite; it was never observed in the ciliary axoneme. In contrast, TRAM-1a::tdTomato was present within the cilia of *tctn-1* mutants (Fig. 3F). Together, these findings indicate that TCTN-1 is not essential for MKS or NPHP protein complex localization to the transition zone, nor for the ciliary localization of ARL-13::GFP, but is required to prevent a non-ciliary protein from entering the cilium.

The NPHP complex and BBS-5 have overlapping functions in *C. elegans* ciliogenesis

The genetic interaction between *tctn-1* and NPHP complex genes strengthens previous indications that the MKS and NPHP complexes perform overlapping functions within the transition zone (31-33, 53). We investigated whether a biochemical complex that does not localize to the transition zone, the IFT-associated BBSome complex, could also have overlapping functions with transition zone complexes. Core BBSome components, BBS-1, BBS-2, BBS-4, BBS-5, BBS-7, BBS-8, and BBS-9 are conserved in *C. elegans*. Except for *bbs-5* mutants, neurons of *C. elegans* BBS mutants do not dye fill, thus precluding the use of dye filling to analyze synthetic interactions with most BBS genes (54). Although the *bbs-5(gk507)* allele contains a 680 bp deletion spanning the first two exons of the *bbs-5* gene, neurons of homozygous *bbs-5(gk507)* mutants do show dye filling, suggesting that this allele is hypomorphic or that BBS-5 is more dispensable for BBSome function than other components. To test for genetic interactions between *bbs-5* and transition zone genes, we examined dye filling in double mutants for *bbs-5* and MKS complex genes or NPHP complex genes. *bbs-5; tctn-1* and *bbs-5; mksr-1* double mutants dye filled to the same extent as their single mutant counterparts, revealing no genetic interaction between *bbs-5* and MKS complex genes (Fig 4A, B). In contrast, dye filling in *bbs-5; nphp-4* and *bbs-5; nphp-1* double mutants was dramatically decreased compared to their respective single mutants (Fig. 4A, B). Therefore, BBS-5 and NPHP complex components have overlapping functions in supporting *C. elegans* ciliary integrity. The finding that *bbs-5* synthetically interacts with NPHP genes but not MKS genes further suggests that the NPHP and MKS complexes perform distinct roles.

To further investigate the interaction between *bbs-5* and NPHP genes, we examined *bbs-5; nphp-4* double mutant cilia by transmission electron microscopy. As predicted by the dye filling assay, *bbs-5* mutants showed normal amphid channel cilium ultrastructure, with a full

complement of ten axonemes extending through the length of each pore (Fig. 4C). Moreover, the transition zones of *bbs-5* mutants contained Y-links, and the ciliary membrane and microtubule core were indistinguishable from wild type (Fig. 4C).

bbs-5; nphp-4 double mutant cilia displayed more pronounced ultrastructural defects than *bbs-5* or *nphp-4* single mutants. Similar to *nphp-4* cilia, *bbs-5; nphp-4* cilia possessed open B-tubules, a reduction in Y-links and vesicle accumulation in some PCMCs (Fig. 4C). However, in contrast to the single mutants, *bbs-5; nphp-4* double mutants were missing 3-4 axonemes in the distal region and one axoneme in the middle region of both amphid pores (Fig. 4C). Thus, BBS-5 has overlapping functions with the NPHP complex in maintaining ciliary axonemal structure.

Murine MKS and NPHP complexes have overlapping functions in limb development

Mutations in human *NPHP4* cause nephronophthisis, either with or without retinal degeneration (26, 55, 56). To test whether the genetic interactions detected in *C. elegans* with MKS complex genes could contribute to the expressivity of *NPHP4*, we investigated whether the same genetic interactions occur in mammals. *Nphp4*$^{nmf192/nmf192}$ mutant mice (hereinafter referred to as *Nphp4*$^{n/n}$) are viable, but develop retinal degeneration and have reduced sperm motility (57). Mouse *Tctn1*$^{-/-}$ mutants die during late gestation and exhibit heterotaxia, microphthalmia, and hindlimb polydactyly, phenotypes associated with ciliary malfunction and similar to those exhibited by MKS affected individuals (26, 42). Several other MKS complex mutants, such as *Tctn2*$^{-/-}$ and *Cc2d2a*$^{-/-}$ (also known as *Mks6*), display highly similar phenotypes (26, 29).
To assess potential genetic interactions between the MKS and NPHP complexes in mammals, we generated mice doubly mutant for *Tctn1* and *Nphp4. Tctn1*$^{-/-}$ mutants exhibited single digit polydactyly restricted to the hindlimbs and *Nphp4*$^{n/n}$ mutants had no limb abnormalities. In contrast, *Tctn1*$^{-/-}$ *Nphp4*$^{n/n}$ double mutants exhibited polydactyly in both the forelimb and hindlimb, and had an increased number of digits per limb (Fig. 5A-C, Supplementary Table 1).

In addition, *Tctn1*$^{-/-}$ *Nphp4*$^{n/n}$ double mutants exhibited partially penetrant exencephaly, which was rarely observed in *Tctn1*$^{-/-}$ single mutants and never in *Nphp4*$^{n/n}$ single mutants (Fig. 5D, Supplementary Table 2). Therefore, *Tctn1* and *Nphp4* display a synergistic genetic interaction in mammals, as they do in *C. elegans*.

Like *NPHP4*, human mutations in *NPHP1* are associated with multiple ciliopathies, including nephronophthisis and Joubert syndrome, characterized by cerebellar vermis hypoplasia (58-60). To determine if the genetic interaction between *Tctn1* and *Nphp4* was specific to *Nphp4* or extended to another NPHP complex gene, we generated *Tctn1*$^{-/-}$ *Nphp1*$^{-/-}$ double mutant mice. As with *Tctn1*$^{-/-}$ *Nphp4*$^{n/n}$ double mutants, *Tctn1*$^{-/-}$ *Nphp1*$^{-/-}$ double mutants displayed more severe polydactyly and a higher penetrance of exencephaly as compared to *Tctn1*$^{-/-}$ mutants (Fig. 5A-D, Supplementary Table 1, 2). These results reveal that in both nematodes and mice, *Tctn1* displays a synthetic genetic interaction with both *Nphp1* and *Nphp4*.

To assess whether the interaction of NPHP complex genes with *Tctn1* extended to other MKS complex genes, we generated double mutants affecting *Nphp4* and *Cc2d2a*. In addition to MKS, human *CC2D2A* mutations are associated with Joubert syndrome (61-63). Like *Tctn1*$^{-/-}$ mutants, mouse *Cc2d2a*$^{-/-}$ mutants displayed single digit polydactyly restricted to the hindlimb (26). Similar to *Tctn1*$^{-/-}$ *Nphp4*$^{n/n}$ double mutants, *Cc2d2a*$^{-/-}$ *Nphp4*$^{n/n}$ double mutants displayed polydactyly in the forelimbs unlike either single mutant (Fig. 5A-C, Supplementary Table 1). Therefore, the genetic interaction between the MKS and NPHP complexes extends to multiple genes of both complexes.

As mutations within the MKS complex or within the NPHP complex do not genetically interact when combined in *C. elegans*, we tested whether this principle held true in mice. We generated

Tctn1$^{-/-}$ *Tctn2*$^{-/-}$ double mutant mice and found that they did not phenotypically differ from *Tctn1*$^{-/-}$ or *Tctn2*$^{-/-}$ single mutants (Fig. 5A-C, Supplementary Table 1). Similarly, we generated *Nphp1*$^{-/-}$ *Nphp4*$^{n/n}$ double mutant mice, which grow into adulthood at rates comparable to control littermates (Supplementary Fig. 4A). Thus, at a gross level in both nematodes and mammals, multiple mutations affecting different MKS complex components or multiple mutations affecting different NPHP complex components do not additively disrupt ciliary function. This suggests that the MKS complex and the NPHP complex do not possess residual function in the absence of individual components.

Murine *Tctn1* and *Nphp4* cooperatively support ciliogenesis

The genetic interaction of *Tctn1* and *Nphp4* suggested that the MKS and NPHP complexes have partially overlapping ciliary functions. To investigate how these two complexes participate in ciliary functions, we examined cilia in the forelimb, a tissue phenotypically affected in *Tctn1*$^{-/-}$ *Nphp4*$^{n/n}$ double mutants. Immunostaining revealed that ciliation in *Tctn1*$^{-/-}$ forelimbs was reduced compared to controls (Fig. 6A). *Tctn1*$^{-/-}$ *Nphp4*$^{n/n}$ forelimbs were further depleted of cilia compared to *Tctn1*$^{-/-}$ forelimbs (Fig. 6A). Transmission electron microscopy confirmed the depletion of cilia in the forelimb buds of *Tctn1*$^{-/-}$ *Nphp4*$^{n/n}$ double mutants, which possessed docked basal bodies, but lacked ciliary axonemes (Fig. 6A, B). Therefore, the greater loss of cilia in *Tctn1*$^{-/-}$ *Nphp4*$^{n/n}$ forelimbs likely accounts for the increased polydactyly, as cilia are required for Shh-dependent patterning of the limb buds.

To further investigate how Tctn1 and Nphp4 participate in ciliary functions, we cultured fibroblasts derived from mutant and control limb buds. Limb bud fibroblasts showed similar degrees of ciliation in vitro as they did in vivo (Fig. 6C, D). Although the majority of *Tctn1*$^{-/-}$ *Nphp4*$^{n/n}$ mutant limb fibroblasts lacked cilia, a small percentage of cells remained ciliated. In the ciliated *Tctn1*$^{-/-}$ *Nphp4*$^{n/n}$ mutant cells, we investigated whether ciliary or transition zone

protein composition was disturbed. The small GTPase Arl13b localized to cilia in control and *Nphp4*$^{n/n}$ mutant fibroblasts, but was absent in *Tctn1*$^{-/-}$ and *Tctn1*$^{-/-}$ *Nphp4*$^{n/n}$ mutant cilia (Fig. 6C).

We examined Nphp1, a member of the NPHP complex, which localizes to the transition zone. In control and *Tctn1*$^{-/-}$ mutant fibroblasts, Nphp1 localized to the transition zone, but in *Nphp4*$^{n/n}$ single and *Tctn1*$^{-/-}$ *Nphp4*$^{n/n}$ double mutant fibroblasts, Nphp1 was absent from the transition zone (Fig. 6E). Hence, mouse Nphp4 is required for the localization of Nphp1, as it is in *C. elegans* (34). Therefore, in mice, ciliary localization of Arl13b depends specifically on Tctn1, and not on Nphp4, whereas transition zone localization of Nphp1 depends specifically on Nphp4, and not on Tctn1. Whereas Tctn1 and Nphp4 have overlapping functions in promoting ciliogenesis, they have distinct roles in controlling ciliary protein localization.

Tctn1 and *Bbs1* have overlapping functions in mammalian ciliogenesis

As the genetic interactions between MKS and NPHP complex genes in *C. elegans* were conserved in mouse, we examined genetic interactions between MKS and NPHP complex genes and BBSome genes in mouse to determine if they also were conserved. In *C. elegans*, we observed a synthetic interaction between NPHP complex genes and *bbs-5* as assessed by dye filling (Fig. 4A, B). Because a *Bbs5* mouse model has not been described, we analyzed another BBSome component in mouse, Bbs1. *Bbs1*$^{-/-}$ mutant mice are obese, lack sperm flagella, and develop retinal degeneration, but do not exhibit polydactyly or renal abnormalities as observed in human BBS affected individuals (64). Mouse *Nphp4*$^{n/n}$ *Bbs1*$^{-/-}$ double mutant embryos survived through the end of embryogenesis with no gross abnormalities, similar to each single mutant (Supplementary Fig. 4B). This indicated a lack of strong genetic interaction between *Nphp4* and *Bbs1* affecting embryogenesis. Therefore, the NPHP complex and BBSome have distinct genetic relationships in *C. elegans* and mouse.

Unlike *C. elegans*, in which *tctn-1* and *bbs-5* did not interact, mouse *Tctn1* and *Bbs1* did genetically interact. *Tctn1*$^{-/-}$ *Bbs1*$^{-/-}$ double mutant embryos displayed dramatically increased polydactyly and exencephaly compared to *Tctn1*$^{-/-}$ embryos (Fig. 7A-D, Supplementary Table 3, 4). Thus, a BBSome gene interacts with NPHP genes in *C. elegans*, but not in mouse, whereas a BBSome gene interacts with an MKS gene in mouse, but not in *C. elegans*. BBSome and transition zone complex genes interact in both organisms, but the specific genetic interactions differ between nematodes and mammals, suggesting that some ciliopathy gene interactions are species and/or cell-type specific.

To analyze the cellular basis of the genetic interaction between *Tctn1* and *Bbs1,* we examined the cilia of fibroblasts derived from developing forelimb buds. *Tctn1*$^{-/-}$ *Bbs1*$^{-/-}$ double mutant cells failed to form cilia, as detected by immunostaining for acetylated tubulin or Arl13b (Fig. 7E). However, *Tctn1*$^{-/-}$ *Bbs1*$^{-/-}$ cells still possessed basal bodies, as identified by γ-tubulin staining (Fig. 7E). *Tctn1*$^{-/-}$ *Bbs1*$^{-/-}$ cells were also still able to localize Nphp1 correctly to the transition zone (data not shown), unlike *Nphp4*$^{n/n}$ or *Tctn1*$^{-/-}$ *Nphp4*$^{n/n}$ cells, suggesting that Tctn1 and Bbs1 have overlapping roles essential for mammalian ciliogenesis, but not for some degree of basal body and transition zone formation.

We hypothesized that the dramatic loss of cilia in *Tctn1*$^{-/-}$ *Bbs1*$^{-/-}$ double mutants compared to *Tctn1*$^{-/-}$ single mutants could account for the exacerbated polydactyly in *Tctn1*$^{-/-}$ *Bbs1*$^{-/-}$ embryos, as decreased ciliary function and consequent decreased Gli3 processing results in polydactyly (1). To test this, we measured the mRNA expression levels of the Shh target genes *Gli1* and *Ptch1* in limb bud fibroblasts stimulated with Smo Agonist (SAG). *Tctn1*$^{-/-}$ mutants showed a reduction in *Gli1* and *Ptch1* expression compared to controls, and *Tctn1*$^{-/-}$ *Bbs1*$^{-/-}$ double mutants showed a further reduction in compared to *Tctn1*$^{-/-}$ (Fig. 7F, G). Thus *Tctn1*$^{-/-}$ *Bbs1*$^{-/-}$ double

mutants have an abrogated response to Shh signaling, likely resulting in the exacerbated phenotypes compared to *Tctn1*$^{-/-}$ single mutants.

Figure 1

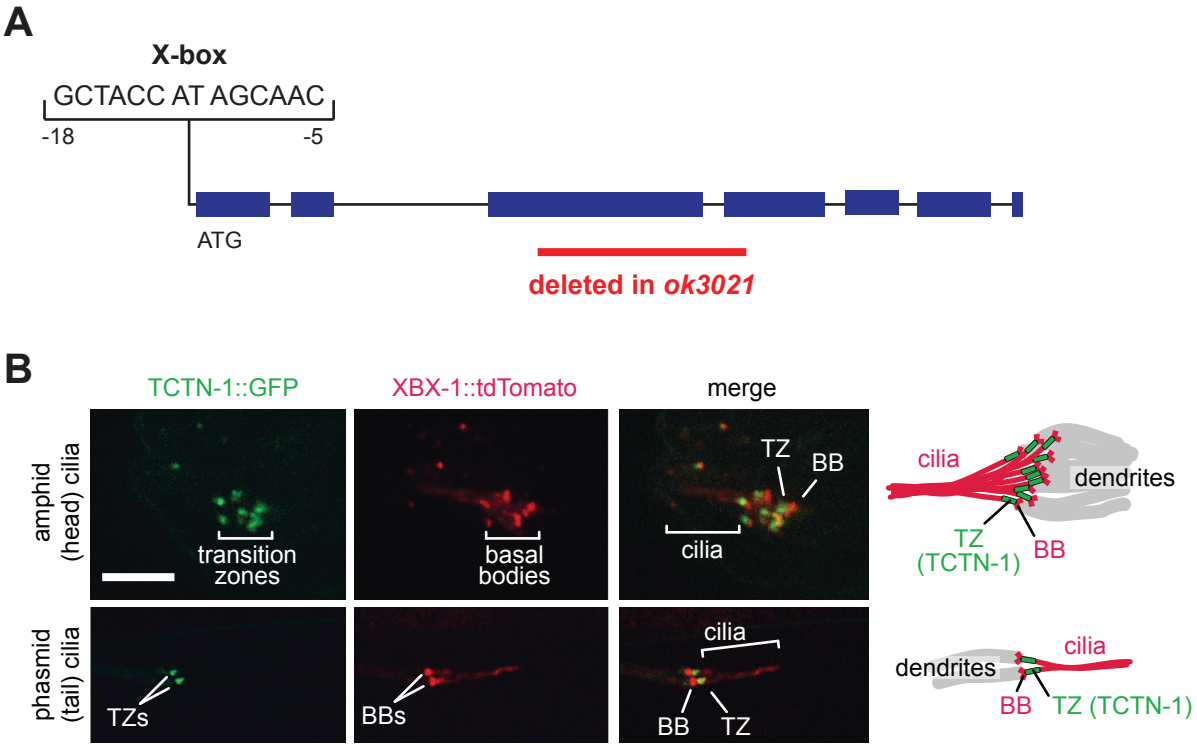
A
X-box
GCTACC AT AGCAAC
-18
-5
ATG
deleted in ok3021
B
TCTN-1::GFP
XBX-1::tdTomato
merge
amphid (head) cilia
transition zones
basal bodies
TZ
BB
cilia
phasmid (tail) cilia
TZs
BBs
cilia
BB
TZ
cilia
dendrites
TZ (TCTN-1)
BB
cilia
dendrites
BB
TZ (TCTN-1)

Figure 1. The *C. elegans* ortholog of Tectonic1 is a transition zone component

(*A*) Schematic of the X-box sequence and *ok3021* allele of *C. elegans tctn-1. (B*) GFP-tagged TCTN-1 localizes specifically to the transition zones (TZs) in head (amphid) and tail (phasmid) cilia of *C. elegans*. Basal bodies (BBs) and ciliary axonemes are marked with tdTomato-tagged XBX-1, a component of the ciliary dynein. Schematics illustrate the position of TCTN-1 at the transition zone with respect to the basal body and axoneme. Scale bar, 5 μm.

Figure 2

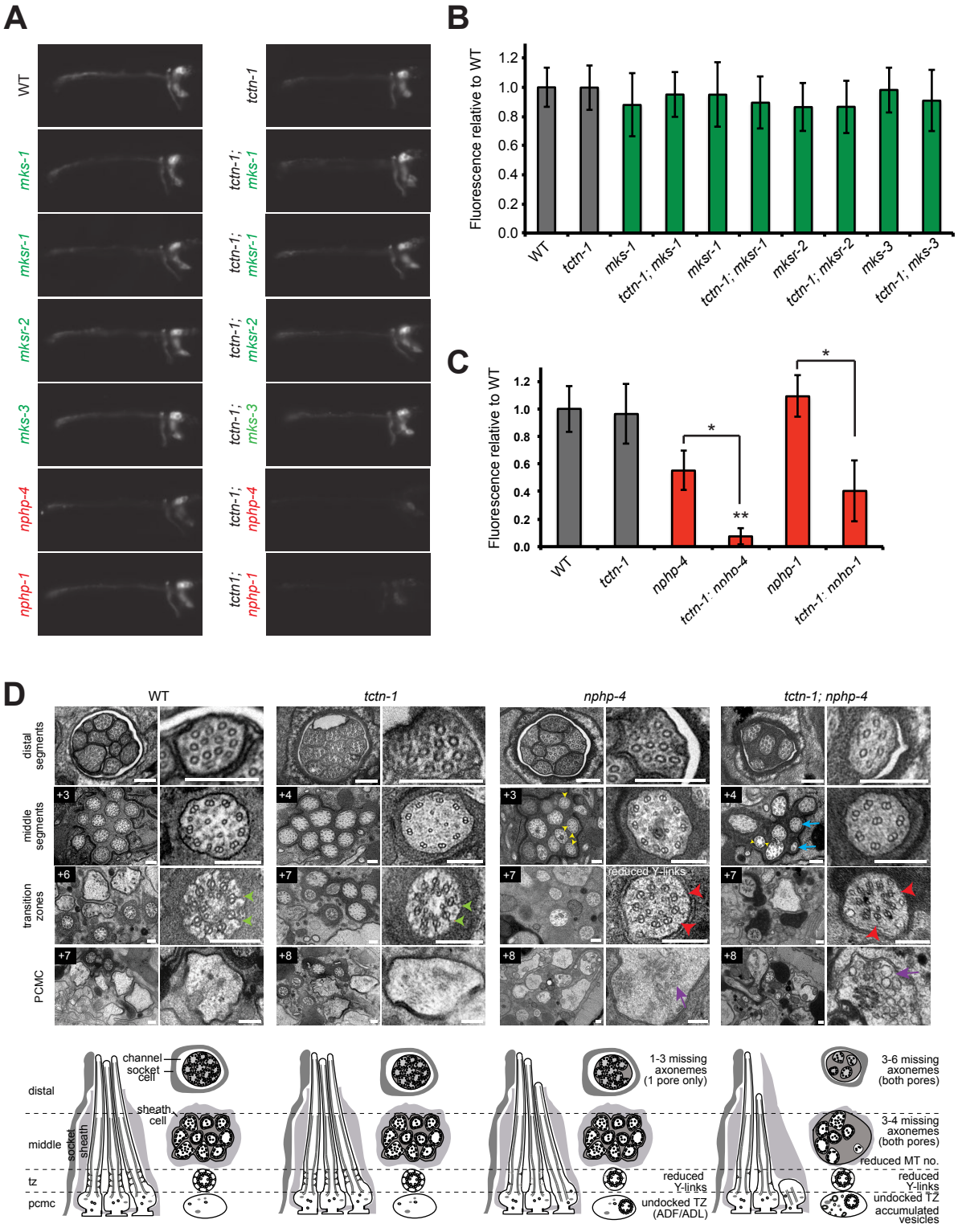
A
WT
mks-1
mksr-1
mksr-2
mks-3
nphp-4
nphp-1
tctn-1
tctn-1; mks-1
tctn-1; mksr-1
tctn-1; mksr-2
tctn-1; mks-3
tctn-1; nphp-4
tctn1; nphp-1
B
Fluorescence relative to WT
1.2
1.0
0.8
0.6
0.4
0.2
0.0
WT
tctn-1
mks-1
tctn-1; mks-1
mksr-1
tctn-1; mksr-1
mksr-2
tctn-1; mksr-2
mks-3
tctn-1; mks-3
C
Fluorescence relative to WT
*
**
*
WT
tctn-1
nphp-4
tctn-1; nphp-4
nphp-1
tctn-1; nphp-1
D
WT
tctn-1
nphp-4
tctn-1; nphp-4
distal segments
middle segments
transition zones
PCMC
+3
+4
+6
+7
+8
reduced Y-links
channel
socket cell
sheath cell
socket
sheath
distal
middle
tz
pcmc
1-3 missing axonemes (1 pore only)
reduced Y-links
undocked TZ (ADF/ADL)
3-6 missing axonemes (both pores)
3-4 missing axonemes (both pores)
reduced MT no.
reduced Y-links
undocked TZ
accumulated vesicles

Figure 2. *C. elegans tctn-1* genetically interacts with NPHP complex genes, but not MKS complex genes to affect ciliary structure

(*A*) Dye filling of amphid neurons in L4 nematodes in the indicated single transition zone mutants (left column) and *tctn-1* double mutants (right column). Lateral views, with anterior to the left. Genotypes including an allele affecting a previously recognized MKS complex component are indicated in green. Genotypes including an allele affecting an NPHP complex component are indicated in red. *(B* and *C)* Fluorescence intensity of DiI filled amphid neurons in single mutants of the MKS complex or NPHP complex, and double mutants with *tctn-1* relative to wild type. Error bars represent the standard deviation. Statistical significance according to unpaired Student's *t*-tests (* $p<0.001$; ** $p<0.001$ compared to *tctn-1*). *(D)* Low and high magnification TEM cross-sections of the distal segment, middle segment, transition zone, and distal dendritic periciliary membrane compartment (PCMC) of amphid cilia with schematics below (lateral and transverse views). Green arrowheads indicate intact Y-links in wild type and *tctn-1* transition zones whereas red arrowheads indicate reduced or missing Y-links, observed in *nphp-4* and *tctn-1; nphp-4* transition zones. Yellow arrowheads indicate open B-tubules and purple arrows indicate vesicle accumulation in the PCMCs of *nphp-4* and *tctn-1; nphp-4* mutants. *tctn-1; nphp-4* mutants display several truncated axonemes and axonemes with fewer microtubule doublets (blue arrows) compared to wild type, *tctn-1* and *nphp-4* mutants. Boxed numbers indicate distance (μM) from the distal tip of the cilium. Scale bars,100 nm.

Figure 3

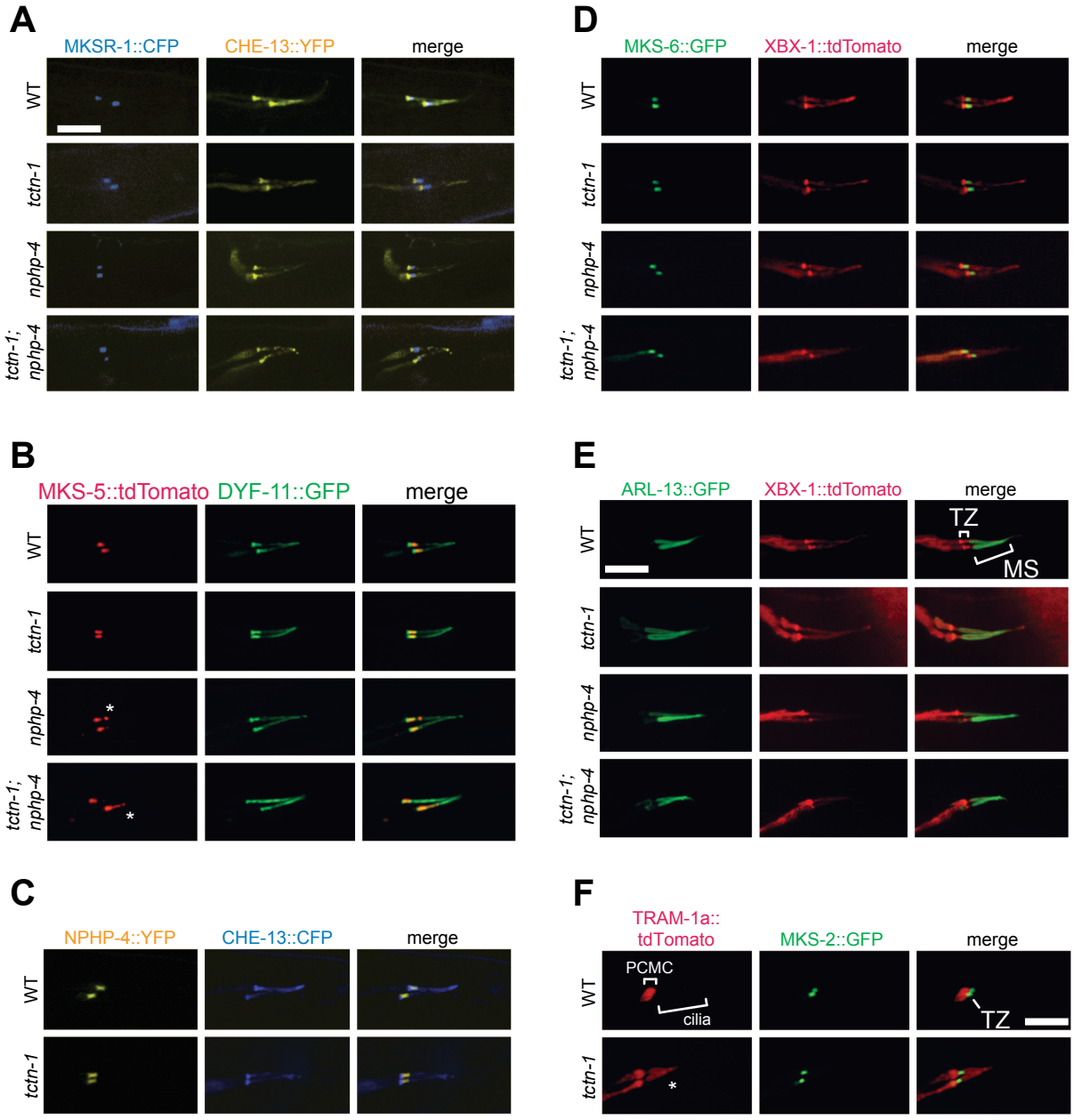
A
MKSR-1::CFP
CHE-13::YFP
merge
WT
tctn-1
nphp-4
tctn-1; nphp-4
D
MKS-6::GFP
XBX-1::tdTomato
merge
WT
tctn-1
nphp-4
tctn-1; nphp-4
B
MKS-5::tdTomato
DYF-11::GFP
merge
WT
tctn-1
nphp-4
tctn-1; nphp-4
E
ARL-13::GFP
XBX-1::tdTomato
merge
TZ
MS
WT
tctn-1
nphp-4
tctn-1; nphp-4
C
NPHP-4::YFP
CHE-13::CFP
merge
WT
tctn-1
F
TRAM-1a:: tdTomato
MKS-2::GFP
merge
PCMC
cilia
TZ
WT
tctn-1

Figure 3. TCTN-1 contributes to maintain ciliary composition in *C. elegans*

(A-D) Localization of different transition zone proteins in phasmid cilia of wild type, *tctn-1*, *nphp-4*, and *tctn-1; nphp-4* mutants. Each GFP, CFP, YFP, or tdTomato-tagged transition zone protein is co-localized with a ciliary marker (CHE-13, DYF-11 or XBX-1), as indicated. Abnormal localization of MKS-5 in the *nphp-4* single and *tctn-1; nphp-4* double mutants is indicated by asterisks. *(E)* ARL-13::GFP localizes to the middle segment (MS) of cilia in wild type, *tctn-1*, *nphp-4*, and *tctn-1; nphp-4* mutants. *(F)* TRAM-1a::tdTomato localizes only to the PCMC in wild type animals, but enters the cilia in *tctn-1* mutants, indicated by asterisks. MKS-2::GFP marks the transition zone. Scale bar, 5 μm.

Figure 4

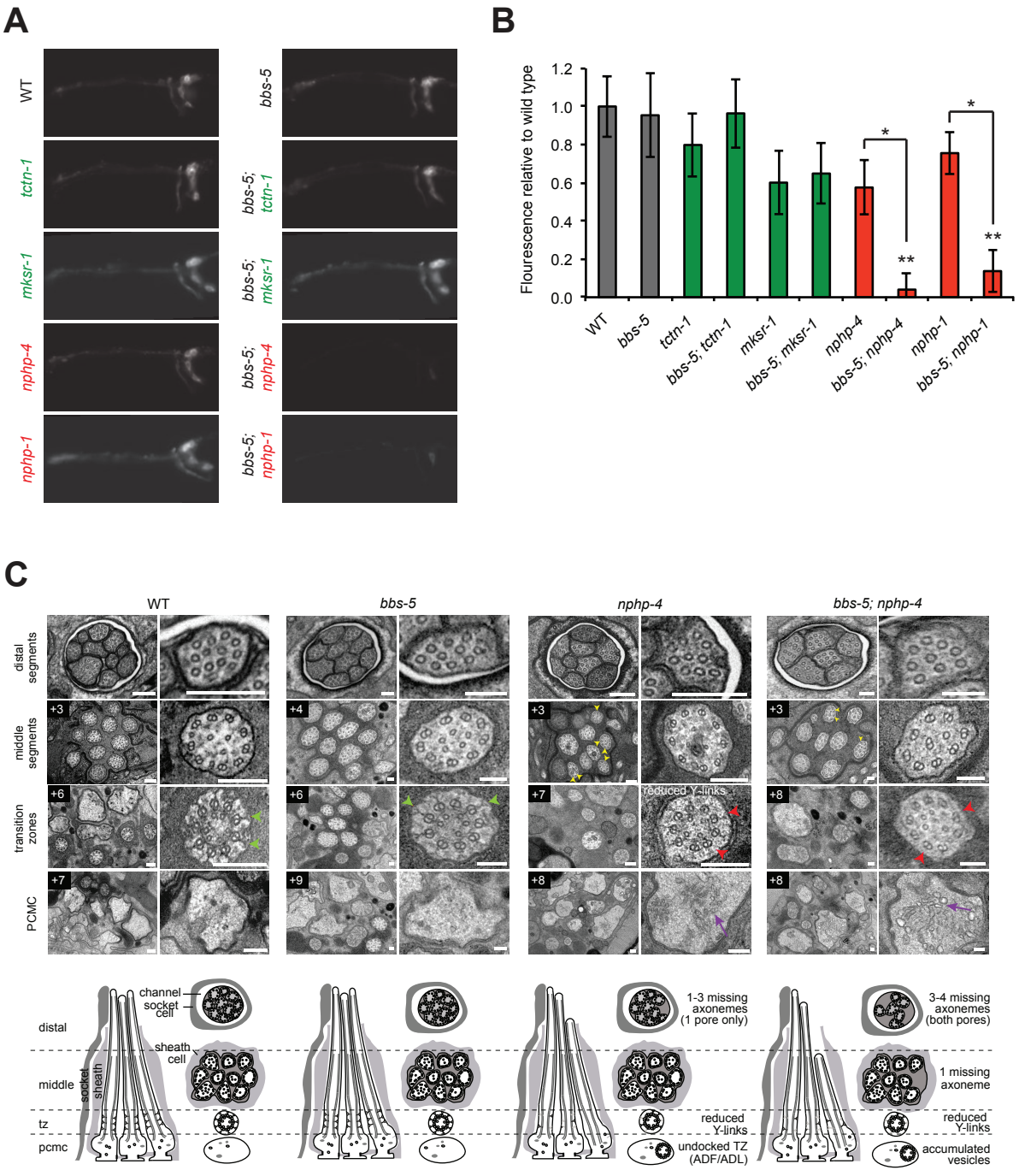
A
WT
tctn-1
mksr-1
nphp-4
nphp-1
bbs-5
bbs-5; tctn-1
bbs-5; mksr-1
bbs-5; nphp-4
bbs-5; nphp-1
B
Flourescence relative to wild type
1.2
1.0
0.8
0.6
0.4
0.2
0.0
*
**
*
**
WT
bbs-5
tctn-1
bbs-5; tctn-1
mksr-1
bbs-5; mksr-1
nphp-4
bbs-5; nphp-4
nphp-1
bbs-5; nphp-1
C
WT
bbs-5
nphp-4
bbs-5; nphp-4
distal segments
middle segments
transition zones
PCMC
+3
+4
+6
+7
+9
+8
reduced Y-links
channel
socket cell
sheath cell
distal
middle
tz
pcmc
socket
sheath
1-3 missing axonemes (1 pore only)
reduced Y-links
undocked TZ (ADF/ADL)
3-4 missing axonemes (both pores)
1 missing axoneme
reduced Y-links
accumulated vesicles

Figure 4. NPHP family genes synthetically interact with *bbs-5* to affect ciliary structure in *C. elegans*

(A) Dye filling of amphid neurons in L4 nematodes in single transition zone mutants (left column) and *bbs-5* double mutants (right column). Lateral views, with anterior to the left. *(B)* Fluorescence intensity of DiI filled amphid neurons relative to wild type. Genotypes including an allele affecting an MKS complex component are indicated in green. Genotypes including an allele affecting an NPHP complex component are indicated in red. Error bars represent the standard deviation. Statistical significance according to unpaired Student's *t*-tests (* $p<0.001$; ** $p<0.001$ compared to *bbs-5*). *(C)* Low and high magnification TEM cross-sections of the distal segment, middle segment, transition zone, and PCMC of amphid cilia with schematics below (lateral and transverse views). *bbs-5* mutants display normal ciliary structures, including intact Y-links (green arrowheads). *bbs-5; nphp-4* mutant cilia display open B-tubules (yellow arrowheads), reduced Y-links (red arrowheads) and vesicle accumulation in the PCMC (purple arrows) similar to *nphp-4* cilia, but have fewer axonemes that fully extend distally in both pores. Boxed numbers indicate distance (μM) from the distal tip of the cilium. Scale bars,100 nm.

Figure 5

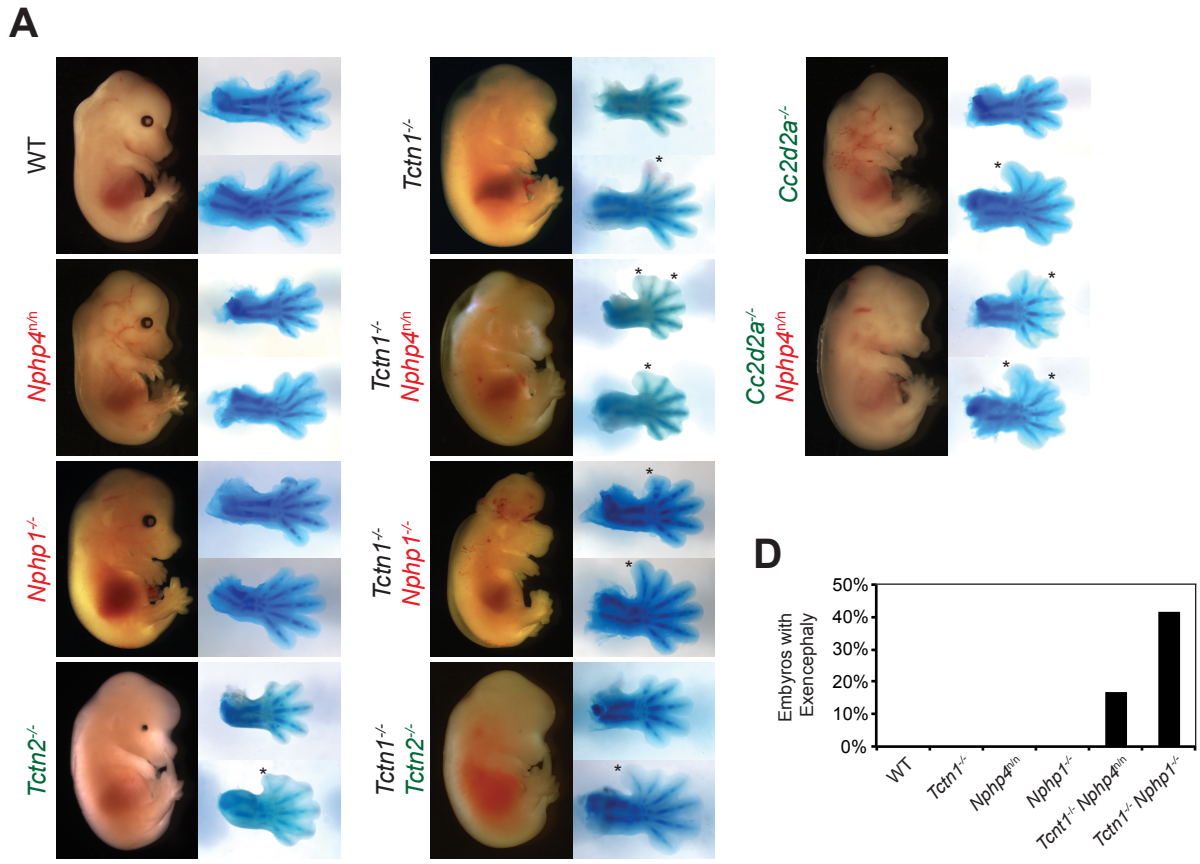
A
WT
Nphp4n/n
Nphp1-/-
Tctn2-/-
Tctn1-/-
Tctn1+/- Nphp4n/n
Tctn1+/- Nphp1-/-
Tctn1-/- Tctn2-/-
Cc2d2a-/-
Cc2d2a-/- Nphp4n/n
D
Embyros with Exencephaly
50%
40%
30%
20%
10%
0%
WT
Tctn1-/-
Nphp4in/in
Nphp1-/-
Tctn1-/- Nphp4in/in
Tctn1-/- Nphp1-/-

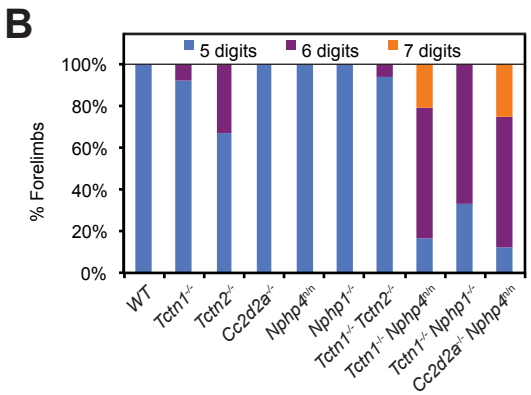
B
5 digits
6 digits
7 digits
% Forelimbs
100%
80%
60%
40%
20%
0%
WT
Tctn1-/-
Tctn2-/-
Cc2d2a-/-
Nphp4in/in
Nphp1-/-
Tctn1-/- Tctn2-/-
Tctn1-/- Nphp4in/in
Tctn1-/- Nphp1-/-
Cc2d2a-/- Nphp4in/in

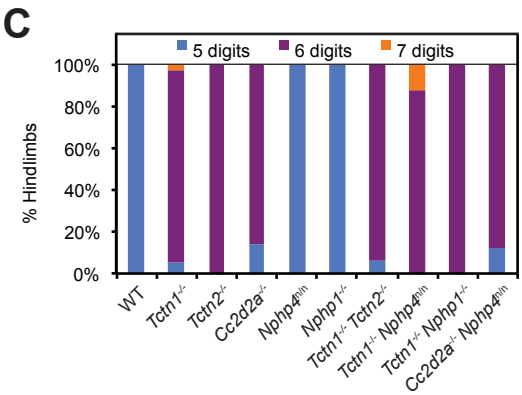
C
5 digits
6 digits
7 digits
% Hindlimbs
100%
80%
60%
40%
20%
0%
WT
Tctn1-/-
Tctn2-/-
Cc2d2a-/-
Nphp4in/in
Nphp1-/-
Tctn1-/- Tctn2-/-
Tctn1-/- Nphp4in/in
Tctn1-/- Nphp1-/-
Cc2d2a-/- Nphp4in/in

Figure 5. Mouse *Tctn1* genetically interacts with NPHP complex genes, but not with MKS complex genes

(A) Lateral views of wild type, single or double mutant mouse embryos of indicated genotype at E14.5. Exencephaly is apparent in the *Tctn1*$^{-/-}$ *Nphp1*$^{-/-}$ double mutant. Corresponding Alcian blue staining of the right forelimb (top) and hindlimb (bottom) are included, with asterisks indicating extra digits. Genes encoding components of the NPHP complex are indicated in red. Genes encoding components of the MKS complex are indicated in green. *(B)* Number of digits in the forelimbs and *(C)* hindlimbs of wild type, single or double mutant embryos of indicated genotypes. *(D)* Incidence of exencephaly in wild type, single or double mutants embryos of indicated genotypes. Numbers of animals analyzed for polydactyly and exencephaly are in Supplementary Tables 1 and 2.

Figure 6

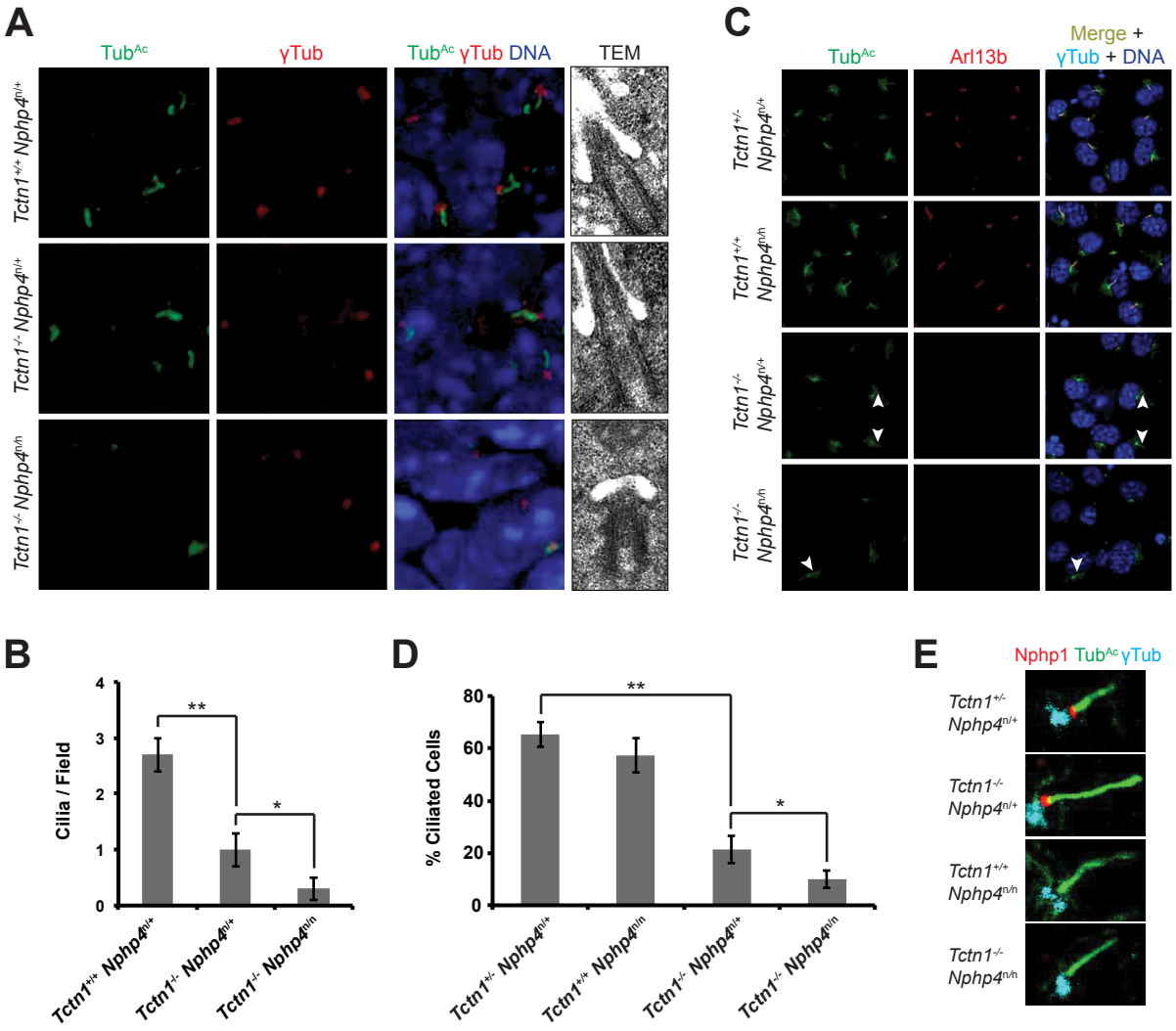
A
TubAc
γTub
TubAc γTub DNA
TEM
Tctn1+/+ Nphp4n/+
Tctn1-/- Nphp4n/+
Tctn1-/- Nphp4n/n
C
TubAc
Arl13b
Merge +
γTub + DNA
Tctn1+/- Nphp4n/+
Tctn1+/+ Nphp4n/n
Tctn1-/- Nphp4n/+
Tctn1-/- Nphp4n/n
B
Cilia / Field
0
1
2
3
4
**
*
Tctn1+/+ Nphp4n/+
Tctn1-/- Nphp4n/+
Tctn1-/- Nphp4n/n
D
% Ciliated Cells
0
20
40
60
80
**
*
Tctn1+/- Nphp4n/+
Tctn1+/+ Nphp4n/n
Tctn1-/- Nphp4n/+
Tctn1-/- Nphp4n/n
E
Nphp1 TubAc γTub
Tctn1+/- Nphp4n/+
Tctn1-/- Nphp4n/+
Tctn1+/+ Nphp4n/n
Tctn1-/- Nphp4n/n

Figure 6. Mouse Tctn1 and Nphp4 have distinct roles in transition zone composition and overlapping roles in ciliogenesis

(A) Limb bud sections (left) from E11.5 embryos were stained for acetylated tubulin (Tub^{Ac}, green) to mark the ciliary axonemes, γ-tubulin (red) to mark the basal bodies and DAPI (blue) to mark nuclei. Transmission electron microscopy (TEM, right) for each genotype. *(B)* Quantification of limb bud cilia in control, *Tctn1*$^{-/-}$ *Nphp4*$^{n/+}$, and *Tctn1*$^{-/-}$ *Nphp4*$^{n/n}$ mutants from TEM fields of view. Error bars represent the standard error of the mean. Statistical significance according to unpaired Student's *t*-tests (* $p<0.05$; ** $p<0.001$). *(C)* Fibroblasts derived from E13.5 embryos limb buds of the indicated genotypes stained for Tub^{Ac} (green), Arl13b (red), γ-tubulin (cyan), and DAPI (blue). White arrowheads indicate cilia in *Tctn1*$^{-/-}$ *Nphp4*$^{n/+}$ and *Tctn1*$^{-/-}$ *Nphp4*$^{-/-}$ mutants. *(D)* Quantification of cilia in cultured limb bud fibroblasts. Error bars represent the standard deviation. Statistical significance according to unpaired Student's *t*-tests (* $p<0.05$; ** $p<0.0001$). *(E)* Immunostaining of limb bud fibroblasts for Nphp1 (red), Tub^{Ac} (green), and γ-tubulin (cyan).

Figure 7

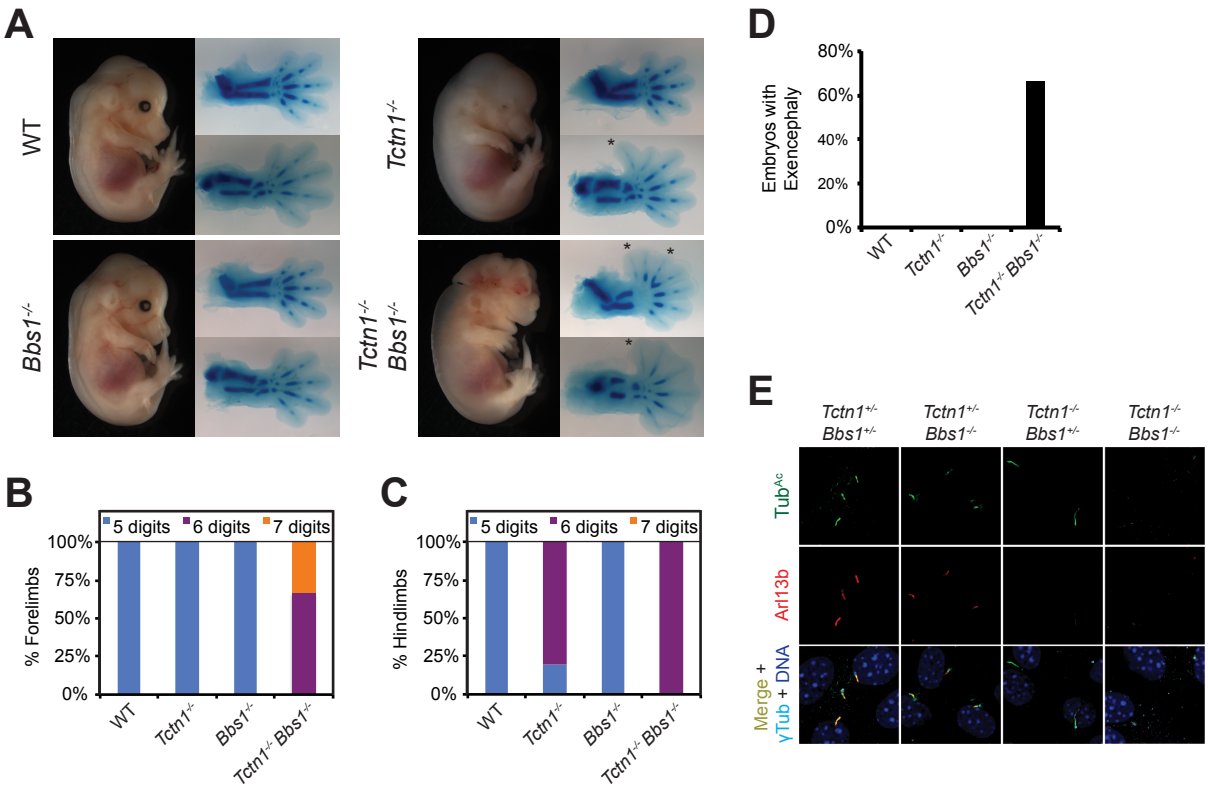
A
WT
Tctn1-/-
Bbs1-/-
Tctn1-/- Bbs1-/-
B
5 digits
6 digits
7 digits
% Forelimbs
100%
75%
50%
25%
0%
WT
Tctn1-/-
Bbs1-/-
Tctn1-/- Bbs1-/-
C
5 digits
6 digits
7 digits
% Hindlimbs
100%
75%
50%
25%
0%
WT
Tctn1-/-
Bbs1-/-
Tctn1-/- Bbs1-/-
D
Embryos with Exencephaly
80%
60%
40%
20%
0%
WT
Tctn1-/-
Bbs1-/-
Tctn1-/- Bbs1-/-
E
Tctn1+/- Bbs1+/-
Tctn1+/- Bbs1-/-
Tctn1-/- Bbs1+/-
Tctn1-/- Bbs1-/-
TubAc
Arl13b
Merge + γTub + DNA

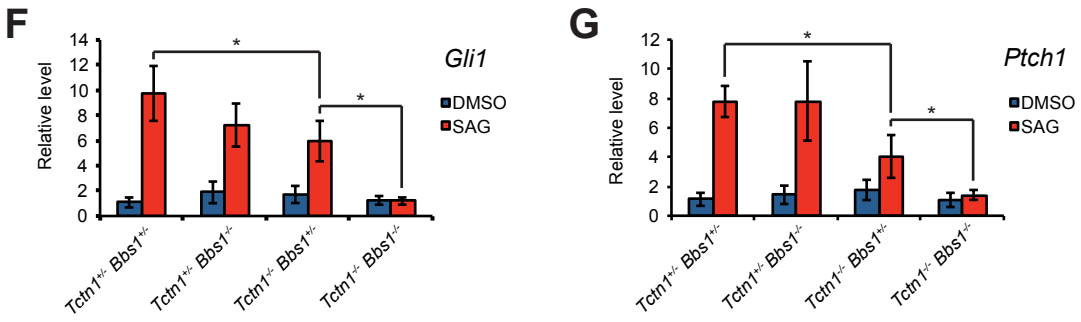
F
Gli1
Relative level
14
12
10
8
6
4
2
0
DMSO
SAG
Tctn1+/- Bbs1+/-
Tctn1+/- Bbs1-/-
Tctn1-/- Bbs1+/-
Tctn1-/- Bbs1-/-
G
Ptch1
Relative level
12
10
8
6
4
2
0
DMSO
SAG
Tctn1+/- Bbs1+/-
Tctn1+/- Bbs1-/-
Tctn1-/- Bbs1+/-
Tctn1-/- Bbs1-/-

Figure 7. Mouse *Tctn1* genetically interacts with *Bbs1*

(A) Lateral views of wild type, *Tctn1*$^{-/-}$, *Bbs1*$^{-/-}$ and *Tctn1*$^{-/-}$ *Bbs1*$^{-/-}$ embryos at E14.5. Exencephaly is apparent in the *Tctn1*$^{-/-}$ *Bbs1*$^{-/-}$ double mutant. Alcian blue staining of the corresponding genotype's forelimb (top) and hindlimb (bottom) are included, with asterisks indicating extra digits. *(B-D)* Number of digits in the *(B)* forelimbs and *(C)* hindlimbs, and *(D)* the incidence of exencephaly for the indicated genotypes. Numbers of animals analyzed for polydactyly and exencephaly are in Supplementary Tables 3 and 4. *(E)* Limb bud fibroblasts of the indicated genotypes immunostained for Tub^{Ac} (green), Arl13b (red), γ-tubulin (cyan), and DAPI (blue). *(F* and *G)* mRNA levels of *Gli1* and *Ptch1* normalized to *β-actin* in forelimb bud cells treated with or without SAG. Error bars represent the standard deviation. Statistical significance according to unpaired Student's *t*-tests (* $p<0.05$).

Figure 8

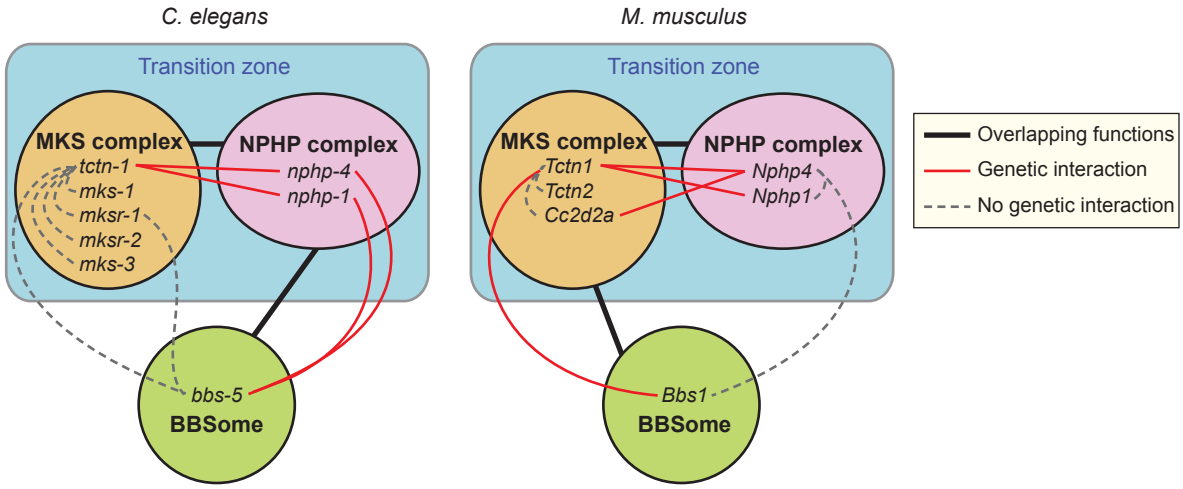
C. elegans
Transition zone
MKS complex
tctn-1
mks-1
mksr-1
mksr-2
mks-3
NPHP complex
nphp-4
nphp-1
bbs-5
BBSome
M. musculus
Transition zone
MKS complex
Tctn1
Tctn2
Cc2d2a
NPHP complex
Nphp4
Nphp1
Bbs1
BBSome
Overlapping functions
Genetic interaction
No genetic interaction

Figure 8. Genetic interactions between transition zone complexes and the BBSome in *C. elegans* and mice

In *C. elegans*, MKS complex genes interact with NPHP complex genes, and BBSome genes interact with NPHP complex genes. In *M. musculus*, MKS complex genes interact with NPHP complex genes and BBSome genes interact with MKS complex genes. Tctn1 behaves as an MKS component in both organisms. Protein complexes that share overlapping functions in ciliogenesis are connected with black lines. Within protein complexes, the specific genes that display a genetic interaction are connected with red lines. Pairs of genes that show no genetic interaction are connected with dashed grey lines.

Discussion

We investigated the genetic interactions between distinct biochemical complexes involved in ciliary function in both nematodes and mammals. We found that TCTN-1, the *C. elegans* ortholog of the mammalian Tectonics, localized to the ciliary transition zone. Loss of *tctn-1* did not abrogate ciliogenesis on its own or in combination with mutations affecting other MKS complex components. However, loss of *tctn-1* in combination with loss of components of the NPHP complex, a biochemically distinct transition zone complex, synergistically abrogated ciliogenesis (Fig. 8). This interaction between MKS and NPHP genes also occurred in mice, which suggests that the overlapping roles for the MKS and NPHP complexes in supporting ciliary structure are evolutionarily conserved. To extend our understanding of how different ciliopathy protein complexes work together, we also analyzed how the BBSome functions with transition zone complexes. The BBSome cooperates with MKS and NPHP complexes, but the specific genetic interactions that support ciliogenesis in *C. elegans* and mice differ (Fig. 8). Thus, we have uncovered evolutionarily conserved functional interactions between three biochemically distinct ciliopathy complexes.

In both mammals and *C. elegans*, MKS and NPHP complex proteins localize to the transition zone, the region at the base of cilia characterized by Y-links. Y-links are hypothesized to be involved in regulating the protein composition of cilia (33, 50). However, *C. elegans nphp-4* and *tctn-1; nphp-4* mutant cilia, which had missing or reduced Y-links, did not have altered protein composition. This suggests that the presence of fully intact Y-links is not, *per se*, a major determinant of ciliary protein composition, although in other instances a more dramatic loss of Y-links correlated with ciliary protein mislocalization (33, 50). More extensive analyses will be required to clarify the composition of Y-links themselves and how Y-link structure and function affect cilia composition.

We have found a genetic interaction between transition zone genes and BBSome genes. Intriguingly, the NPHP complex synergizes with the BBSome in *C. elegans* whereas the MKS complex synergizes with the BBSome in mice (Fig. 8). No interactions were found between the MKS complex and BBSome in *C. elegans* and the NPHP complex and BBSome in mice. However, we cannot exclude the possibly that these interactions may exist, but were undetectable by our methods. For example, functional differences between *bbs-5* and *Bbs1* may account for the different genetic interactions observed in nematodes and mice. Despite these limitations, the specificity of the synergistic interactions between *Bbs1* and *Tctn1* in mice, and between *bbs-5* and *nphp-4* or *nphp-1* in *C. elegans* suggests that the transition zone has altered its relationship to the BBSome through evolution.

How compromising the MKS and NPHP complexes, MKS and BBS complexes in mammals, or NPHP and BBS complexes in nematodes results in synthetic ciliary defects remains unclear. In mammals, Tctn1 is required for the localization of select transition zone proteins and MKS family members are required for the localization of a subset of ciliary membrane proteins (26). Given that the BBSome facilitates the ciliary localization of GPCRs (38), the MKS complex and the BBSome may cooperate in ciliary protein transport such that compromising both BBSome and MKS complex function abrogates this transport sufficiently to disrupt ciliogenesis. Physical interaction between Tctn1 and the BBSome has not been detected, but intriguingly, the MKS complex interactor, Cep290, binds to Bbs4 (26, 41). Furthermore, loss of Bbs4 exacerbates the mislocalization of Rhodopsin in *Cep290* mutant retinas (41), indicating that MKS complex interactors and the BBSome can cooperate to transport proteins to cilia.

As the MKS and NPHP complexes also have overlapping functions in supporting ciliogenesis in mice, the NPHP complex may, like the MKS complex, regulate protein trafficking to cilia. Likewise, in *C. elegans*, in which the NPHP complex genes interact with both MKS and BBS

genes, the NPHP complex may have overlapping functions in regulating ciliary protein composition. In support of this possibility, *C. elegans* NPHP-4 is required for proper ciliary localization of certain IFT proteins and *Chlamydomonas* Nphp4 regulates the entry of a subset of membrane proteins into flagella (23, 65).

As phenotypes reflect gene function, new phenotypes generated by the interaction of multiple mutations can reveal previously unknown functions of the genes involved. On their own, *Nphp4* and *Nphp1* do not play critical roles in limb bud or neural tube development. However, mutation of *Nphp4* or *Nphp1* modifies the *Tctn1*$^{-/-}$ limb and neural tube phenotypes, thereby demonstrating their involvement in the affected tissues. Similarly, human BBS patients have extra digits, yet mouse models of BBS have thus far not displayed polydactyly. Our results demonstrate that mouse *Bbs1* does indeed affect limb patterning, exposed in the context of a *Tctn1*$^{-/-}$ mutation. Therefore, studying genes in combination can reveal roles for those genes that might otherwise be masked by the overlapping function of other genes. By identifying overlapping functions for genes, particularly those from distinct biochemical complexes, we may be able to predict which genes interact and which do not.

Thus far, understanding how human genotypes predict phenotypes is insufficient except for the most straightforward traits. For ciliopathy affected individuals, even when the principal disease-causing mutation is identified, how mutations in that gene manifest as a range of phenotypes in different populations remains unknown. Genome-wide association studies (GWAS) have identified polymorphisms associated with many diseases and traits. However, these only account for a small percentage of the estimated heritability, provoking searches for sources of "missing heritability" (66, 67). Work in simple organisms such as yeast has suggested that more extensive accounting for the effects of allelic variation can explain the phenotypic variation in disease and common traits (68). Our work suggests that in heterogeneous, oligogenic disorders

such as ciliopathies, missing heritability could arise not from the effects of polymorphisms by themselves but from gene specific interactions between polymorphisms, which GWAS fail to detect. Our double mutant analyses demonstrate that the phenotypes that arise for a given mutation depend on the genetic context, such that an innocuous mutation in one genetic background may alter a disease phenotype in another. In support of this notion in ciliopathies, human genetic studies have found NPHP and BBS patients with multiple genetic lesions that contribute to their phenotypes (20, 69, 70). As common or rare variants may be shared within a family, they may be a source of heritability and significant modifiers of disease phenotypes. Detecting variants that affect expressivity only in specific genetic contexts will require power and computation not currently present in GWAS. Therefore, as a complement to GWAS, animal genetic models provide a valuable means to identify the oliogenic interactions that define inherited disease phenotypes.

Materials and Methods

C. elegans Strains

All strains (Supplementary Table 5) were generated and maintained under standard conditions(71)(71)(71)(70)(69)(68)(68)(68). The *tctn-1* mutant strain, E04A4.6*(ok3021)* IV*,* was obtained from the *C. elegans* Gene Knockout Consortium via the *Caenorhabditis* Genetics Center and outcrossed to wild type (N2) six times. Standard mating procedures were used to generate double mutants and to introduce fluorescently tagged protein constructs into the specified genetic backgrounds.

Subcellular protein localization

Strains bearing TCTN-1 C-terminal GFP translational fusion constructs were generated by stitch-PCR, essentially as described in Inglis *et al.* (2009). In brief, the *bbs-8* promoter region, followed by the complete genomic coding region of the *tctn-1* gene, was fused in-frame to EGFP, and used to create transgenic lines. Live animals were anaesthetized using 10 mM levamisole, mounted on 5% agarose pads, and observed by spinning-disc confocal microscopy. The subcellular localization patterns of the fluorescent marker-tagged proteins were assessed in either wild type (N2) animals or in the indicated mutant backgrounds. Mislocalization phenotypes were confirmed by analyzing at least 50 animals for each strain.

C. elegans assays

To assess sensory neuron dye filling, 300 synchronized L4 worms were washed with S-basal and immersed in 10 mg/ml DiI in S-basal for two hours. Worms were rinsed with S-basal, and plated onto an OP50 seeded plate. After one hour, the animals were anesthetized with 0.2 M sodium azide, mounted on a 2% agarose pad, and imaged on a Zeiss Axioplan microscope at

16x. Assays were performed on at least three separate occasions for each genotype. Statistical significance was assessed using the unpaired Student's *t* test.

To measure growth, 150 synchronized L1 larvae were plated on OP50 and incubated at 20°C. After 45 hours, the animals were counted and staged. Assay was repeated three times. To measure size, DIC images of synchronized day 1 gravid adults were captured on a Zeiss Axioplan microscope. Perimeter and area were measured using Fiji software for 20-35 animals of each genotype. Egg laying was measured by picking synchronized day 1 gravid adults onto individual plates. One hour later, the number of eggs on the plate was counted. Brood size was measured by plating synchronized L4 animals, and transferring the animals onto fresh plates daily until the end of the reproductive period. Progeny from each plate was counted for at least ten animals. Standard osmotic avoidance and chemotaxis assays were performed as previously described using 8M glycerol to create high osmolarity, and diacytyl (1:1000 dilution) and butanone (1:1000 dilution) as chemoattractants (5, 72).

Mouse alleles

Tctn1^{-} (*Tctn1*$^{Gt(KST296)Byg}$), *Tctn2*$^{-}$(*Tctn2*$^{tm1.1Reit}$), *Nphp4*^{n}(*Nphp4*^{nmf192}), *Nphp1*$^{-}$(*Nphp1*^{tm1Jgg}) *Cc2d2a*$^{-}$(*Cc2d2a*$^{Gt(AA0274)Wtsi}$), and *Bbs1*$^{-}$(*Bbs1*^{tm1Vcs}) alleles have been previously described (26, 29, 42, 57, 64, 73). Mouse protocols were approved by the Institutional Animal Care and Use Committee at the University of California, San Francisco.

Mouse mutant analysis

Single and double mutant embryos were generated by timed matings of trans-heterozygous animals. For gross phenotypic examination, embryos were harvested at E14.5, fixed in 4% paraformaldehyde, and imaged at 8x magnification on a Zeiss Discovery V12 steREO microscope. At least three embryos of each double mutant combination were analyzed. Limb

bud digits were visualized by fixing E14.5 embryos in ethanol and staining in Alcian blue and Alizarin red, as previously described (74).

Limb fibroblast derivation

Limb fibroblast cell lines were generated from E13.5 mouse embryos that were harvested and transferred into Dulbecco's PBS with penicillin, streptomycin and fungizone (P/S/F) at 37ºC. For each embryo, both forelimb buds were extracted and incubated for 2 minutes at room temperature in 0.05% Trypsin-EDTA solution, after which they were disaggregated by pipetting. The resulting cell suspensions were immediately transferred into DMEM medium supplemented with 20% fetal bovine serum (FBS) and P/S/F, and incubated overnight with gentle shaking at 37ºC and 5% CO_2. The next day cells were confluent and were passaged using the trypsinization procedure described above. Cells were maintained in DMEM+15%FBS+P/S/F and were not diluted more than five times when passaging. All analyses were performed in cells passaged less than ten times.

Immunofluorescence

For immunostaining, confluent limb bud fibroblasts were starved for 48 hours in OptiMEM medium to induce ciliation. Cells were fixed by incubating them first in DPBS+4% paraformaldehyde (10 min, RT), followed by cold methanol (3 min, -20ºC). Cells were blocked and permeabilized for at least 15 min at RT in blocking solution (PBS+2% donkey serum+0.1% Triton-X100+0.02% sodium azide). Coverslips were then incubated with primary antibodies diluted in blocking solution for 3 hours at RT. After two rinses in PBS, coverslips were incubated with fluorophore (Alexa Fluor)-conjugated donkey secondary antibodies and the DNA dye Hoechst-33342 for 1 hour at RT in darkness. This was followed by two rinses in milliQ water and the mounting of coverslips on slides using gelvatol mounting medium. Slides were imaged on a Leica TCS SPE confocal microscope. Antibodies used were: acetylated tubulin (clone 6-11B-1;

Sigma), γ-tubulin (C-20; Santa Cruz), Arl13b (N295B/66; NeuroMab) and Nphp1 (gift from Dr. Greg Pazour). For quantitation of cilia numbers, fields of cells were imaged at seven positions spanning the whole sample. Acetylated tubulin-positive cilia associated with a γ-tubulin-positive basal body were counted in each field and normalized to the number of nuclei in the field. Statistical significance was assessed using the unpaired Student's *t* test. Immunostaining of limb bud cryosections was performed as previously described (26).

Shh signaling assay

To measure Shh signaling, confluent limb bud fibroblasts were starved in OptiMEM for 24 hours, then treated with DMSO or 200nM SAG (Cayman Chemical) for 24 hours. RNA was extracted from these cells using the RNeasy Mini Kit (Qiagen) and cDNA was synthesized using the SuperScript III First-Strand Synthesis System (Invitrogen). Quantitative PCR was performed using EXPRESS SYBR GreenER qPCR Supermix, with premixed ROX (Invitrogen) on a 7300 Real-Time PCR machine (Applied Biosystems). Transcript levels of *Gli1* and *Ptch1* were normalized to levels of *β-actin.* The primers used were Gli1F, 5'-GGTGCTGCCTATAGCCAGTGTCCTC-3'; Gli3R, 5'-GTGCCAATCCGGTGGAGTCAGACCC-3'; Ptch1F, 5'-CTCTGGAGCAGATTTCCAAGG-3'; Ptch1R, 5'-TGCCGCAGTTCTTTTGAATG-3'; β-actinF*,* 5'-CACAGCTTCTTTGCAGCTCCTT-3'; and β-actinR, 5'-CGTCATCCATGGCGAACTG-3'. Experiments were performed in triplicate and repeated at least three times. Statistical significance was assessed using the unpaired Student's *t* test.

Electron microscopy

Transmission electron microscopy of *C. elegans* amphid cilia was performed as previously described (33, 52). Images depicting *nphp-4* single mutant cilia were of strain PT709: *nphp-4(tm925) him-5(e1490)* V. No differences in ciliary structure were detected between *nphp-4* and *nphp-4 him-5* genotypes (data not shown). For TEM analysis of limb cilia in mice, we isolated

forelimb buds from E11.5 embryos, washed with Dulbecco's PBS and incubated in fixative solution containing 0.1M sodium cacodylate (pH 7.2), 4% formaldehyde, 4% glutaraldehyde, 4% tannic acid and 5% sucrose, where they remained for two days. The limb buds were processed for TEM as previously described (26). Images were acquired using a JEOL JEM-1400 electron microscope. For quantification of limb bud cilia, axonemes with docked basal bodies were counted per field in at least seven fields. Statistical significance was assessed using the unpaired Student's *t* test.

Figure S1

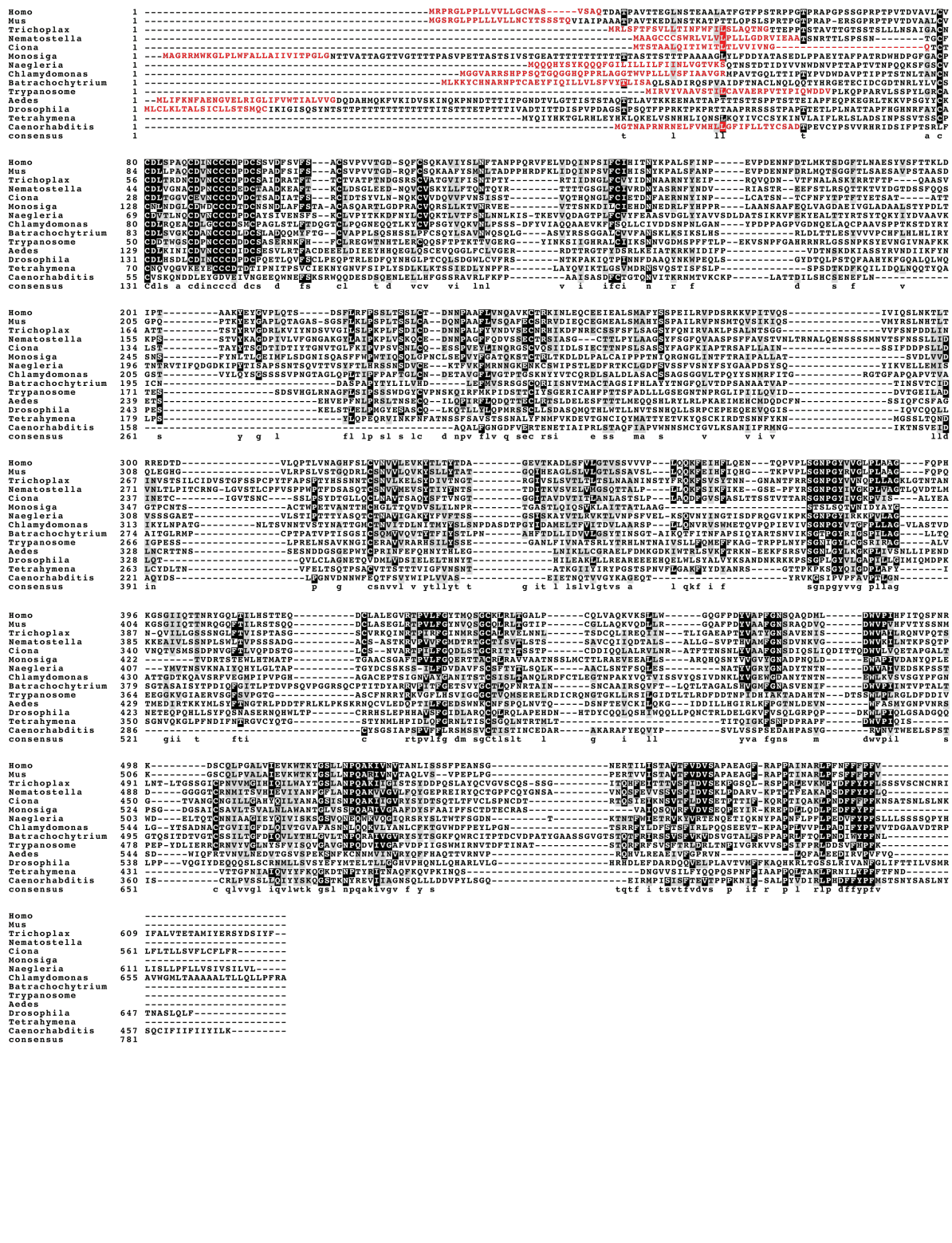

Figure S1. Orthologs of Tectonic1

Sequence alignment of Tectonic1 orthologs of *Homo sapiens, Mus musculus, Ciona intestinalis* (sea squirt)*, Drosophila virilis* (fruit fly)*, Aedes aegypti* (mosquito)*, Nematostella vectensis* (sea anemone)*, Trichoplax* (Placozoan)*, Monosiga brevicollis* (choanoflagellate)*, Naegleria gruberi* (amoeboflagellate)*, Batrachochytrium dendrobatidis* (chytrid fungus)*, Tetrahymena thermophile, Trypanosome brucei, Chlamydomonas reinhardtii,* and *Caenorhabditis elegans*. Predicted signal peptides are indicated in red. *C. elegans tctn-1* is most homologous to other Tectonics in the C-terminal region.

Figure S2

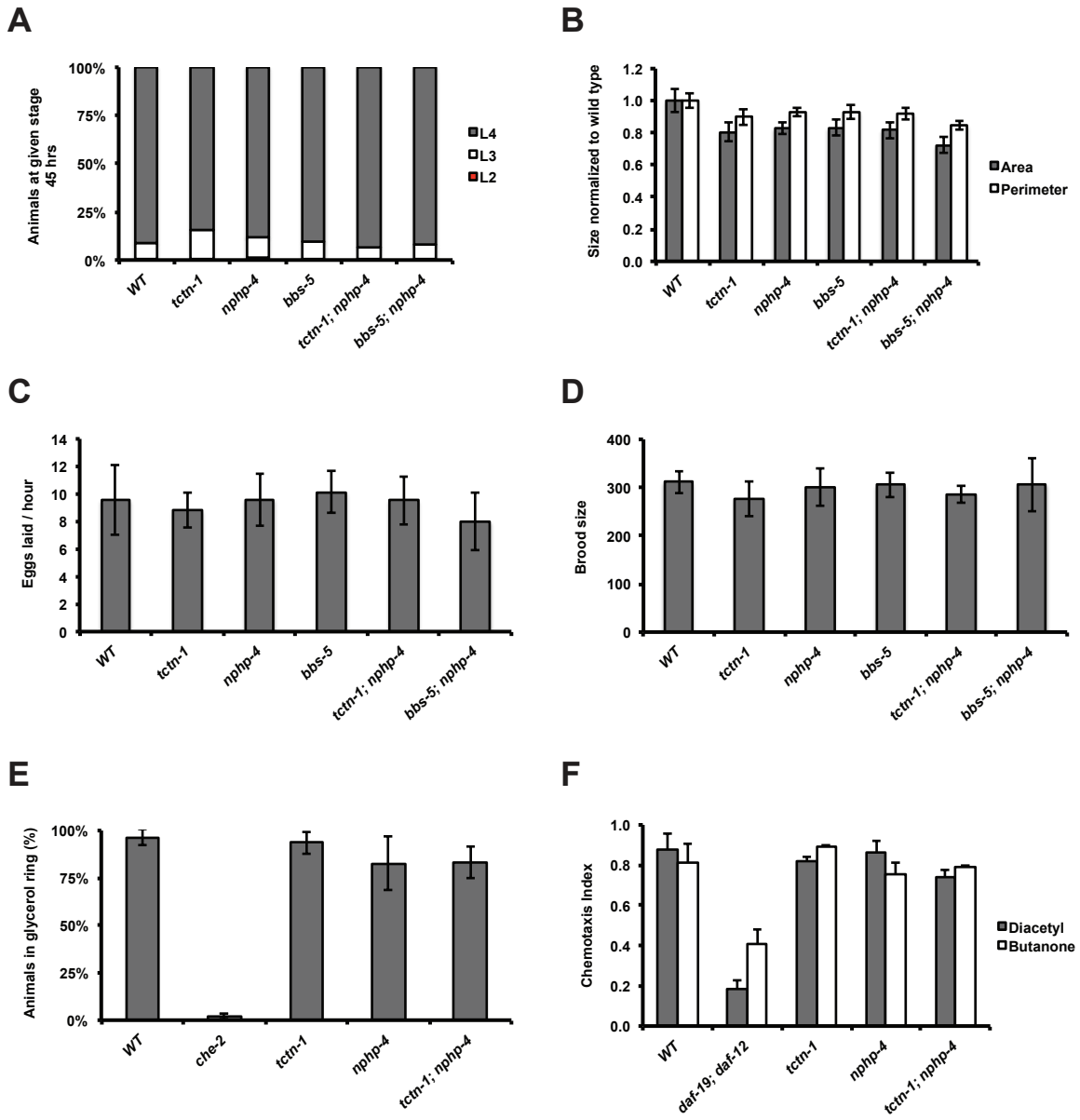
A
Animals at given stage 45 hrs
100%
75%
50%
25%
0%
L4
L3
L2
WT
tctn-1
nphp-4
bbs-5
tctn-1; nphp-4
bbs-5; nphp-4
B
Size normalized to wild type
1.2
1.0
0.8
0.6
0.4
0.2
0.0
Area
Perimeter
C
Eggs laid / hour
14
12
10
8
6
4
2
0
D
Brood size
400
300
200
100
0
E
Animals in glycerol ring (%)
che-2
F
Chemotaxis Index
Diacetyl
Butanone
daf-19; daf-12

Figure S2. *tctn-1* mutants are grossly normal *in C. elegans*

(A) Growth, *(B)* size, *(C)* egg laying, *(D)* brood size, *(E)* response to high osmolarity, and *(F)* chemotaxis abilities to diacytyl and butanone were assessed in *tctn-1* mutants. Additional single and double mutant genotypes were included as indicated.

Figure S3

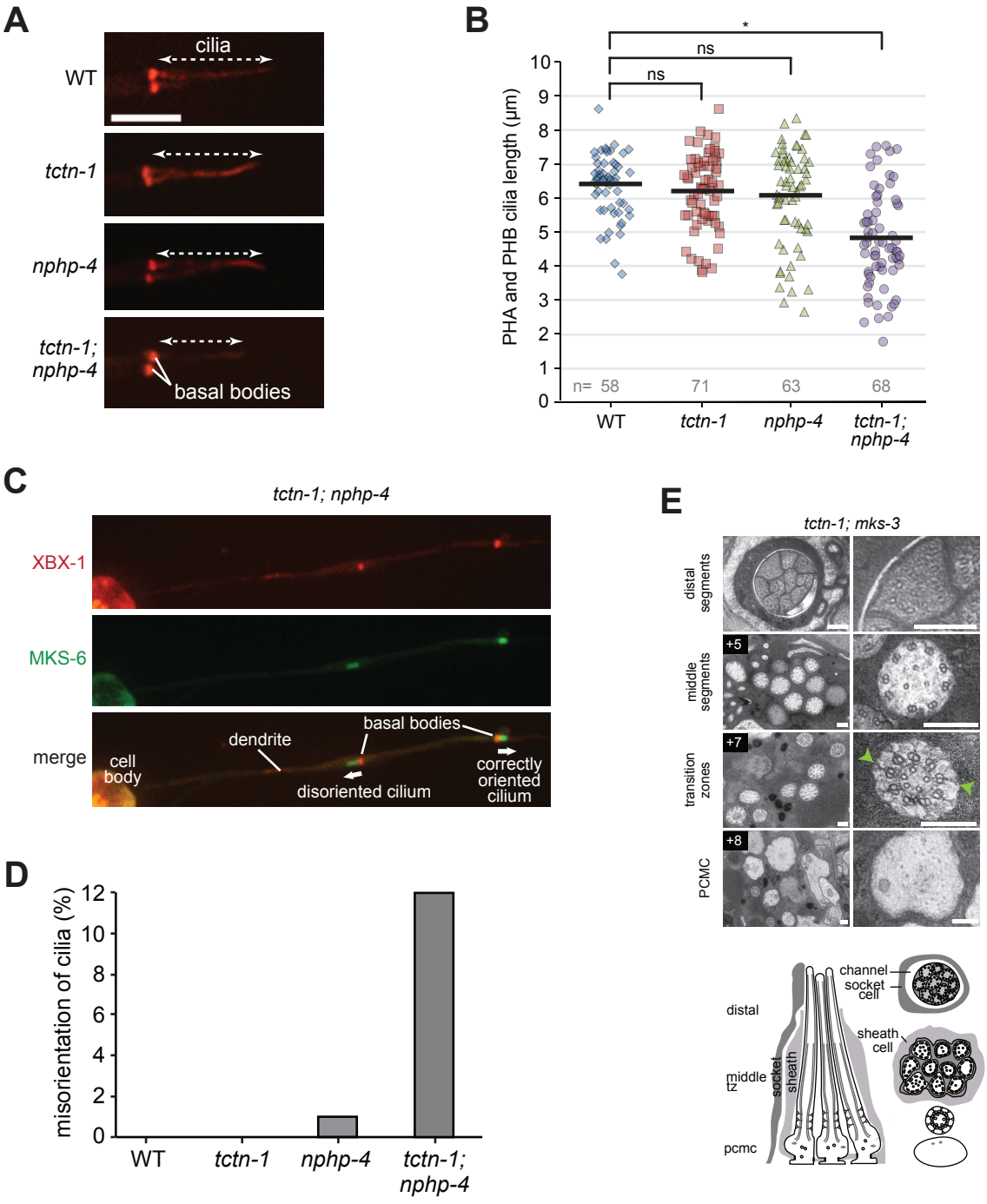
A
cilia
WT
tctn-1
nphp-4
tctn-1; nphp-4
basal bodies
B
PHA and PHB cilia length (µm)
ns
ns
*
n= 58
71
63
68
WT
tctn-1
nphp-4
tctn-1; nphp-4
C
tctn-1; nphp-4
XBX-1
MKS-6
merge
cell body
dendrite
basal bodies
disoriented cilium
correctly oriented cilium
D
misorientation of cilia (%)
WT
tctn-1
nphp-4
tctn-1; nphp-4
E
tctn-1; mks-3
distal segments
middle segments
transition zones
PCMC
+5
+7
+8
channel
socket cell
sheath cell
distal
middle tz
pcmc
socket
sheath

Figure S3. Affected cilia in *tctn-1; nphp-4* mutants and unaffected cilia in *tctn-1; mks-3* mutants in *C. elegans*

tctn-1; nphp-4 double mutants display morphologically abnormal cilia. *(A) tctn-1; nphp-4* PHA and PHB cilia, visualized with XBX-1::tdTomato, are slightly shorter compared to controls. *(B)* Measurements of cilia lengths as shown in *(A),* * $p<0.001$, ns: no significant difference. *(C) tctn-1; nphp-4* mutants display mis-oriented PHA and PHB cilia visualized with XBX-1::tdTomato and MKS-6::GFP. *(D)* Percentage of mis-oriented *tctn-1; nphp-4* cilia as shown in *(C)* compared to controls. (*E*) *tctn-1; mks-3* mutants do not have defects in ciliary structure. Low and high magnification TEM cross-sections of the distal segment, middle segment, transition zone, and PCMC of amphid cilia of *tctn-1; mks-3* double mutants. Schematics below (lateral and transverse views). Green arrows indicate intact Y-links at the transition zone. Boxed numbers indicate distance (μM) from the distal tip of the cilium. Scale bars,100 nm.

Figure S4

A

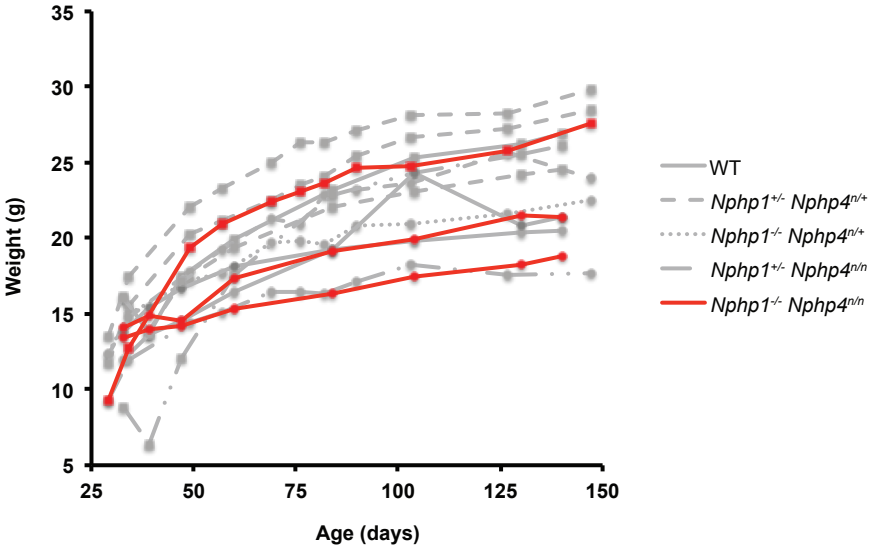
35
30
25
20
15
10
5
Weight (g)
25
50
75
100
125
150
Age (days)
WT
Nphp1+/- Nphp4n/+
Nphp1-/- Nphp4n/+
Nphp1+/- Nphp4n/n
Nphp1-/- Nphp4n/n

B

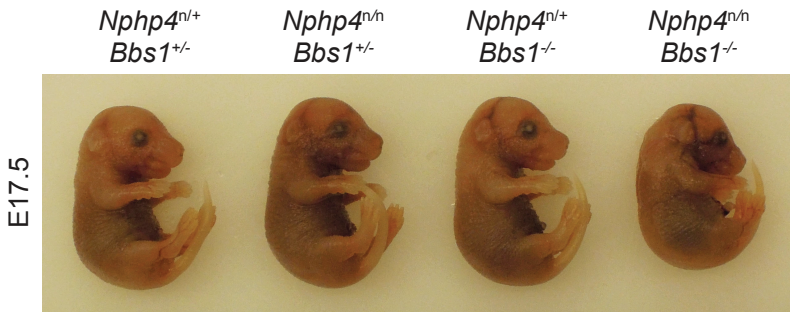
Nphp4n/+ Bbs1+/-
Nphp4n/n Bbs1+/-
Nphp4n/+ Bbs1-/-
Nphp4n/n Bbs1-/-
E17.5

Figure S4. Mouse *Nphp4* does not genetically interact with *Nphp1* or *Bbs1*

(A) Nphp1$^{-/-}$ *Nphp4*$^{n/n}$ double mutants are viable and grow at the same rate as their littermates of indicated genotypes. Two litters are shown with each line representing one animal. Squares represent males and circles represent females. *(B) Nphp4*$^{n/n}$ *Bbs1*$^{-/-}$ double mutant embryos at E17.5 resemble wild type, *Nphp4*$^{n/n}$ and *Bbs1*$^{-/-}$ single mutant embryos.

Table S1. Polydactyly in MKS and NPHP complex mutants

Genotype	Forelimbs (%)			Total forelimbs	Hindlimbs (%)			Total hindlimbs
	5 digits	6 digits	7 digits	examined	5 digits	6 digits	7 digits	examined
WT	34 (100)	0 (0)	0 (0)	34	34 (100)	0 (0)	0 (0)	34
***Tctn1*$^{-/-}$**	35 (92)	3 (8)	0 (0)	38	2 (5)	35 (92)	1 (3)	38
***Tctn2*$^{-/-}$**	8 (67)	4 (33)	0 (0)	12	0 (0)	12 (100)	0 (0)	12
***Cc2d2a*$^{-/-}$**	14 (100)	0 (0)	0 (0)	14	2 (14)	12 (86)	0 (0)	24
***Nphp4*$^{n/n}$**	36 (100)	0 (0)	0 (0)	36	36 (100)	0 (0)	0 (0)	36
***Nphp1*$^{-/-}$**	28 (100)	0 (0)	0 (0)	28	28 (100)	0 (0)	0 (0)	28
***Tctn1*$^{-/-}$ *Tctn2*$^{-/-}$**	17 (94)	1 (6)	0 (0)	18	1 (6)	17 (94)	0 (0)	18
***Tctn1*$^{-/-}$ *Nphp4*$^{n/n}$**	4 (17)	15 (62)	5 (21)	24	0 (0)	21 (88)	3 (12)	24
***Tctn1*$^{-/-}$ *Nphp1*$^{-/-}$**	8 (33)	16 (67)	0 (0)	24	0 (0)	24 (100)	0 (0)	24
***Cc2d2a*$^{-/-}$ *Nphp4*$^{n/n}$**	1 (12)	5 (63)	2 (25)	8	1 (12)	7 (88)	0 (0)	8

The number of limbs with the indicated number of digits observed, with the percentage in parentheses.

Table S2. Exencephaly in MKS and NPHP complex mutants

Genotype	Embryos with exencephaly (%)
WT	0/17 (0)
***Tctn1*$^{-/-}$**	0/19 (0)
***Nphp4*$^{n/n}$**	0/18 (0)
***Nphp1*$^{-/-}$**	0/14 (0)
***Tctn1*$^{-/-}$ *Nphp4*$^{n/n}$**	2/12 (17)
***Tctn1*$^{-/-}$ *Nphp1*$^{-/-}$**	5/12 (42)

The number of embryos with exencephaly among the total examined, with the percentage in parentheses.

Table S3. Polydactyly in *Tctn1*$^{-/-}$ *Bbs1*$^{-/-}$ mutants

Genotype	Forelimbs (%)			Total forelimbs	Hindlimbs (%)			Total hindlimbs
	5 digits	6 digits	7 digits	examined	5 digits	6 digits	7 digits	examined
WT	12 (100)	0 (0)	0 (0)	12	12 (100)	0 (0)	0 (0)	12
***Tctn1*$^{-/-}$**	8 (100)	0 (0)	0 (0)	8	2 (20)	8 (80)	0 (0)	10
***Bbs1*$^{-/-}$**	12 (100)	0 (0)	0 (0)	12	12 (100)	0 (0)	0 (0)	12
***Tctn1*$^{-/-}$ *Bbs1*$^{-/-}$**	0 (0)	4 (67)	2 (33)	6	0 (0)	6 (100)	0 (0)	6

The number of limbs with the indicated number of digits observed, with the percentage in parentheses.

Table S4. Exencephaly in *Tctn1*$^{-/-}$ *Bbs1*$^{-/-}$ mutants

Genotype	Embryos with exencephaly (%)
WT	0/6 (0)
***Tctn1*$^{-/-}$**	0/5 (0)
***Bbs1*$^{-/-}$**	0/6 (0)
***Tctn1*$^{-/-}$ *Bbs1*$^{-/-}$**	2/3 (67)

The number of embryos with exencephaly among the total examined, with the percentage in parentheses.

Table S5. *C. elegans* strains used in this study

Strain	Genotype
N2	wild type
KQ2175	*tctn-1(ok3021)* IV
KQ1456	*nphp-4(tm925)* V
KQ2206	*nphp-1(ok500)* II
KQ2333	*mks-1 (tm2705)* III
KQ2209	*mksr-1(ok2092)* X
KQ2245	*mksr-2 (tm2452)* IV
KQ2185	*mks-3(tm2547)* II
KQ2187	*tctn-1(ok3021)* IV; *nphp-4(tm925)* V
KQ2232	*nphp-1(ok500)* II; *tctn-1(ok3021)* IV
KQ2372	*mks-1(tm2705)* III; *tctn-1(ok3021)* IV
KQ2233	*tctn-1(ok3021)* IV; *mksr-1(ok2092)* X
KQ2290	*mksr-2(tm2452)* IV; *tctn-1(ok3021)* IV
KQ2188	*mks-3(tm2547)* II; *tctn-1(ok3021)* IV
KQ1681	*bbs-5(gk507)* III
KQ2544	*bbs-5(gk507)* III; *nphp-4(tm925)* V
KQ2545	*bbs-5(gk507)* III; *tctn-1(ok3021)* IV
KQ2547	*nphp-1(ok500)* II; *bbs-5(gk507)* III
KQ2548	*bbs-5(gk507)* III; *mksr-1(ok2092)* X
CB1033	*che-2(e1033)* X
JT6924	*daf-19(m86)* II; *daf-12(sa204)* X
PT709	*nphp-4(tm925) him-5(e1490)* V
MX1758	N2; nxEx[P*bbs-8*::*tctn-1*::gfp + P*osm-5*::*xbx-1*::tdTomato + *rol-6(su1006)*]
YH372	N2; Ex[*mksr-1*::cfp + *che-13*::yfp + *rol-6(su1006)*]
MX1674	*nphp-4*; nxEx[*mksr-1*::cfp + *che-13*::yfp + *rol-6(su1006)*]
MX1723	*tctn-1*; nxEx[*mksr-1*::cfp + *che-13*::yfp + *rol-6(su1006)*]
MX1726	*tctn-1; nphp-4*; nxEx[*mksr-1*::cfp + *che-13*::yfp + *rol-6(su1006)*]
YH751	N2; yhEx419[P*osm-5*::*mks-6*::gfp + P*osm-5*::*xbx-1*::tdTomato + *rol-6(su1006)*]
YH776	*nphp-4*; yhEx419[P*osm-5*::*mks-6*::gfp + P*osm-5*::*xbx-1*::tdTomato + *rol-6(su1006)*]
MX1675	*tctn-1*; nxEx[P*osm-5*::*mks-6*::gfp + P*osm-5*::*xbx-1*::tdTomato + *rol-6(su1006)*]
MX1727	*tctn-1; nphp-4*; nxEx[P*osm-5*::*mks-6*::gfp + P*osm-5*::*xbx-1*::tdTomato + *rol-6(su1006)*]
MX1388	N2; nxEx[*arl-13*::gfp+ P*osm-5*::*xbx-1*::tdTomato + *rol-6(su1006)*]
MX1751	*nphp-4*; nxEx[*arl-13*::gfp+ P*osm-5*::*xbx-1*::tdTomato + *rol-6(su1006)*]
MX1725	*tctn-1*; nxEx[*arl-13*::gfp+ P*osm-5*::*xbx-1*::tdTomato + *rol-6(su1006)*]
MX1728	*tctn-1;nphp-4*; nxEx[*arl-13*::gfp+ P*osm-5*::*xbx-1*::tdTomato + *rol-6(su1006)*]
YH930	N2; Ex[P*osm-5*::*mks-5*::tdTomato + P*osm-5*::*dyf-11*::gfp + *rol-6(su1006)*]
MX1219	*nphp-4*; nxEx[P*osm-5*::*mks-5*::tdTomato + P*osm-5*::*dyf-11*::gfp + *rol-6(su1006)*]
MX1722	tctn-1; nxEx[Posm-5::mks-5::tdTomato + Posm-5::*dyf-11*::gfp + *rol-6(su1006)*]
MX1750	*tctn-1; nphp-4*; nxEx[P*osm-5*::*mks-5*::tdTomato + P*osm-5*::*dyf-11*::gfp+ *rol-6(su1006)*]
YH224	N2; Ex[*nphp-4*::yfp + *che-13*::cfp + *rol-6(su1006)*]
MX1721	*tctn-1*; nxEx[*nphp-4*::yfp + *che-13*::cfp + *rol-6(su1006)*]
MX1420	N2; nxEx[P*bbs-8*::*tram-1*::tdTomato + P*bbs-8*::*mks-2*::gfp + *rol-6(su1006)*]
MX1724	*tctn-1*; nxEx[P*bbs-8*::*tram-1*::tdTomato + P*bbs-8*::*mks-2*::gfp + *rol-6(su1006)*]

Chapter 3: Odr4, a potential ciliary targeting gene and Ufm1 regulator, is required for embryonic development in mammals

Abstract

Primary cilia are specialized signaling compartments that project from the surface of most cells. To properly function, subsets of proteins are trafficked to cilia through several mechanisms whereas others proteins are excluded. Here we investigate the gene responsible for one such mechanism, *Odr4*, which is required for the localization of select GPCRs to cilia in *C. elegans.* In mice, we find that *Odr4* is expressed ubiquitously throughout development. *Odr4* mutants die at midgestion with possible signs of anemia and cardiovascular abnormalities. Odr4 physically interacts with UfSP2, a cysteine protease for the ubiquitin-like protein Ufm1. Similar to *odr-4* mutants, *ufsp-2* mutants do not localize a GPCR to the cilium, suggesting that the functions of *odr-4* and *ufsp-2* are indeed related. These preliminary results suggest that in mice, Odr4 may have functions other than regulating the ciliary localization of GPCRs as in *C. elegans.*

Introduction

Cells employ complex and diverse mechanisms to ensure the proper trafficking of proteins to functional compartments. One such compartment is the primary cilium, a highly specialized organelle that emanates from the cell surface. Cilia are present on many cell types, and thus carry out several tissue-specific roles. For example, cilia transduce the Hh signaling pathway in the developing neural tube, sense fluid flow in the kidney, and sense external stimuli such as light and odors (2). To perform these functions, cilia must generate and maintain membrane and protein compositions distinct from those of the cell proper.

Odorant receptors (ORs) and their associated signaling machinery concentrate to cilia in mammalian olfactory sensory neurons (OSNs) and *C. elegans* chemosensory neurons. In mice, 10-30 immotile cilia project from the dendritic knob of each olfactory sensory neuron into the mucus of the nasal cavity, overlapping with cilia from other cells (75). Mature OSNs express only one OR out of more than a thousand OR genes, with every OSN expressing a given OR projecting to the same glomeruli in the olfactory bulb (76-78). In *C. elegans*, chemosensation is primarily mediated by the amphid neurons in the head. Cilia extend from the dendritic tips of amphid neurons to the anterior of the animal where they are exposed to the external environment. Unlike mouse OSNs, which only express one receptor per cell, amphid neurons express a characteristic set of receptors, and consequently respond to characteristic set of odorants (5, 6).

Odorant receptors belong to the large family of G-protein coupled receptors (GPCRs), 7-pass transmembrane proteins at the cell surface that are involved in numerous cellular processes. Several GPCRs that are not ORs localize to cilia, the mislocalization of which can lead to

defective signaling (79, 80). GPCRs traffic to cilia through diverse mechanisms. For example, ciliary localization sequences (e.g. those in the third intracellular loop or at the C-terminal tail) recognized by adaptors (81-83); the BBSome, a protein complex comprised of many proteins disrupted in Bardet-Biedl syndrome (37, 38, 79, 84); and interaction between the intraflagellar protein complex IFT-A and TULP3 (85-87), are required for the ciliary localization of at least a subset of GPCRs.

The ciliary localization of olfactory receptors in particular involve yet another set of accessory proteins. In mice, RTP1 and RTP2 are expressed specifically in olfactory sensory neurons, can bind to ORs, and facilitate OR trafficking to the cell surface in heterologous cells (88). In *C. elegans*, trafficking of ORs to the cilium involves vesicular transport, as disruption of the AP-clathrin adaptor complex or clathrin results in the indiscriminate localization of ORs to ciliary and non-ciliary membranes. (89, 90). Through a forward genetic screen, several mutants defective in detecting volatile odorants were isolated and classified as *odr* mutants (5). Of these, *odr-4* and *odr-8* mutants do not traffic the diacetyl receptor ODR-10 to the cilium of AWA neurons and thus are unresponsive to diacetyl (7). Remarkably, *C. elegans odr-4* is able to facilitate the localization of one OR, but not another OR to the cell surface in heterologous mammalian cells (91). These results suggest a protein and/or cell type specific function for Odr4 in ciliary localization of ORs may be conserved.

Posttranslational modifications are an additional layer of regulation that affect OR and GPCR maturation and function at the cell surface. N-linked glycosylation, phosphorylation, and palmitoylation are common posttranslational modifications of GPCRs (92). Additionally, ubiquitin and ubiquitin like proteins such as SUMO can bind GPCRs or functionally related proteins (93-95). Ubiquitin-fold modifier 1 (Ufm1) is a recently identified, ubiquitin-like posttranslational

modification that is conserved in almost all eukaryotes, but not present in fungi (96, 97). Whether GPCRs are modified by Ufm1 is unknown.

Ufm1 attaches to target proteins (ufmylation) through a series of enzymatic events similar to ubiquitination: Uba5 functions as an E1 to activate Ufm1, Ufc1 functions as an E2, and Ufl1 functions as an E3 (98-100). Ufm1 is synthesized as a precursor, and is cleaved by the proteases UfSP1 and UfSP2 to expose a C-terminal glycine before activation by Uba5. UfSP1 and UfSP2 also function to deconjugate Ufm1 from target proteins (101).

The functions of Ufm1 and the proteins of its conjugation system are largely unknown. Ufm1 may be involved in maintaining ER homeostasis, as several Ufm1 components localize to the cytosolic side of the ER and are upregulated during ER stress (102-106). In mice that lack Uba5 or Ufl1, erythroid differentiation is impaired, resulting in extreme anemia and embryonic lethality (107, 108). Ufl1 also stabilizes the tumor suppressor CdK5Rap3 and regulates the NF-κB pathway (106). Most recently, poly-Ufm1 chains on the nuclear receptor coactivator ASC1 have been shown act as a scaffold for the recruitment of several transcriptional co-factors to the promoters ERα target genes (109).

In *C. elegans,* mutants of the Ufm1 cascade display increased resistance to pathogen, heat, and oxidative stress(110). Ufm1 components are expressed primarily the intestine, but the protease UfSP-2 is expressed specifically in sensory neurons. Like *odr-4, ufsp-2* is required for the proper localization of ODR-10, though this requirement appears to be independent of the Ufm1 cascade (111).

In this work, we have performed preliminary experiments that explore the function of *Odr4* in mice. We found that *Odr4* mutant embryos die at mid-gestation, and have a potential

cardiovascular defect. Odr4 binds to UfSP2, a protease for Ufm1. We hypothesize that for a subset of GPCRs, ufmylation is important for proper ciliary localization, a process that may depend on Odr4. However, the possible functions of Odr4 are not restricted to GPCR trafficking or ufmylation. These results will provide a basis for future studies on Odr4.

Results

Mouse Odr4 shares 22% sequence identity and 45% homology with its *C. elegans* ortholog. Accordingly, it contains no recognized protein domains except for a transmembrane region at the C-terminus (Figure 1A). The Reiter lab obtained a gene trap allele of *Odr4*, BC003331$^{tm1a(EUCOMM)Wtsi}$ (herein thereafter referred to as *Odr4*^{gt}) from the European Conditional Mouse Mutagenesis Program (EUCOMM), in which the first three exons of *Odr4* are captured (Figure 1B). The gene trap vector contains an IRES-lacZ sequence surrounded by two FRT sites, enabling the creation of a conditional allele by recombining with *β-actin-FlpE* (Fig 1B). LoxP sites flanking exons 4 and 5 enable the generation of a null allele by recombining with *β-actin-Cre* (Figure 1B). As Odr4 protein was not detected by immunoblot in *Odr4*$^{gt/gt}$ mutant tissue, the majority of experiments were performed using the gene trap allele (Figure 1C).

To assess where and when *Odr4* is expressed, we performed whole-mount X-gal staining on heterozygous *Odr4*$^{gt/+}$ embryos. In all stages examined (E8.5-E11.5), *Odr4* was ubiquitously expressed throughout the embryo (Figure 2A). Additionally, *Odr4* expression was found in the yolk sac and placenta of E11.5 embryos (Figure 2B). Thus, unlike *C. elegans*, in which a GFP-tagged version of ODR-4 is expressed exclusively in ten types of amphid neurons and the phasmid neurons (7), in mice *Odr4* is more broadly expressed, suggesting it may have broader functions. As efforts to detect the intracellular localization of endogenous Odr4 were unsuccessful, we stably expressed a C-terminal GFP fusion of Odr4 in mouse fibroblasts (3T3s). Odr4-GFP diffusely localized to intracellular membranes as in *C. elegans* (Figure 2C) (7). The localization pattern of Odr4-GFP was also similar in kidney epithelial cells (IMCD3s, data not shown).

Odr4$^{gt/gt}$ embryos died at approximately E12.5 (Table 1) in a C57/Bl6 background and a mixed C57/Bl6-CD1 background. Beginning at E9.5, *Odr4*$^{gt/gt}$ mutants appeared smaller or developmentally delayed compared to control littermates (Figure 3A). Within litters, *Odr4*$^{gt/gt}$ siblings also displayed variation in size. Additionally, *Odr4*$^{gt/gt}$ mutants were often pale, but otherwise did not display obvious defects between E9.5-E11.5 (Figure. 3A). Odr4 null (*Odr4*$^{n/n}$) embryos were also runted, but superficially normal, similar to *Odr4*$^{gt/gt}$ mutants (Fig. 3B).

Although *Odr4*$^{gt/gt}$ embryos appeared grossly normal, they sometimes displayed pericardial edema (Figure 4A). H&E stained sections revealed that *Odr4*$^{gt/gt}$ mutant hearts had thinner ventricular walls with reduced trabeculation than controls (Figure 4B). However, because of the disparity in size, and thus perhaps age, a direct comparison between mutants and controls was difficult to make. The paleness sometimes observed in *Odr4*$^{gt/gt}$ mutants suggested that there might be a defect in circulation. Indeed, *Odr4*$^{gt/gt}$ mutants did not display vitelline vessels in the yolk sac whereas control animals had yolk sacs with prominent vitelinne vessels throughout (Figure 4C). To test whether *Odr4*$^{gt/gt}$ mutants had a defect in the formation of the blood vessels in the embryo itself, we performed whole-mount immunostaining against CD31, a marker for endothelial cells. The staining pattern of CD31 in *Odr4*$^{gt/gt}$ mutants was equivalent to control animals, indicating that any defect in circulation was likely not due to defects in blood vessel formation in the embryo proper (Figure 4D). Taken together, these data suggest that *Odr4*$^{gt/gt}$ mutants potentially have a cardiovascular defect. Additional stage-matched mutant and control embryos must be analyzed to definitely define or exclude the phenotype.

Because *odr-4* is required for the localization of certain GPCRs to cilia in *C. elegans*, we tested whether this was also true in mice (7). *Odr4*$^{gt/gt}$ embryonic fibroblasts (MEFs) were ciliated to the same extent as control MEFs (Figure 5A). Somatostatin receptor 3 (SSTR3) is a ciliary GPCR present in neurons (81, 112), therefore we tested whether its localization was perturbed in the

absence of Odr4. When transiently expressed, an N-terminal EGFP-tagged version of SSTR3 localized to cilia equivalently in *Odr4*$^{+/+}$ and *Odr4*$^{gt/gt}$ MEFs (Figure 5A). Next we assessed the orphan GPCR mOR256-17, which localizes to cilia and the dendritic knob, as well as axonal processes of olfactory sensory neurons (113). In both *Odr4*$^{+/+}$ and *Odr4*$^{+/+}$ MEFs, mOR256-17 localized to the ciliary base, but not the axoneme (Figure 5A). Additionally, Smoothened, a seven-transmembrane protein that traffics to cilia in response to Shh signaling (80), localized to cilia treated with SAG in *Odr4*$^{gt/gt}$ MEFs as in controls (Figure 5B). Consistent with components of the Shh signaling cascade functioning properly in the absence of *Odr4*, *Odr4*$^{gt/gt}$ embryos displayed normal patterning of the neural tube, a process dependent on Shh (Figure 5C) (1). Thus, a GPCR that localizes to the ciliary axoneme, one that localizes to the ciliary base, and one that dynamically enters and exits the cilium do not require Odr4 to do so in vitro.

To test whether *Odr4* was required for olfactory receptor localization in vivo, we deleted *Odr4* in the olfactory epithelium using the *Foxg1-Cre* line. *Odr4*$^{n/c}$ *Foxg1-Cre* mice survive at least until birth; whether they survive until adulthood has not been determined. The localization of ORs (e.g. mOR28, mOR256-17, C6, M7 and M50) in mOSNs and the staining pattern of their glomeruli in the olfactory bulb are currently being analyzed. In addition, examining the localization of G-protein signaling machinery (e.g. $G\gamma_{13}$, $G_{olf,}$ CNGA2, and AC3) in *Odr4*$^{n/c}$ *Foxg1-Cre* mutants will be informative as will examining the localization of vomeronasal receptors on vomeronasal sensory neurons.

As a complementary approach to investigating Odr4 through mutant analysis, we took a biochemical approach to identify interacting partners of Odr4. We created 3T3 cell lines stably expressing the localization and affinity purification (LAP) tag fused to Odr4 at the C-terminus (3T3-pgLAP5-Odr4) (Figure 2C). We purified Odr4-LAP, subjected the precipitated proteins to SDS-PAGE (Figure 6A). Through mass spectrometry analysis, we detected a single protein

highly enriched with Odr4, Ufm-1 specific protease 2 (UfSP2). Additional proteins were co-purified with Odr4, but had significantly lower peptide counts than UfSP2 (Table 3). Physical interaction between Odr4 and UfSP2 was confirmed by co-immunoprecipation of overexpressed Odr4 and endogenous UfSP2 in the 3T3pgLAP5-Odr4 cell line used for mass spectrometry (Figure 6B).

UfSP2 is a cysteine protease that cleaves the posttranslational modification Ufm1 into its mature form and removes Ufm1 from target proteins (Figure 6C). We hypothesized that through UfSP2, Odr4 plays a role in conjugating Ufm1 to its target proteins. Alternatively, Odr4 could play a role in removing Ufm1 from its target proteins, also through UfSP2. As an initial experiment to broadly assess ufmylation in *Odr4*$^{+/+}$ and *Odr4*$^{gt/gt}$ cells we probed for Ufm1 in whole cell lysates. Several discrete bands of various molecular weights were Ufm1 positive in the lysates, representing Ufm1 conjugated proteins. Notably, a band corresponding to approximately 35 kDa was more intense in the *Odr4*$^{gt/gt}$ lysate than in the control lysate (Figure 6D). Thus, for this unidentified protein of 35 kDa, Odr4 negatively regulates its conjugation to Ufm1. If Odr4 affects ufmylation, it may affect the localization of Ufm1. However, loss of Odr4 did not alter the localization of transiently expressed EGFP-Ufm1 (Figure 6E).

The targets of Ufm1 remain largely unknown, which limits functional studies of Ufm1 to some extent. Purification Ufm1 and subsequent mass spectrometry of co-purified proteins has identified c20orf116 (also known as UFBP1), CDK5RAP3, and ASC1 as proteins that are modified by Ufm1 (99, 104, 109). To identify additional ufmylated proteins, we searched the Odr4 mass spectrometry dataset for peptides with a signature Ufm1 modification. Candidate ufmylated proteins included probable G-protein coupled receptor 115 (Gpr115), olfactory receptor 1383 (Olfr1383), and olfactory receptor 448 (Olfr448), which were of particular interest because of the association of ODR-4 with GPCRs. We hypothesized that if Gpr115, Olfr1383,

and Olfr448 were indeed Ufm1 targets, there ufmylation would be regulated by Odr4. Ufmylation would be tested by co-immunoprecipitation in the presence and absence of Odr4. As a positive control, we demonstrated that overexpressed Ufm1 binds to overexpressed c20orf116 in HEK293 cells as previously found (99, 104). We created stable HEK293 cell lines and *Odr4* mutant lines that expressed GFP-tagged versions of Gpr115, Olfr1383, and Olfr448, but were not able to affectively purify them and detect them by Western blot. Thus additional experiments and conditions that enable the immunoprecipitation of Gpr115, Olfr1383, and Olfr448 will be required to determine if these receptors are Ufm1 substrates.

As UfSP2 binds to Odr4, it may share functions with Odr4 in both mammals and *C.elegans*. We therefore examined *ufsp-2* in C. *elegans*. The mutant *ufsp-2* allele in *C. elegans* contains a 1000 bp deletion across exons 2-6 in addition to a 4 bp insertion at the same site (Figure 7A). As a result, a premature stop codon is generated near the insertion site, likely creating a loss of function allele. Like in *odr-4* mutants, in *ufsp-2* mutants, ODR-10::GFP failed to localize to the cilium of AWA neurons, localizing to the cell body instead (Figure 7B). As expected from the mislocalization of ODR-10, *ufsp-2* mutants did not chemotax properly to diacetyl, the odorant that binds ODR-10 (Figure 7C). Studies from a recent paper also confirm these findings (111). Additionally, *odr-4* suppresses the group feeding behavior of mutants in *npr-1,* a putative neuropeptide receptor homologous to the mammalian neuropeptide Y (NPY) receptor (114). *odr-4; npr-1* double mutants exhibit individual feeding behavior like *odr-4* single mutants and wild type animals. *ufsp-2* single mutants feed individually, and *ufsp-2; npr-1* double mutants also restored individual feeding behavior to *npr-1* (Figure 7D, E). Thus, *ufsp-2* phenocopies *odr-4*, suggesting that they have related functions, and that the interaction between these proteins in mammals is conserved in *C. elegans*.

Figure 1

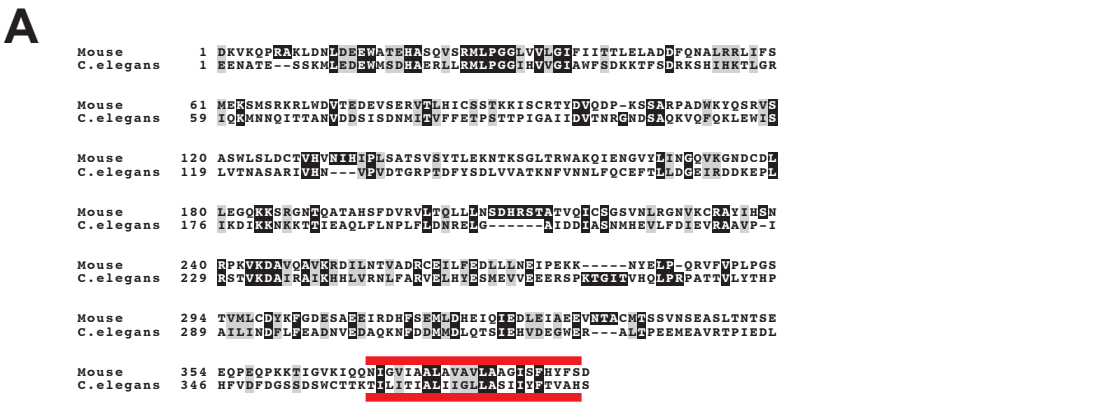
A
Mouse 1 DKVKQPRAKLDNPDEEWATEHASQVSRMLPGGLVVLGIFIITTLELADPFQNALRRLIFS
C.elegans 1 EENATE--SSKMPEDEWMSDHAERLLRMLPGGIHVVGIAWFSDKKTFSPRKSHIHKTLGR
Mouse 61 MEKSMSRKRLWDVTEDEVSERVTLHICSSTKKISCRTYDVQDP-KSSARPADWKYQSRVS
C.elegans 59 IQKMNNQITTANVDDSISDNMITVFFETPSTTPIGAIIDVTNRGNDSAQKVQFQKLEWIS
Mouse 120 ASWLSLDCTVHVNIHIPLSATSVSYTLEKNTKSGLTRWAKQIENGVYLINGQVKGNDCDL
C.elegans 119 LVTNASARIVHN---VPVDTGRPTDFYSDLVVATKNFVNNLFQCEFTLLDGEIRDDKEPL
Mouse 180 LEGQKKSRGNTQATAHSFDVRVLTQLLTNSDHRSTATVQHCSGSVNLRGNVKCRAYIHSN
C.elegans 176 IKDIKKNKKTTIEAQLFLNPLPLDNREIG------AIDDIASNMHEVLFDIEVRAAVP-I
Mouse 240 RPKVKDAVQAVKRDILNTVADFCEILFDDLLLNSIPEKK-----NYELF-QRVFVPLPGS
C.elegans 229 RSTVKDAIRAIKHHLVRNLFAFVELHYESMEVVEEERSPKTGITVHQLPRPATTVLYTHP
Mouse 294 TVMLCDYKFGDESAEEIRDHFSEMLDHEIQHEDLEIAESVNTACMPSSVNSEASLTNTSE
C.elegans 289 AILINDFLFEADNVEDAQKNFDDMMDLQTSIEHVDEGWER---ALLPEEMEAVRTPIEDL
Mouse 354 EQPEQPKKTIGVKIQQNIGVIAALAVAVLAAGISFHYFSD
C.elegans 346 HFVDFDGSSDSWCTTKTILITIALIIGLLASIIYFTVAHS
B
Gene trap
FRT
loxP
FRT
loxP
loxP
5'
IRES
lacZ
neo
3'
Exons 2 & 3
4 & 5
6 & 7
Conditional
FRT
loxP
loxP
5'
3'
Exons 2 & 3
4 & 5
6 &7
Null
FRT
loxP
5'
3'
Exons 2 & 3
6 & 7
C
kDa
Odr4+/+
Odr4gt/gt
70
55
anti-Odr4
anti-β-actin

Figure 1. The Structure of Odr4 and *Odr4* mutant alleles

(A) Sequence alignment of Odr4 orthologs from mouse and *C. elegans*. Both proteins lack recognized domains other than a C-terminal transmembrane region highlighted in red. *(B)* Schematics of the Odr4 genetrap, conditional, and null alleles. The *Odr4* genetrap, inserted downstream of exon 3, contains a lacZ locus flanked by two *FRT* sites as well as two *loxP* sites flanking exons 4 &5. Recombination with β-actin-FlpE excises the lacZ locus, creating the conditional allele. Recombination with β-actin-Cre generates the null allele, which lacks exons 4 and 5. *(C)* Westen blot displaying an absence of Odr4 protein (~49 kD) in $Odr4^{gt/gt}$ MEFS compared to wild type.

Figure 2

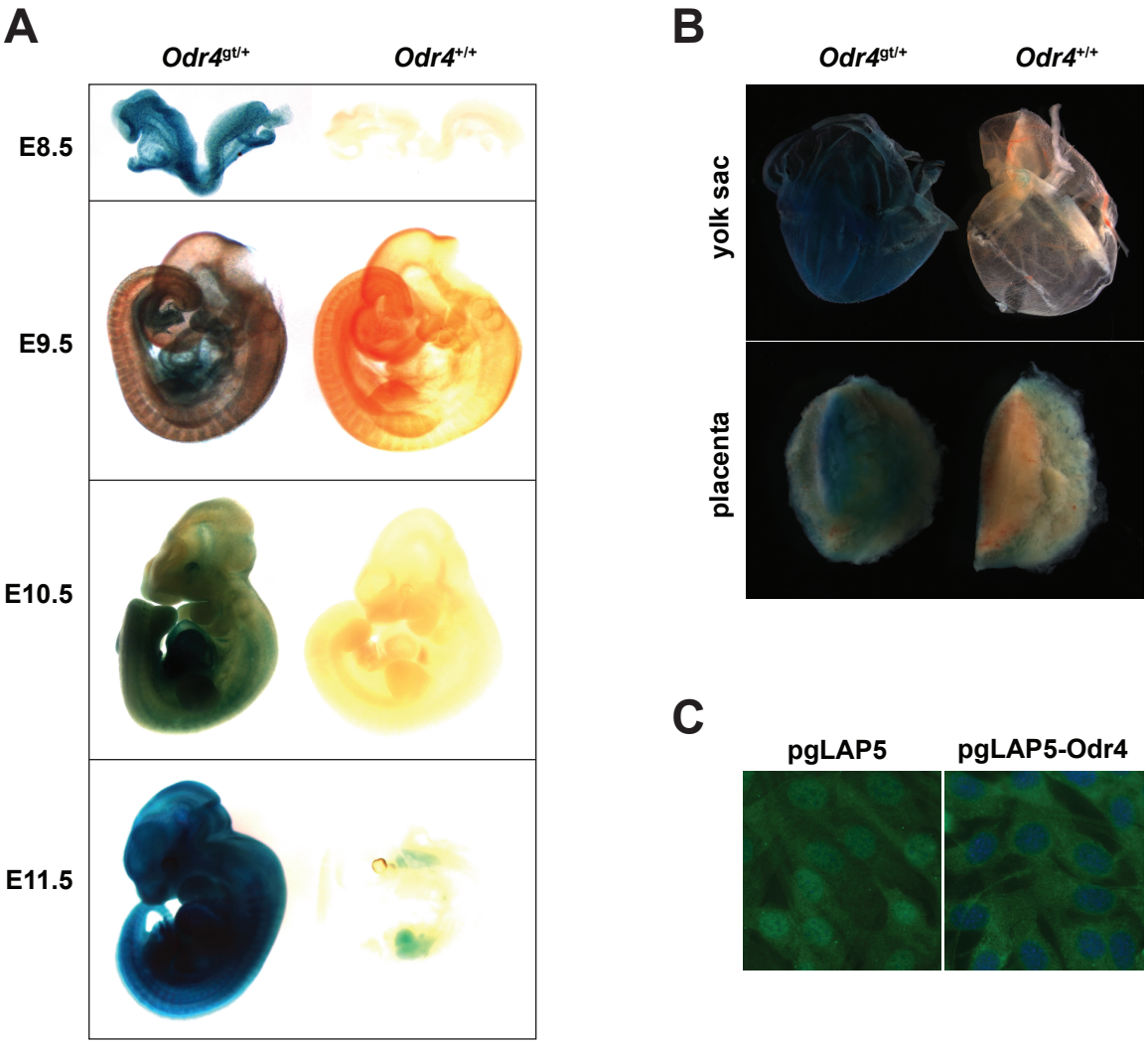
A
Odr4gt/+
Odr4+/+
E8.5
E9.5
E10.5
E11.5
B
Odr4gt/+
Odr4+/+
yolk sac
placenta
C
pgLAP5
pgLAP5-Odr4

Figure 2. *Odr4* is expressed ubiquitously throughout development

(A) Left lateral views of X-gal staining of *Odr4*$^{gt/+}$ and *Odr4*$^{+/+}$ embryos at indicated stages. *Odr4* expression is found throughout the embryo at all stages examined. *(B)* X-gal staining of extra-embryonic tissues (yolk sac and placenta) of *Odr4*$^{gt/+}$ and *Odr4*$^{+/+}$ embryos at E11.5. *(C)* Immunofluorescence of GFP (green) in 3T3 cells stably expressing GFP (pgLAP5) or Odr4-GFP (pgLAP5-Odr4). Nuclei are marked with DAPI (blue).

Figure 3

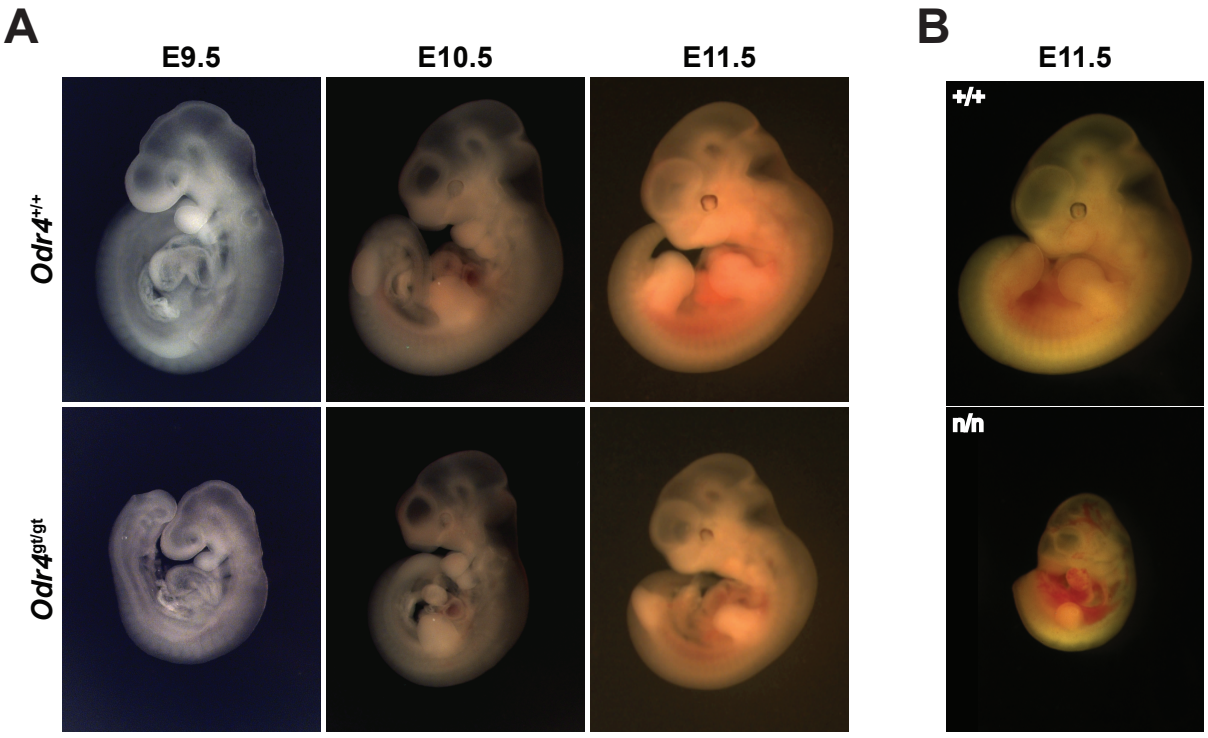

Table 1. Survival of *Odr4* mutants

Age	gt/gt	gt/+	+/+	Total
E9.5	7 (20%)	21 (60%)	7 (20%)	35 (100%)
E10.5	8 (27%)	15 (50%)	7 (23%)	30 (100%)
E11.5	8 (19%)	25 (58%)	10 (23%)	43 (100%)
E12.5	1 (3%)	23 (62%)	13 (35%)	37 (100%)
E13.5	0 (%)	8 (57%)	9 (64%)	14 (100%)
E14.5	0 (%)	14 (67%)	7 (33%)	21 (100%)
E15.5	0 (%)	6 (75%)	2 (25%)	8 (100%)
P0	0 (%)	51 (82%)	11 (18%)	62 (100%)

Number of surviving embryos with percentages in parentheses

Figure 3. *Odr4* is required for embryonic development

(A) Right lateral views of *Odr4*$^{gt/gt}$ mutant embryos and control littermates at E9.5, E10.5, and E11.5. *Odr4*$^{gt/gt}$ mutant embryos are runted and pale, but otherwise do not display gross abnormalities. *(B)* Right lateral views of Odr4$^{n/n}$ mutants and control littermates at E11.5.

Figure 4

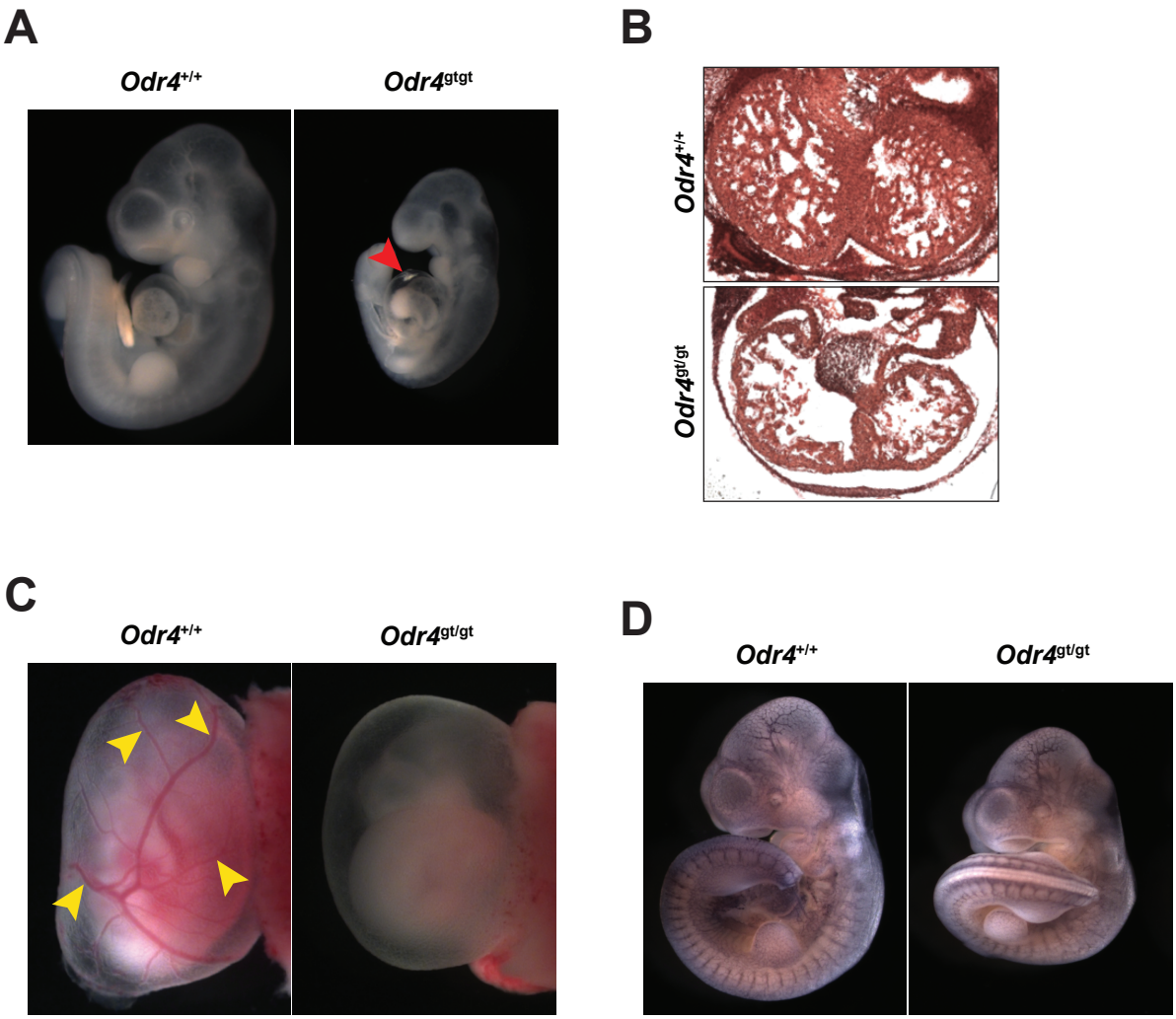
A
Odr4+/+
Odr4gtgt
B
Odr4+/+
Odr4gt/gt
C
Odr4+/+
Odr4gt/gt
D
Odr4+/+
Odr4gt/gt

Figure 4. *Odr4*$^{gt/gt}$ mutants have possible cardiovascular defects

(A) Odr4$^{gt/gt}$ mutants (E10.5) sometimes display pericardial edema, indicated by a red arrowhead. *(B)* Hematoxylin and eosin staining of transverse sections of the heart of E11.5 embryos. The ventricular walls of *Odr4*$^{gt/gt}$ hearts appear thinner and more sparse compared to controls, but because of the difference in size, and thus perhaps age, a comparison is difficult to make. *(C)* At E10.5, vitelline vessels (yellow arrowheads) form a visible network throughout the yolk sac of control embryos, but are not visible in *Odr4*$^{gt/gt}$ mutants. *(D)* Whole mount staining of CD31 *Odr4*$^{+/+}$ and *Odr4*$^{gt/gt}$ embryos at E10.5.

Figure 5

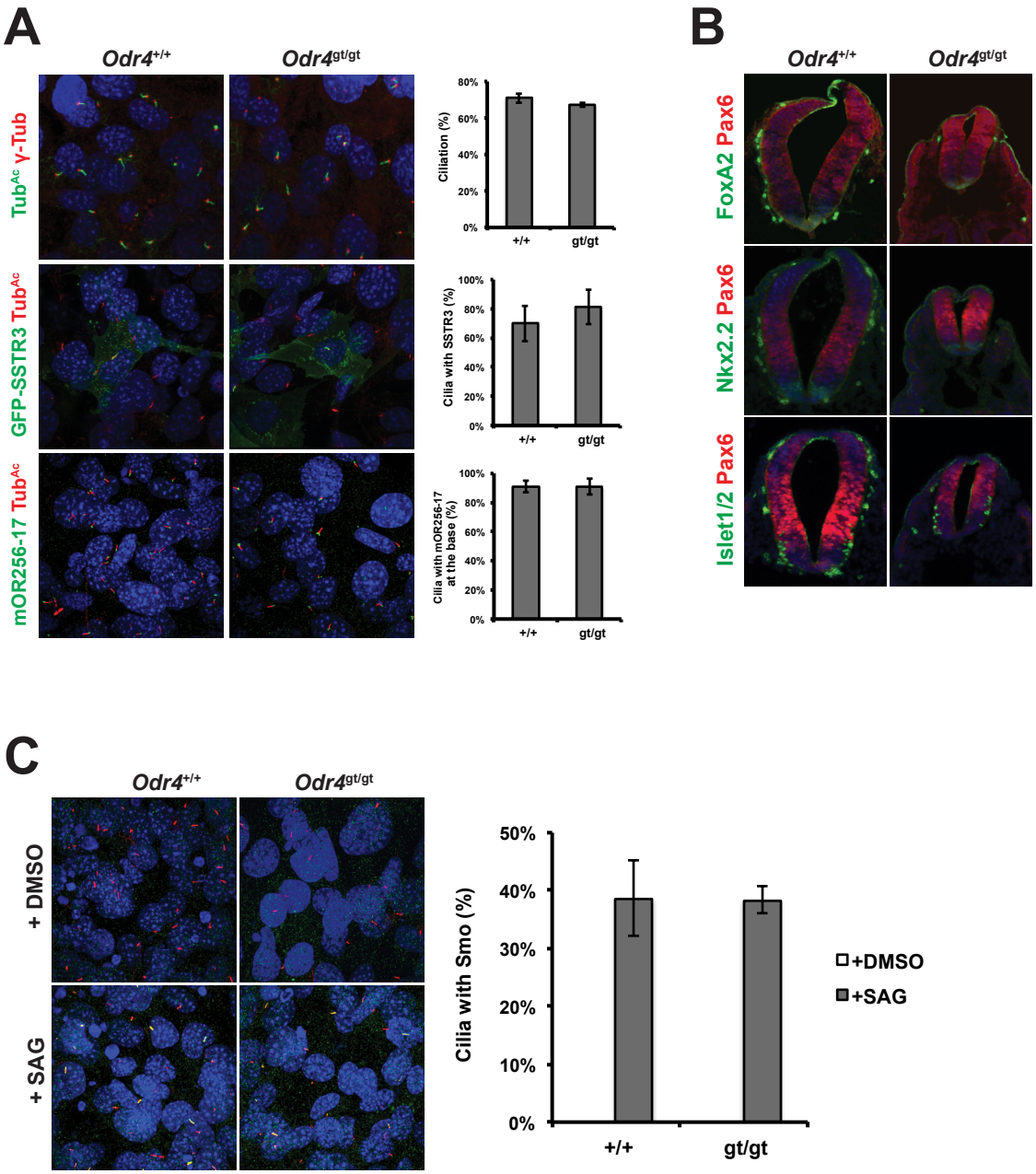
A
Odr4+/+
Odr4gt/gt
TubAc γ-Tub
GFP-SSTR3 TubAc
mOR256-17 TubAc
Ciliation (%)
Cilia with SSTR3 (%)
Cilia with mOR256-17 at the base (%)
80%
60%
40%
20%
0%
100%
+/+
gt/gt
B
Odr4+/+
Odr4gt/gt
FoxA2 Pax6
Nkx2.2 Pax6
Islet1/2 Pax6
C
Odr4+/+
Odr4gt/gt
+ DMSO
+ SAG
Cilia with Smo (%)
50%
40%
30%
20%
10%
0%
+/+
gt/gt
+DMSO
+SAG

Figure 5. Odr4 is not required for ciliogenesis or Shh signaling

(A). Immunofluorescence of cilia and ciliary proteins in *Odr4*$^{+/+}$ and *Odr4*$^{gt/gt}$ MEFs with quantification to the right. Error bars represent the SEM. Top panels: cilia are identified with acetylated tubulin (green) and γ-tubulin (red) to mark the basal body. Middle panels: transiently expressed EGFP-SSTR3 (green) localizes to cilia marked with acetylated tubulin (red). Bottom panels: mOR256-17 (green) localizes to the base of cilia proximal to the axoneme (marked with acetylated tubulin, red). *(B)* Localization of Smo (green) to cilia (marked with acetylated tubulin, red) upon treatment with SAG or DMSO in *Odr4*$^{+/+}$ and *Odr4*$^{gt/gt}$ MEFs. Quantification to the right with error bars representing the SEM. *(C)* Immunofluorescence of Fox2A (green), Nkx2.2 (green), Islet1/2 (green)and Pax6 (red) in transverse sections of the neural tube in *Odr4*$^{g+/+}$ and *Odr4*$^{gt/gt}$ E9.5 embryos. In all panels, nuclei are stained with DAPI.

Figure 6

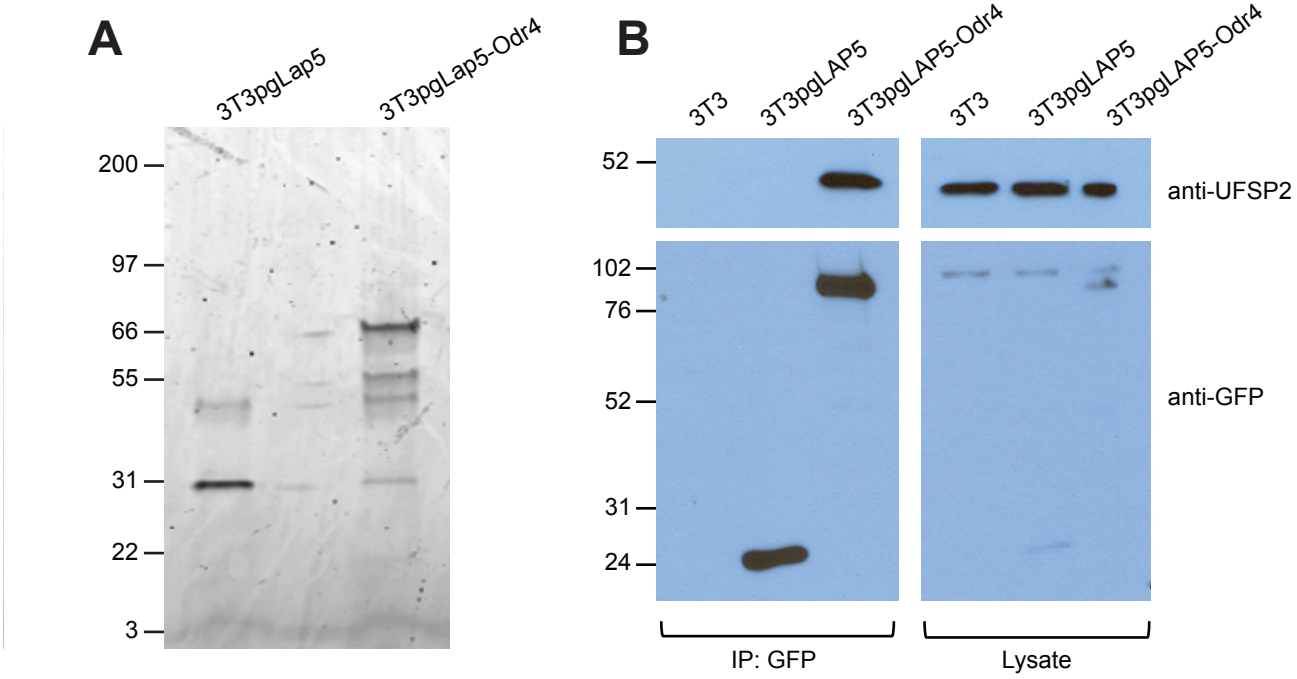
A
3T3pgLap5
3T3pgLap5-Odr4
200
97
66
55
31
22
3
B
3T3
3T3pgLAP5
3T3pgLAP5-Odr4
3T3
3T3pgLAP5
3T3pgLAP5-Odr4
52
anti-UFSP2
102
76
52
anti-GFP
31
24
IP: GFP
Lysate

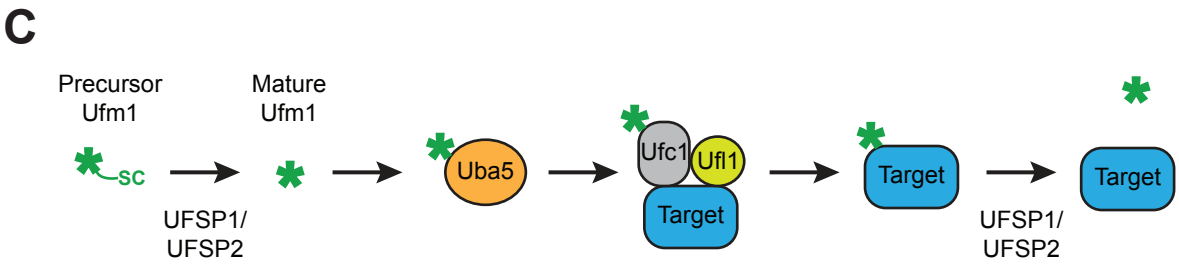
C
Precursor Ufm1
Mature Ufm1
SC
UFSP1/ UFSP2
Uba5
Ufc1
Ufl1
Target
Target
UFSP1/ UFSP2
Target

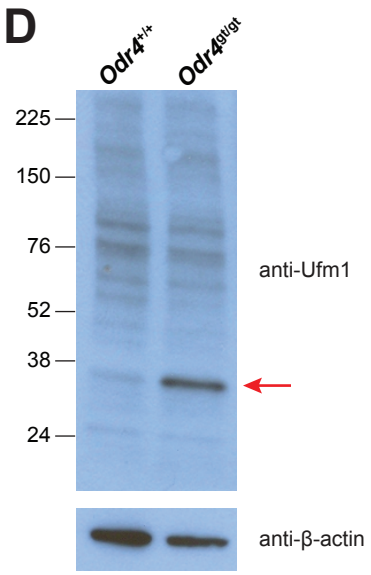
D
Odr4+/+
Odr4gt/gt
225
150
76
52
38
24
anti-Ufm1
anti-β-actin

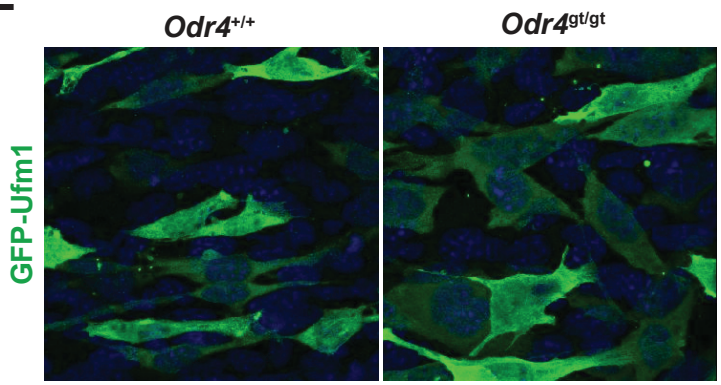
E
Odr4+/+
Odr4gt/gt
GFP-Ufm1

Figure 6. Odr4 physically interacts with UfSP2

(A) SYPRO ruby staining of 3T3pgLAP5 and 3T3pgLAP5-Odr4 cells that were purified and analyzed by mass spectrometry. *(B)* Immunoprecipitation of GFP (left) and whole cell lysates (right) of indicated cell lines, blotted with anti-UFSP2 antibody (top) or anti-GFP antibody (bottom). *(C)* Schematic of the Ufm1-conjugation pathway. The precursor form of Ufm1 (green asterisk) contains a C-terminal serine and cysteine, which are cleaved by UFSP1 and UFSP2 to create the mature form of Ufm1. Similar to ubiquitination, mature Ufm1 is conjugated to its target protein through a serious of enzymatic reactions involving Uba5, Ufc1, and Ufl1. UFSP1 and UFSP2 also function to remove Ufm1 from the target protein. *(D)* Whole cell lysates from *Odr4*$^{gt/gt}$ and *Odr4*$^{+/+}$ MEFs were probed with anti-Ufm1 antibodies. Arrow indicates an unidentified Ufm1-associated protein in control, but not *Odr4*$^{gt/gt}$ MEFs. (*E)* Transient expression of EGFP-Ufm1 in *Odr4*$^{gt/gt}$ and *Odr4*$^{+/+}$ MEFs.

Table 2. Mass Spectrometry results from Odr4 purification

Gene	Description	Molecular Weight	Odr4LAP peptides	LAP peptides	Odr4LAP % coverage	LAP % coverage
ODR4	Protein odr-4 homolog	50 kDa	37	3	44.5%	4.9%
UFSP2	Ufm1-specific protease 2	53 kDa	34	3	52.7%	5.2%
FAR1	Fatty acyl-CoA reductase 1	59 kDa	6	0	12.0%	0.0%
SLC25A11	Mitochondrial 2-oxoglutarate/ malate carrier protein	34 kDa	4	0	14.6%	0.0%
TXNRD1	Thioredoxin reductase 1, cytoplasmic	67 kDa	4	0	3.8%	0.0%
SQRDL	Sulfide:quinone oxidoreductase, mitochondrial	50 kDa	5	1	13.8%	2.2%
SLC25A3	Phosphate carrier protein, mitochondrial	40 kDa	6	2	10.1%	2.2%
PRDX1	Peroxiredoxin-1	22 kDa	20	16	37.7%	36.2%
CACNA1D	Voltage-dependent L-type calcium channel subunit α-1D	247 kDa	3	0	0.4%	0.0%
NPAS3	Neuronal PAS domain-containing protein 3	100 kDa	3	0	2.7%	0.0%
SFXN3	Sideroflexin-3	35 kDa	3	0	11.8%	0.0%
RBMX	RNA-binding motif protein, X chromosome	42 kDa	3	0	9.0%	0.0%
DYSF	Dysferlin	238 kDa	3	0	1.3%	0.0%
ESRP2	Epithelial splicing regulatory protein 2	77 kDa	3	0	4.0%	0.0%
VCL	Vinculin	117 kDa	13	10	12.1%	9.6%
SLC25A12	Calcium-binding mitochondrial carrier protein Aralar1	75 kDa	5	2	6.8%	1.8%
SYNE2	Nesprin-2	783 kDa	4	1	0.4%	0.0%
ATAD3	ATPase family AAA domain-containing protein 3	67 kDa	3	0	5.3%	0.0%
PHGDH	D-3-phosphoglycerate dehydrogenase	57 kDa	8	5	11.3%	9.0%
ANXA2	Annexin A2	39 kDa	22	19	27.4%	29.2%

Figure 7

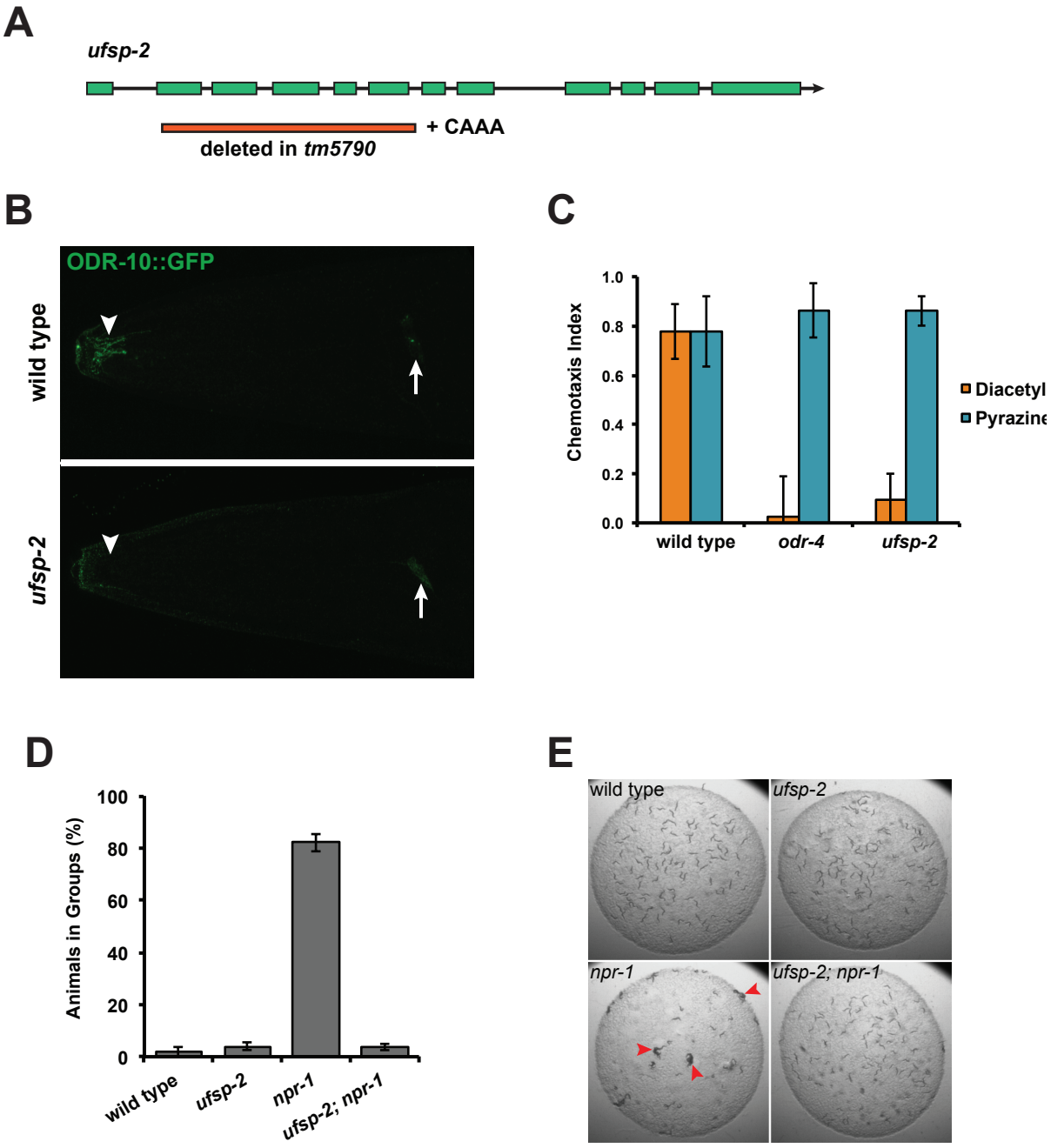
A
ufsp-2
+ CAAA
deleted in tm5790
B
ODR-10::GFP
wild type
ufsp-2
C
Chemotaxis Index
1.0
0.8
0.6
0.4
0.2
0.0
wild type
odr-4
ufsp-2
Diacetyl
Pyrazine
D
Animals in Groups (%)
100
80
60
40
20
0
wild type
ufsp-2
npr-1
ufsp-2; npr-1
E
wild type
ufsp-2
npr-1
ufsp-2; npr-1

Figure 7. *ufsp-2* mutants phenocopy *odr-4* mutants in *C. elegans*

(A) Schematic of the *ufsp-2* gene in *C. elegans.* The *ufsp-2(tm5790)* allele consists of a 4 bp insertion (CAAA) at the site of a 1000 bp deletion spanning exons 2-6. *(B)* Localization of ODR-10::GFP in wild type and *ufsp-2* mutants. Arrowhead indicates AWA sensory cilia. Arrow indicates AWA cell body. *(C)* Chemotaxis responses to diacetyl and pyrazine in wild type, *odr-4*, and *ufsp-2* mutants. *(D)* Quantification of group feeding behavior of wild type, *ufsp-2*, *npr-1*, and *ufsp-2; npr-1* mutants. *(E)* Still images of ~100 animals of the indicated genotype feeding on a bacterial lawn after 1 hour. Red arrowheads point to prominent examples of group feeding.

Discussion

How the cell localizes specific proteins to specialized cellular compartments such as the cilium is of great interest to the Reiter lab. Inspired by the finding that *odr-4*, an otherwise uncharacterized gene, is required for the localization of a subset of olfactory receptors to cilia in *C. elegans*, we investigated the function of *Odr4* in mammals. *Odr4* is required for embryonic development and is ubiquitously expressed. Cells lacking Odr4 do not display obvious ciliation defects nor do mutant embryos display phenotypes typical of ciliary mutants (8). Odr4 physically interacts with UfSP2, a protease for the newly identified posttranslational modification, Ufm1. In *C. elegans*, like *odr-4*, *ufsp-2* is required for the localization of ODR-10 to the cilium, further suggesting that these genes have similar functions or may function in the same pathway. In mammals, *Odr4* may be involved in the trafficking of GPCRs as in *C. elegans,* or it may function in the Ufm1 pathway. Whether GPCR localization and Ufm1 modification are connected is unknown, but these processes provide starting points from which to further examine *Odr4*.

Odr4 is essential for embryonic development, but the primary cause of death of *Odr4* mutants remains unknown. *Odr4* mutants display a nonspecific growth phenotype, and display possible indications of cardiovascular defects (paleness, reduced vitelline vessels, and occasional pericardial edema), but these defects have not been well defined. Additionally, adult $Odr4^{fl/fl}$ animals that express a ubiquitously expressed inducible Cre (*UBC-Cre-ER*^{T2}) die without overt causes upon treatment with tamoxifen, (personal communication with Christian Vaisse), demonstrating a requirement for *Odr4* in both embryonic and adult life. Mutants deficient in the Ufm1-activating enzyme Uba5 die at approximately the same time as *Odr4* mutants, with defects in the differentiation of megakaryocytes and erythrocytes (107). Similarly, in mutants deficient in the Ufm1 E3 ligase Ufl1, erythrocyte differentiation and hematopoietic stem cell survival are impaired (108). If *Odr4* plays a role in the Ufm1 pathway, *Odr4* mutants may display

phenotypes similar to *Uba5* and *Ufl1* mutants. Examination of erythroid differentiation in *Odr4* mutants may reveal specific defects and implicate Odr4 in this process.

In vitro, Odr4 was not required for the localization of the select proteins that were examined. Experiments in which *Odr4* is deleted in the olfactory epithelium (*Odr4*$^{n/fl}$ *Foxg1-Cre*) followed by immunostaining for ORs, may more closely resemble the system in *C. elegans*, and thus may recapitulate the phenotype. Furthermore, perturbation of OR localization to the cilium may lead to defects in olfactory receptor choice thus OSN maturation. Upon expression of a single OR, a feedback mechanism prevents the expression of additional ORs (115). Defects in OR expression or function can lead to olfactory receptor choice switching and a loss of OSN maturation (116, 117). It will be interesting to see if defects in OR ciliary localization have the same effects. If so, a more dramatic phenotype in *Odr4* mutants may be observed, an expansion of immature OSNs, and a reduction of mature OSNs.

Whether or not *Odr4* affects the localization of olfactory receptors, *Odr4* may affect the localization of other GPCRs to the cilium or cell surface. *Odr4* is ubiquitously expressed and required for viability, thus *Odr4* likely plays critical roles extending beyond the olfactory epithelium. If an erythroid, circulation, or cardiovascular defect is uncovered in *Odr4* mutants, examining candidate GPCR localization in the affected tissue may be fruitful.

The relationship between Odr4 and the Ufm1 pathway has not yet been determined. Odr4 itself may be a substrate for Ufm1. Alternatively, it may act as a regulator of Ufm1 conjugation. Recently, it has been shown that UfSP2 prevents the ufmylation of ASC1. c20orf116, itself an Ufm1 substrate, promotes ASC1 ufmylation (109). It will be interesting to test whether Odr4 also prevents ufmylation of ASC1 or if Odr4 antagonizes the actions of UfSP2. In addition to the core E1, E2, E3 conjugating enzymes and UfSP1/2, ufmylation is likely tightly controlled by other

regulatory proteins. Thus the auxiliary machinery that determines which proteins are ufmylated, when, and for how long, will be intriguing to uncover. Perhaps like c20orf116, Odr4 contributes to these functions.

Do the putative functions of Odr4 in OR trafficking and ufmylation overlap? One parsimonious hypothesis is that ORs are modified by Ufm1, and this modification facilitates trafficking to the cilium through an Odr4 dependent mechanism. As Odr4 localizes to intracellular membranes, perhaps the ER, and Ufm1 conjugating machinery also associate with the ER, Ufm1 and Odr4 may be involved the folding of nascent ORs or correcting misfolded ERs before they are trafficked to the cilium. Similar to its role in ASC1, poly-Ufm1 chains may even serve scaffolds on ORs during their maturation processing, concentrating chaperones to the OR of interest. Thus far, odorant receptors or GPCRs have not been definitively identified as Ufm1 substrates. Mass spectrometry from immunoprecipitation of Flag-His-Ufm1 identified ORFR561 (Olfactory receptor 561) (109), and we identified Gpr115, Olfr1383, and Olfr448 as potential candidates for ufmylation. Determining whether these and other GPCRs are Ufm1 substrates should be actively pursued as the role of Ufm1 likely depends on its substrates.

While Odr4 physically interacts with UfSP2, it may have functions unrelated to ufmylation. We and others have found that in *C. elegans*, *ufsp-2* is required for the localization of ODR-10, as is *odr-4* (111). However, mutations in other Ufm1 components do not affect ODR-10 localization, suggesting that the ability to conjugate Ufm1 is not necessary for this process (111). Thus, the function of UfSP-2 with regards to ODR-10 is distinct from its function in the Ufm1 pathway. Likewise, Odr4 may have functions entirely separate from the Ufm1 pathway, but still related to UfSP2 and GPCR transport.

To gain better insight into Odr4 function, a well-defined and specific phenotype of *Odr4* mutants will need to be uncovered. If Odr4 is indeed required for the localization of GPCRs to cilia or the cell surface in mammals, how this process is achieved will be an imminent question. Odr4 may act through the Ufm1 conjugation system to target proteins to their cellular destinations, act with other chaperones, or act independently. Although little is known about this novel gene, it is evident and promising that *Odr4* plays a critical role in mammalian development, potentially affecting a multitude of systems.

Materials and Methods

Mouse husbandry

Mouse protocols were performed with approval from the Institutional Animal Care and Use Committee (IACUC) at the University of California, San Francisco. *Odr4*$^{gt/-}$ animals were maintained in a C57BL/6J background, except when they were outcrossed to CD1 mice for two generations to create the mixed B6J/CD1 background. To generate the Odr4 conditional allele (*Odr4*^{fl}), *Odr4*$^{gt/+}$ mice were crossed to mice ubiquitously expressing FLPe recombinase (*Tg(ACTFLPe)9205Dym/J*). To generate the Odr4 null allele (*Odr4*^{n}), *Odr4*$^{fl/fl}$ mice were crossed to mice ubiquitously expressing Cre recombinase (*Tg(ACTB-cre)2Mrt/J*). Genotyping for Odr4 used a common forward primer and allele specific reverse primers. Primer sequences are: Odr4Fwd, gcagtcctatgggaggtgaa; Odr4wtRev, gcagtcctatgggaggtgaa; Odr4gtRev, ccacaacgggttcttctgtt; Odr4floxRev; ACGAAGTTATCTCGACGAAGTTCC; and Odr4nullRev, gcggatttctgagttcaagg. The Foxg1-Cre mouse has been previously described (118).

Mouse experiments

Timed matings were used to generate animals at a given stage. The embryos were dissected in cold PBS with 10% FBS, fixed in 4% paraformaldehyde at 4°C for 1 hour, then washed in PBS three times and imaged on a Zeiss Discovery V12 steREO microscope. LacZ staining of whole embryos was performed as previously described, except that samples were incubated in X-gal solution at 37°C instead of room temperature (119). Hematoxylin and eosin staining was performed on 12 μm paraffin sections according to standard procedures. Whole mount IHC was performed using rat anti-C31 (BD Biosciences, 1:200) as previously described (120).

Cell culture and Immunofluorescence

To generate *Odr4* embryonic fibroblasts, embryos at E10.5 were harvested and disaggregated into cell suspensions by pipetting. The cells were immortalized with SV40 large T-antigen and clonal lines were isolated. Cells were maintained in DMEM+15% FBS. To induce ciliation, cells were grown to confluency and starved for 24 hours in OptiMEM. For transient gene expression, cells were transfected at 70% confluency using either Jetprime or Fugene 6 transfection reagents. Expression of the transgene was assessed 24 or 48 hours post-transfection. pEGFP-SSTR3 was a gift from K. Mykytyn, and pGFP-Ufm1 was a gift from M. Komatsu. To assess the ciliary localization of Smo, MEFs were grown to confluency and starved in OptiMEM for 24 hours, followed by treatment with DMSO or 200nM SAG for 24 hours.

Immunofluorescence of cultured cells was performed on cells grown to confluency on coverslips in 24 well plates. The cells were rinsed once in cold PBS and fixed in 4% PFA for 5 minutes at room temperature, followed by 3 minutes in cold methanol at -20°C. The samples were washed 3X in PBS, and submerged in blocking solution (2.5% BSA, 0.1% Triton X-100, 0.03% sodium azide in PBS) for 1 hour. The samples were incubated in primary antibody for 1.5 hours at room temperature, washed 3X in PBS, incubated in secondary antibody for 1 hour at room temperature, washed in 3X PBS, and mounted with Gelvatol.

For neural tube analysis, E9.5 embryos were dissected in cold PBS with 10% FBS. After fixation in 4% paraformaldehyde for 1 hour at 4°C, embryos were washed 3X in PBS, and equilibrated in 30% sucrose overnight at 4°C. The samples were embedded in OCT, frozen in a dry ice/ethanol bath, and stored at -80°C. 12 μm transverse sections of the neural tube were incubated in blocking solution (10% goat serum, 0.1% Triton-X 100 in PBS) and stained previously described (9, 42). The following antibodies were used: rabbit α-Pax6 (1:100, Covance), mouse α-Nkx2.2 (1:20), mouse α-FoxA2 (1:20), and mouse α-Islet1/2 (1:20, Developmental Studies Hybridoma Bank).

Immunoprecipitation and Western Blot

For immunoprecipitation, 3T3pgLap5-Odr4 cells and control cells were grown on 10cm plates to confluency, and lysed in 50mM Tris pH 7.4, 1% NP-40, 150mM NaCl and protease inhibitors (Calbiochem, 539134). Following centrifugation, 25 ul of GFP-Trap beads (Chromotek, gta-20) were added to 1 mg total lysate and incubated for 2 hours at 4°C. GFP-trap beads were washed three times with lysis buffer, and boiled in Laemmli sample buffer. Western blots were performed according to standard protocols. The following primary antibodies were used: rabbit anti-Odr4 (Sigma, 1:500), rabbit anti-UfSP2 (Proteintech, 1:1500), rabbit anti-Ufm1 (Proteintech 1:1000), goat anti-GFP (Rockland, 1:1000), and rabbit anti-β-actin (Sigma, 1:5000).

Mass spectrometry

Full length mouse Odr4 was amplified (Fwd primer: ATG GGA AGA ACC TAC ATT GTA GAA, Rev primer: ATC, ACT, GAA, GTA, ATG GAA, GGA, GAT), cloned into pCR8/GW, then recombined into pGLAP5 using LR clonase II. 3T3pgLAP5-Odr4 stable cell lines were created by co-transfecting pgLAP5-Odr4 and pOG44-FlpE (Invitrogen) into 3T3/Flp-In cells (Invitrogen). Colonies that had stable expression of Odr4 were selected for and maintained in DMEM + 10% calf serum + 150 µg/ml hygromycin B. LAP purification was performed as previously described using fifty 15-cm plates each of 3T3pgLAP5-Odr4 stable cells and control 3T3pgLAP5 cells, GFP-trap beads (Chromotek, gta-20) were used instead of anti-GFP antibodies (121). Purified proteins were resolved on a 4%–15% Tris-glycine gradient gel and stained with SYPRO Ruby (Invitrogen). Control and 3T3pgLAP5-Odr4 lanes were excised, divided into three gel slices each, and subjected to tandom mass spectrometry analysis.

***C. elegans* strains**

C. elegans stains were maintained on OP-50 seeded plates under standard conditions. The *ufsp-2* mutant F38A5.1*(tm5790)*IV was generated by the National BioResource Project, Tokyo, Japan, which is part of the International C. elegans Gene Knockout Consortium. F38A5.1*(tm5790)*IV was outcrossed to wild type N2 six times. Double mutants and transgenic animals were generated by standard mating procedures. The following strains were used: N2 wild type, MT5300 *odr-4(n2144)* III, CX3344 N2; kyIs53[*odr-10*::GFP], DA609 *npr-1(ad609)* X, KQ2513 *ufsp-2(tm5790)* IV, KQ2527; *ufsp-2(tm5790)* IV; kyIs53[*odr-10*::GFP], and KQ2526, *ufsp-2(tm5790)* IV; *npr-1(ad609)* X.

Chemotaxis assay

Chemotaxis assays were performed as previously described (7). Odorants were diluted in ethanol at 1:1000 for diacetyl and 10 mg/ml for pyrazine. Assays were performed at least six times using approximately 100 animals per assay. The chemotaxis index was calculated as (# of animals at odorant – # of animals at control (ethanol)) / total # of animals.

Social feeding assay

Social feeding assays were performed essentially as previously described (114, 122). Approximately 100 synchronized young adult (not gravid) animals were picked onto a 200 ul bacterial lawn seeded the day before. After one hour at room temperature, social feeding was assessed. Animals in contact with two or more animals covering at least 50% of their body length were considered in a group. Assays were performed on four separate occasions.

Protein localization in *C. elegans*

Translational GFP fusion proteins were expressed in the genetic background of interest. In the case of visualizing ODR-10::GFP, the fluorescent signal was amplified by immunostaining against GFP following the protocol for Antibody Staining of Formaldehyde-fixed Worms by Gary

Ruvkun and Michael Finney (123). Antibodies used were goat anti-GFP at 1:1000 (Rockland 600-101-215) and donkey α-goat Alexa Fluor 488 at 1:250 (Invitrogen A-11055).

Chapter 4: Conclusion

In these projects we have studied the genetic interactions and functions of ciliary genes in both *C. elegans* and mice. We report that synergistic interactions between genes of the MKS complex, NPHP complex, and BBSome are largely conserved between these species. We have also started to analyze the mammalian ortholog of Odr4, and found unexpectedly that it associates with the Ufm1 post-translational modification system.

What might synergistic genetic interactions reveal about ciliary biology? Single mutations of MKS complex components in mice result in polydactyly restricted to the hindlimb. Only when combined with an additional mutation of an NPHP complex gene or a BBSome gene does polydactyly extend to the forelimb. This suggests that the requirement of transition zone proteins in forelimb cilia is distinct from the requirement of transition proteins in hindlimb cilia. Different types of cilia are present on different tissues, but whether the transition zone also differs has not been explored. The transition zone may vary in composition or function, and certain types of cilia may have different requirements for proper transition zone function. Conversely, distinct transition zones may distinguish otherwise similar cilia, such as forelimb and hindlimb cilia. Variation in the transition zone may also exist in the cilia of *C. elegans*, as not all cilia are disrupted in *mks/nphp* double mutants. While this may reflect incomplete penetrance, different amphid neurons may have distinct responses to the loss of transition zone proteins. Thus, tissue-specific analysis of transition zone genes and transition zone gene interactions will shed light on the possibility different types of transition zones and whether this affects human ciliopathies

The role of Odr4 in mammals has not yet been defined, but clues from mutant animals and biochemical interactors have generated several possibilities. Odr4 binds to UfSP2, and mutants

of both these genes in *C. elegans* do not traffic ODR-10 to the cilium. However, recent work suggests that ODR-10 ciliary localization does not require ufmylation (111). Thus, if Odr4 works with UfSP2 to promote ODR-10 location, it likely does so independently of Ufm1. Alternatively, Odr4 may function with UfSP2 through the Ufm1 conjugation pathway to affect a process other than GPCR localization to the cilium. In either case, it is becoming clear that mammalian Odr4 does not behave exactly as its *C. elegans* ortholog. Mammalian Odr4 may still facilitate GPCR localization to the cilium, but it may also have additional roles in several tissue types.

That genetic interactions between MKS, NPHP, and BBS complexes are conserved in both *C. elegans* and mice demonstrate the importance of these complexes in ciliogenesis. However, how these complexes functionally overlap within the transition zone has yet to be determined. Similarly, the role of many specialized proteins affecting ciliary function in a highly specific manner, such as Odr4 has yet to be uncovered. That is for another PhD.

Chapter 5: References

1. Goetz SC, Anderson KV. The primary cilium: a signalling centre during vertebrate development. Nat Rev Genet. 2010;11(5):331-44.
2. Singla V, Reiter JF. The primary cilium as the cell's antenna: signaling at a sensory organelle. Science. 2006;313(5787):629-33.
3. Hildebrandt F, Benzing T, Katsanis N. Ciliopathies. N Engl J Med. 2011;364(16):1533-43.
4. Waters AM, Beales PL. Ciliopathies: an expanding disease spectrum. Pediatr Nephrol. 2011;26(7):1039-56.
5. Bargmann CI, Hartwieg E, Horvitz HR. Odorant-selective genes and neurons mediate olfaction in C. elegans. Cell. 1993;74(3):515-27.
6. Troemel ER, Chou JH, Dwyer ND, Colbert HA, Bargmann CI. Divergent seven transmembrane receptors are candidate chemosensory receptors in C. elegans. Cell. 1995;83(2):207-18.
7. Dwyer ND, Troemel ER, Sengupta P, Bargmann CI. Odorant receptor localization to olfactory cilia is mediated by ODR-4, a novel membrane-associated protein. Cell. 1998;93(3):455-66.
8. Huangfu D, Liu A, Rakeman AS, Murcia NS, Niswander L, Anderson KV. Hedgehog signalling in the mouse requires intraflagellar transport proteins. Nature. 2003;426(6962):83-7.
9. Dowdle WE, Robinson JF, Kneist A, Sirerol-Piquer MS, Frints SG, Corbit KC, et al. Disruption of a ciliary B9 protein complex causes Meckel syndrome. Am J Hum Genet. 2011;89(1):94-110.
10. Roberson EC, Dowdle WE, Ozanturk A, Garcia-Gonzalo FR, Li C, Halbritter J, et al. TMEM231, mutated in orofaciodigital and Meckel syndromes, organizes the ciliary transition zone. J Cell Biol. 2015;209(1):129-42.
11. Garcia-Gonzalo FR, Corbit KC, Sirerol-Piquer MS, Ramaswami G, Otto EA, Noriega TR, et al. A transition zone complex regulates mammalian ciliogenesis and ciliary membrane composition. Nat Genet. 2011;43(8):776-84.
12. Morell RJ, Brewer CC, Ge D, Snieder H, Zalewski CK, King KA, et al. A twin study of auditory processing indicates that dichotic listening ability is a strongly heritable trait. Hum Genet. 2007;122(1):103-11.
13. Adato A, Kalinski H, Weil D, Chaib H, Korostishevsky M, Bonne-Tamir B. Possible interaction between USH1B and USH3 gene products as implied by apparent digenic deafness inheritance. Am J Hum Genet. 1999;65(1):261-5.
14. Floeth M, Bruckner-Tuderman L. Digenic junctional epidermolysis bullosa: mutations in COL17A1 and LAMB3 genes. Am J Hum Genet. 1999;65(6):1530-7.
15. Vincent S, Planells R, Defoort C, Bernard MC, Gerber M, Prudhomme J, et al. Genetic polymorphisms and lipoprotein responses to diets. Proc Nutr Soc. 2002;61(4):427-34.
16. Hichri H, Stoetzel C, Laurier V, Caron S, Sigaudy S, Sarda P, et al. Testing for triallelism: analysis of six BBS genes in a Bardet-Biedl syndrome family cohort. Eur J Hum Genet. 2005;13(5):607-16.
17. Abu-Safieh L, Al-Anazi S, Al-Abdi L, Hashem M, Alkuraya H, Alamr M, et al. In search of triallelism in Bardet-Biedl syndrome. Eur J Hum Genet. 2012;20(4):420-7.
18. Nakane T, Biesecker LG. No evidence for triallelic inheritance of MKKS/BBS loci in Amish Mckusick-Kaufman syndrome. Am J Med Genet A. 2005;138(1):32-4.
19. Katsanis N, Eichers ER, Ansley SJ, Lewis RA, Kayserili H, Hoskins BE, et al. BBS4 is a minor contributor to Bardet-Biedl syndrome and may also participate in triallelic inheritance. Am J Hum Genet. 2002;71(1):22-9.
20. Katsanis N, Ansley SJ, Badano JL, Eichers ER, Lewis RA, Hoskins BE, et al. Triallelic inheritance in Bardet-Biedl syndrome, a Mendelian recessive disorder. Science. 2001;293(5538):2256-9.

21. Garcia-Gonzalo FR, Reiter JF. Scoring a backstage pass: mechanisms of ciliogenesis and ciliary access. J Cell Biol. 2012;197(6):697-709.
22. Rosenbaum JL, Witman GB. Intraflagellar transport. Nat Rev Mol Cell Biol. 2002;3(11):813-25.
23. Jauregui AR, Nguyen KC, Hall DH, Barr MM. The Caenorhabditis elegans nephrocystins act as global modifiers of cilium structure. J Cell Biol. 2008;180(5):973-88.
24. Gilula NB, Satir P. The ciliary necklace. A ciliary membrane specialization. J Cell Biol. 1972;53(2):494-509.
25. Perkins LA, Hedgecock EM, Thomson JN, Culotti JG. Mutant sensory cilia in the nematode Caenorhabditis elegans. Dev Biol. 1986;117(2):456-87.
26. Garcia-Gonzalo FR, Corbit KC, Sirerol-Piquer MS, Ramaswami G, Otto EA, Noriega TR, et al. A transition zone complex regulates mammalian ciliogenesis and ciliary membrane composition. Nat Genet. 2011;43(8):776-84.
27. Dowdle WE, Robinson JF, Kneist A, Sirerol-Piquer MS, Frints SG, Corbit KC, et al. Disruption of a ciliary B9 protein complex causes Meckel syndrome. Am J Hum Genet. 2011;89(1):94-110.
28. Chih B, Liu P, Chinn Y, Chalouni C, Komuves LG, Hass PE, et al. A ciliopathy complex at the transition zone protects the cilia as a privileged membrane domain. Nat Cell Biol. 2011;14(1):61-72.
29. Sang L, Miller JJ, Corbit KC, Giles RH, Brauer MJ, Otto EA, et al. Mapping the NPHP-JBTS-MKS protein network reveals ciliopathy disease genes and pathways. Cell. 2011;145(4):513-28.
30. Roberson EC, Dowdle WE, Ozanturk A, Garcia-Gonzalo FR, Li C, Halbritter J, et al. TMEM231, mutated in orofaciodigital and Meckel syndromes, organizes the ciliary transition zone. J Cell Biol. 2015;209(1):129-42.
31. Williams CL, Winkelbauer ME, Schafer JC, Michaud EJ, Yoder BK. Functional redundancy of the B9 proteins and nephrocystins in Caenorhabditis elegans ciliogenesis. Mol Biol Cell. 2008;19(5):2154-68.
32. Williams CL, Masyukova SV, Yoder BK. Normal ciliogenesis requires synergy between the cystic kidney disease genes MKS-3 and NPHP-4. J Am Soc Nephrol. 2010;21(5):782-93.
33. Williams CL, Li C, Kida K, Inglis PN, Mohan S, Semenec L, et al. MKS and NPHP modules cooperate to establish basal body/transition zone membrane associations and ciliary gate function during ciliogenesis. J Cell Biol. 2011;192(6):1023-41.
34. Winkelbauer ME, Schafer JC, Haycraft CJ, Swoboda P, Yoder BK. The C. elegans homologs of nephrocystin-1 and nephrocystin-4 are cilia transition zone proteins involved in chemosensory perception. J Cell Sci. 2005;118(Pt 23):5575-87.
35. Liu L, Zhang M, Xia Z, Xu P, Chen L, Xu T. Caenorhabditis elegans ciliary protein NPHP-8, the homologue of human RPGRIP1L, is required for ciliogenesis and chemosensation. Biochem Biophys Res Commun. 2011;410(3):626-31.
36. Nachury MV, Loktev AV, Zhang Q, Westlake CJ, Peranen J, Merdes A, et al. A core complex of BBS proteins cooperates with the GTPase Rab8 to promote ciliary membrane biogenesis. Cell. 2007;129(6):1201-13.
37. Berbari NF, Lewis JS, Bishop GA, Askwith CC, Mykytyn K. Bardet-Biedl syndrome proteins are required for the localization of G protein-coupled receptors to primary cilia. Proc Natl Acad Sci U S A. 2008;105(11):4242-6.
38. Jin H, White SR, Shida T, Schulz S, Aguiar M, Gygi SP, et al. The conserved Bardet-Biedl syndrome proteins assemble a coat that traffics membrane proteins to cilia. Cell. 2010;141(7):1208-19.
39. Blacque OE, Reardon MJ, Li C, McCarthy J, Mahjoub MR, Ansley SJ, et al. Loss of C. elegans BBS-7 and BBS-8 protein function results in cilia defects and compromised intraflagellar transport. Genes Dev. 2004;18(13):1630-42.

40. Leitch CC, Zaghloul NA, Davis EE, Stoetzel C, Diaz-Font A, Rix S, et al. Hypomorphic mutations in syndromic encephalocele genes are associated with Bardet-Biedl syndrome. Nat Genet. 2008;40(4):443-8.
41. Zhang Y, Seo S, Bhattarai S, Bugge K, Searby CC, Zhang Q, et al. BBS mutations modify phenotypic expression of CEP290-related ciliopathies. Hum Mol Genet. 2014;23(1):40-51.
42. Reiter JF, Skarnes WC. Tectonic, a novel regulator of the Hedgehog pathway required for both activation and inhibition. Genes Dev. 2006;20(1):22-7.
43. Swoboda P, Adler HT, Thomas JH. The RFX-type transcription factor DAF-19 regulates sensory neuron cilium formation in C. elegans. Mol Cell. 2000;5(3):411-21.
44. Emery P, Durand B, Mach B, Reith W. RFX proteins, a novel family of DNA binding proteins conserved in the eukaryotic kingdom. Nucleic Acids Res. 1996;24(5):803-7.
45. Chen N, Mah A, Blacque OE, Chu J, Phgora K, Bakhoum MW, et al. Identification of ciliary and ciliopathy genes in Caenorhabditis elegans through comparative genomics. Genome Biol. 2006;7(12):R126.
46. Phirke P, Efimenko E, Mohan S, Burghoorn J, Crona F, Bakhoum MW, et al. Transcriptional profiling of C. elegans DAF-19 uncovers a ciliary base-associated protein and a CDK/CCRK/LF2p-related kinase required for intraflagellar transport. Dev Biol. 2011;357(1):235-47.
47. Colosimo ME, Brown A, Mukhopadhyay S, Gabel C, Lanjuin AE, Samuel AD, et al. Identification of thermosensory and olfactory neuron-specific genes via expression profiling of single neuron types. Curr Biol. 2004;14(24):2245-51.
48. Ansley SJ, Badano JL, Blacque OE, Hill J, Hoskins BE, Leitch CC, et al. Basal body dysfunction is a likely cause of pleiotropic Bardet-Biedl syndrome. Nature. 2003;425(6958):628-33.
49. Starich TA, Herman RK, Kari CK, Yeh WH, Schackwitz WS, Schuyler MW, et al. Mutations affecting the chemosensory neurons of Caenorhabditis elegans. Genetics. 1995;139(1):171-88.
50. Craige B, Tsao CC, Diener DR, Hou Y, Lechtreck KF, Rosenbaum JL, et al. CEP290 tethers flagellar transition zone microtubules to the membrane and regulates flagellar protein content. J Cell Biol. 2010;190(5):927-40.
51. Caspary T, Larkins CE, Anderson KV. The graded response to Sonic Hedgehog depends on cilia architecture. Dev Cell. 2007;12(5):767-78.
52. Cevik S, Hori Y, Kaplan OI, Kida K, Toivenon T, Foley-Fisher C, et al. Joubert syndrome Arl13b functions at ciliary membranes and stabilizes protein transport in Caenorhabditis elegans. J Cell Biol. 2010;188(6):953-69.
53. Huang L, Szymanska K, Jensen VL, Janecke AR, Innes AM, Davis EE, et al. TMEM237 is mutated in individuals with a Joubert syndrome related disorder and expands the role of the TMEM family at the ciliary transition zone. Am J Hum Genet. 2011;89(6):713-30.
54. Lee BH, Liu J, Wong D, Srinivasan S, Ashrafi K. Hyperactive neuroendocrine secretion causes size, feeding, and metabolic defects of C. elegans Bardet-Biedl syndrome mutants. PLoS Biol. 2011;9(12):e1001219.
55. Mollet G, Salomon R, Gribouval O, Silbermann F, Bacq D, Landthaler G, et al. The gene mutated in juvenile nephronophthisis type 4 encodes a novel protein that interacts with nephrocystin. Nat Genet. 2002;32(2):300-5.
56. Otto E, Hoefele J, Ruf R, Mueller AM, Hiller KS, Wolf MT, et al. A gene mutated in nephronophthisis and retinitis pigmentosa encodes a novel protein, nephroretinin, conserved in evolution. Am J Hum Genet. 2002;71(5):1161-7.
57. Won J, Marin de Evsikova C, Smith RS, Hicks WL, Edwards MM, Longo-Guess C, et al. NPHP4 is necessary for normal photoreceptor ribbon synapse maintenance and outer segment formation, and for sperm development. Hum Mol Genet. 2011;20(3):482-96.

58. Hildebrandt F, Otto E, Rensing C, Nothwang HG, Vollmer M, Adolphs J, et al. A novel gene encoding an SH3 domain protein is mutated in nephronophthisis type 1. Nat Genet. 1997;17(2):149-53.
59. Konrad M, Saunier S, Heidet L, Silbermann F, Benessy F, Calado J, et al. Large homozygous deletions of the 2q13 region are a major cause of juvenile nephronophthisis. Hum Mol Genet. 1996;5(3):367-71.
60. Parisi MA, Bennett CL, Eckert ML, Dobyns WB, Gleeson JG, Shaw DW, et al. The NPHP1 gene deletion associated with juvenile nephronophthisis is present in a subset of individuals with Joubert syndrome. Am J Hum Genet. 2004;75(1):82-91.
61. Gorden NT, Arts HH, Parisi MA, Coene KL, Letteboer SJ, van Beersum SE, et al. CC2D2A is mutated in Joubert syndrome and interacts with the ciliopathy-associated basal body protein CEP290. Am J Hum Genet. 2008;83(5):559-71.
62. Noor A, Windpassinger C, Patel M, Stachowiak B, Mikhailov A, Azam M, et al. CC2D2A, encoding a coiled-coil and C2 domain protein, causes autosomal-recessive mental retardation with retinitis pigmentosa. Am J Hum Genet. 2008;82(4):1011-8.
63. Tallila J, Jakkula E, Peltonen L, Salonen R, Kestila M. Identification of CC2D2A as a Meckel syndrome gene adds an important piece to the ciliopathy puzzle. Am J Hum Genet. 2008;82(6):1361-7.
64. Davis RE, Swiderski RE, Rahmouni K, Nishimura DY, Mullins RF, Agassandian K, et al. A knockin mouse model of the Bardet-Biedl syndrome 1 M390R mutation has cilia defects, ventriculomegaly, retinopathy, and obesity. Proc Natl Acad Sci U S A. 2007;104(49):19422-7.
65. Awata J, Takada S, Standley C, Lechtreck KF, Bellve KD, Pazour GJ, et al. Nephrocystin-4 controls ciliary trafficking of membrane and large soluble proteins at the transition zone. J Cell Sci. 2014.
66. Manolio TA, Collins FS, Cox NJ, Goldstein DB, Hindorff LA, Hunter DJ, et al. Finding the missing heritability of complex diseases. Nature. 2009;461(7265):747-53.
67. Frazer KA, Murray SS, Schork NJ, Topol EJ. Human genetic variation and its contribution to complex traits. Nat Rev Genet. 2009;10(4):241-51.
68. Bloom JS, Ehrenreich IM, Loo WT, Lite TL, Kruglyak L. Finding the sources of missing heritability in a yeast cross. Nature. 2013;494(7436):234-7.
69. Hoefele J, Wolf MT, O'Toole JF, Otto EA, Schultheiss U, Deschenes G, et al. Evidence of oligogenic inheritance in nephronophthisis. J Am Soc Nephrol. 2007;18(10):2789-95.
70. Beales PL, Badano JL, Ross AJ, Ansley SJ, Hoskins BE, Kirsten B, et al. Genetic interaction of BBS1 mutations with alleles at other BBS loci can result in non-Mendelian Bardet-Biedl syndrome. Am J Hum Genet. 2003;72(5):1187-99.
71. Brenner S. The genetics of Caenorhabditis elegans. Genetics. 1974;77(1):71-94.
72. Culotti JG, Russell RL. Osmotic avoidance defective mutants of the nematode Caenorhabditis elegans. Genetics. 1978;90(2):243-56.
73. Louie CM, Caridi G, Lopes VS, Brancati F, Kispert A, Lancaster MA, et al. AHI1 is required for photoreceptor outer segment development and is a modifier for retinal degeneration in nephronophthisis. Nat Genet. 2010;42(2):175-80.
74. Nagy A, Gertsensten, M., Vintersten, K., and Behringer, R. Manipulating the Mouse Embryo: A Laboratory Manual. 3rd ed. Cold Spring Harbor, New York: Cold Spring Harbor Press; 2003.
75. McEwen DP, Jenkins PM, Martens JR. Olfactory cilia: our direct neuronal connection to the external world. Curr Top Dev Biol. 2008;85:333-70.
76. Buck L, Axel R. A novel multigene family may encode odorant receptors: a molecular basis for odor recognition. Cell. 1991;65(1):175-87.
77. Ressler KJ, Sullivan SL, Buck LB. Information coding in the olfactory system: evidence for a stereotyped and highly organized epitope map in the olfactory bulb. Cell. 1994;79(7):1245-55.

78. Vassar R, Chao SK, Sitcheran R, Nuñez JM, Vosshall LB, Axel R. Topographic organization of sensory projections to the olfactory bulb. Cell. 1994;79(6):981-91.
79. Loktev AV, Jackson PK. Neuropeptide Y family receptors traffic via the Bardet-Biedl syndrome pathway to signal in neuronal primary cilia. Cell Rep. 2013;5(5):1316-29.
80. Corbit KC, Aanstad P, Singla V, Norman AR, Stainier DY, Reiter JF. Vertebrate Smoothened functions at the primary cilium. Nature. 2005;437(7061):1018-21.
81. Berbari NF, Johnson AD, Lewis JS, Askwith CC, Mykytyn K. Identification of ciliary localization sequences within the third intracellular loop of G protein-coupled receptors. Mol Biol Cell. 2008;19(4):1540-7.
82. Mazelova J, Astuto-Gribble L, Inoue H, Tam BM, Schonteich E, Prekeris R, et al. Ciliary targeting motif VxPx directs assembly of a trafficking module through Arf4. EMBO J. 2009;28(3):183-92.
83. Brear AG, Yoon J, Wojtyniak M, Sengupta P. Diverse cell type-specific mechanisms localize G protein-coupled receptors to Caenorhabditis elegans sensory cilia. Genetics. 2014;197(2):667-84.
84. Nachury MV, Loktev AV, Zhang Q, Westlake CJ, Peränen J, Merdes A, et al. A core complex of BBS proteins cooperates with the GTPase Rab8 to promote ciliary membrane biogenesis. Cell. 2007;129(6):1201-13.
85. Mukhopadhyay S, Wen X, Chih B, Nelson CD, Lane WS, Scales SJ, et al. TULP3 bridges the IFT-A complex and membrane phosphoinositides to promote trafficking of G protein-coupled receptors into primary cilia. Genes Dev. 2010;24(19):2180-93.
86. Mukhopadhyay S, Wen X, Ratti N, Loktev A, Rangell L, Scales SJ, et al. The ciliary G-protein-coupled receptor Gpr161 negatively regulates the Sonic hedgehog pathway via cAMP signaling. Cell. 2013;152(1-2):210-23.
87. Sun X, Haley J, Bulgakov OV, Cai X, McGinnis J, Li T. Tubby is required for trafficking G protein-coupled receptors to neuronal cilia. Cilia. 2012;1(1):21.
88. Saito H, Kubota M, Roberts RW, Chi Q, Matsunami H. RTP family members induce functional expression of mammalian odorant receptors. Cell. 2004;119(5):679-91.
89. Dwyer ND, Adler CE, Crump JG, L'Etoile ND, Bargmann CI. Polarized dendritic transport and the AP-1 mu1 clathrin adaptor UNC-101 localize odorant receptors to olfactory cilia. Neuron. 2001;31(2):277-87.
90. Kaplan OI, Molla-Herman A, Cevik S, Ghossoub R, Kida K, Kimura Y, et al. The AP-1 clathrin adaptor facilitates cilium formation and functions with RAB-8 in C. elegans ciliary membrane transport. J Cell Sci. 2010;123(Pt 22):3966-77.
91. Gimelbrant AA, Haley SL, McClintock TS. Olfactory receptor trafficking involves conserved regulatory steps. J Biol Chem. 2001;276(10):7285-90.
92. Law YQP-Y. Posttranslational Regulation of G Protein-Coupled Receptors. In: Stevens CW, editor. Methods for the Discovery and Characterization of G Protein-Coupled Receptors. Neuromethods. 602011. p. 133-52.
93. Alonso V, Friedman PA. Minireview: ubiquitination-regulated G protein-coupled receptor signaling and trafficking. Mol Endocrinol. 2013;27(4):558-72.
94. Wyatt D, Malik R, Vesecky AC, Marchese A. Small ubiquitin-like modifier modification of arrestin-3 regulates receptor trafficking. J Biol Chem. 2011;286(5):3884-93.
95. Tang Z, El Far O, Betz H, Scheschonka A. Pias1 interaction and sumoylation of metabotropic glutamate receptor 8. J Biol Chem. 2005;280(46):38153-9.
96. Komatsu M, Chiba T, Tatsumi K, Iemura S, Tanida I, Okazaki N, et al. A novel protein-conjugating system for Ufm1, a ubiquitin-fold modifier. EMBO J. 2004;23(9):1977-86.
97. Cort JR, Chiang Y, Zheng D, Montelione GT, Kennedy MA. NMR structure of conserved eukaryotic protein ZK652.3 from C. elegans: a ubiquitin-like fold. Proteins. 2002;48(4):733-6.

98. Mizushima T, Tatsumi K, Ozaki Y, Kawakami T, Suzuki A, Ogasahara K, et al. Crystal structure of Ufc1, the Ufm1-conjugating enzyme. Biochem Biophys Res Commun. 2007;362(4):1079-84.
99. Tatsumi K, Sou YS, Tada N, Nakamura E, Iemura S, Natsume T, et al. A novel type of E3 ligase for the Ufm1 conjugation system. J Biol Chem. 2010;285(8):5417-27.
100. Bacik JP, Walker JR, Ali M, Schimmer AD, Dhe-Paganon S. Crystal structure of the human ubiquitin-activating enzyme 5 (UBA5) bound to ATP: mechanistic insights into a minimalistic E1 enzyme. J Biol Chem. 2010;285(26):20273-80.
101. Kang SH, Kim GR, Seong M, Baek SH, Seol JH, Bang OS, et al. Two novel ubiquitin-fold modifier 1 (Ufm1)-specific proteases, UfSP1 and UfSP2. J Biol Chem. 2007;282(8):5256-62.
102. Azfer A, Niu J, Rogers LM, Adamski FM, Kolattukudy PE. Activation of endoplasmic reticulum stress response during the development of ischemic heart disease. Am J Physiol Heart Circ Physiol. 2006;291(3):H1411-20.
103. Lu H, Yang Y, Allister EM, Wijesekara N, Wheeler MB. The identification of potential factors associated with the development of type 2 diabetes: a quantitative proteomics approach. Mol Cell Proteomics. 2008;7(8):1434-51.
104. Lemaire K, Moura RF, Granvik M, Igoillo-Esteve M, Hohmeier HE, Hendrickx N, et al. Ubiquitin fold modifier 1 (UFM1) and its target UFBP1 protect pancreatic beta cells from ER stress-induced apoptosis. PLoS One. 2011;6(4):e18517.
105. Zhang Y, Zhang M, Wu J, Lei G, Li H. Transcriptional regulation of the Ufm1 conjugation system in response to disturbance of the endoplasmic reticulum homeostasis and inhibition of vesicle trafficking. PLoS One. 2012;7(11):e48587.
106. Wu J, Lei G, Mei M, Tang Y, Li H. A novel C53/LZAP-interacting protein regulates stability of C53/LZAP and DDRGK domain-containing Protein 1 (DDRGK1) and modulates NF-kappaB signaling. J Biol Chem. 2010;285(20):15126-36.
107. Tatsumi K, Yamamoto-Mukai H, Shimizu R, Waguri S, Sou YS, Sakamoto A, et al. The Ufm1-activating enzyme Uba5 is indispensable for erythroid differentiation in mice. Nat Commun. 2011;2:181.
108. Zhang M, Zhu X, Zhang Y, Cai Y, Chen J, Sivaprakasam S, et al. RCAD/Ufl1, a Ufm1 E3 ligase, is essential for hematopoietic stem cell function and murine hematopoiesis. Cell Death Differ. 2015.
109. Yoo HM, Kang SH, Kim JY, Lee JE, Seong MW, Lee SW, et al. Modification of ASC1 by UFM1 is crucial for ERα transactivation and breast cancer development. Mol Cell. 2014;56(2):261-74.
110. Hertel P, Daniel J, Stegehake D, Vaupel H, Kailayangiri S, Gruel C, et al. The ubiquitin-fold modifier 1 (Ufm1) cascade of Caenorhabditis elegans. J Biol Chem. 2013;288(15):10661-71.
111. Chen C, Itakura E, Weber KP, Hegde RS, de Bono M. An ER complex of ODR-4 and ODR-8/Ufm1 specific protease 2 promotes GPCR maturation by a Ufm1-independent mechanism. PLoS Genet. 2014;10(3):e1004082.
112. Händel M, Schulz S, Stanarius A, Schreff M, Erdtmann-Vourliotis M, Schmidt H, et al. Selective targeting of somatostatin receptor 3 to neuronal cilia. Neuroscience. 1999;89(3):909-26.
113. Strotmann J, Levai O, Fleischer J, Schwarzenbacher K, Breer H. Olfactory receptor proteins in axonal processes of chemosensory neurons. J Neurosci. 2004;24(35):7754-61.
114. de Bono M, Tobin DM, Davis MW, Avery L, Bargmann CI. Social feeding in Caenorhabditis elegans is induced by neurons that detect aversive stimuli. Nature. 2002;419(6910):899-903.
115. Dalton RP, Lyons DB, Lomvardas S. Co-opting the unfolded protein response to elicit olfactory receptor feedback. Cell. 2013;155(2):321-32.
116. Shykind BM, Rohani SC, O'Donnell S, Nemes A, Mendelsohn M, Sun Y, et al. Gene switching and the stability of odorant receptor gene choice. Cell. 2004;117(6):801-15.

117. Lyons DB, Allen WE, Goh T, Tsai L, Barnea G, Lomvardas S. An epigenetic trap stabilizes singular olfactory receptor expression. Cell. 2013;154(2):325-36.
118. Hébert JM, McConnell SK. Targeting of cre to the Foxg1 (BF-1) locus mediates loxP recombination in the telencephalon and other developing head structures. Dev Biol. 2000;222(2):296-306.
119. Dodou E, Xu SM, Black BL. mef2c is activated directly by myogenic basic helix-loop-helix proteins during skeletal muscle development in vivo. Mech Dev. 2003;120(9):1021-32.
120. Joyner A, Wall N. Immunohistochemistry of whole-mount mouse embryos. Cold Spring Harbor Protocols2008.
121. Cheeseman IM, Desai A. A combined approach for the localization and tandem affinity purification of protein complexes from metazoans. Sci STKE. 2005;2005(266):pl1.
122. de Bono M, Bargmann CI. Natural variation in a neuropeptide Y receptor homolog modifies social behavior and food response in C. elegans. Cell. 1998;94(5):679-89.
123. WormAtlas. WormAtlas 2002-2015. http://www.wormatlas.org]. Available from: http://www.wormatlas.org.

Publishing Agreement

It is the policy of the University to encourage the distribution of all theses, dissertations, and manuscripts. Copies of all UCSF theses, dissertations, and manuscripts will be routed to the library via the Graduate Division. The library will make all theses, dissertations, and manuscripts accessible to the public and will preserve these to the best of their abilities, in perpetuity.

Please sign the following statement:

I hereby grant permission to the Graduate Division of the University of California, San Francisco to release copies of my thesis, dissertation, or manuscript to the Campus Library to provide access and preservation, in whole or in part, in perpetuity.

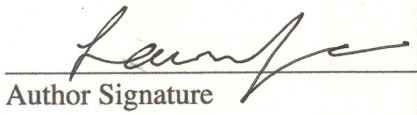

Author Signature

6/12/15

Date